Jari-Pascal Curty
Michel Declercq
Catherine Dehollain
Norbert Joehl

Design and Optimization of Passive UHF RFID Systems

Springer

DESIGN AND OPTIMIZATION OF PASSIVE UHF RFID SYSTEMS

DESIGN AND OPTIMIZATION OF PASSIVE UHF RFID SYSTEMS

Jari-Pascal Curty, Michel Declercq
Catherine Dehollain, Norbert Joehl
École Polytechnique Fédérale de Lausanne, Switzerland

Springer

Jari-Pascal Curty
Michel Declercq
Catherine Dehollain
Norbert Joehl
École Polytechnique Fédérale de Lausanne, Switzerland

Design and Optimization of Passive UHF RFID Systems

Library of Congress Control Number: 2006932387

ISBN 0-387-35274-0 e-ISBN 0-387-44710-5
ISBN 9780387352749

Printed on acid-free paper.

9 8 7 6 5 4 3 2 1

springer.com

Contents

Preface

RADIOFrequency IDentification (RFID) is an automatic identification method, relying on storing and remotely retrieving data using devices called RFID tags or transponders. An RFID tag is a small object that can be attached to or incorporated into a product, animal or person. An RFID tag contains an antenna to enable it to receive and respond to Radio-Frequency (RF) queries from an RFID reader or interrogator. Passive tags require no internal power source, whereas active tags require a power source.

As of today (2006), the concepts of ubiquitous computing and ambient intelligence are becoming widespread. In order for these to become a reality, a number of key technologies are required. In brief, these technologies need to be sensitive, responsive, interconnected, contextualised, transparent and intelligent. RFID, and in particular passive RFID tags, are such a technology. In order to deliver the necessary characteristics that could lead to ambient intelligence, however, there are some challenges that need to be addressed.

Remote powering of the tags is probably the most important challenge. Issues concerning the antenna-tag interface and the rectifier design, that allow the RF signal to be converted to Direct Current (DC) are top priorities. Secondly, the communication link and the reader should be optimized. The RF signal that contains the tag data suffers from a power of four decay with the distance between tag and reader. As a result, both the reader sensitivity and the tag backscattered power efficiency have to be maximized. Long-range powering, as well as sufficient communication quality, are the guidelines of this work.

This work proposes a linear two-port model for an N-stage modified-Greinacher full wave rectifier. It predicts the overall conversion efficiency at low power levels where the diodes are operating near their threshold voltage. The output electrical behavior of the rectifier is calculated as a function of the received power and the antenna parameters. Moreover, the two-port parameter values are computed for particular input voltages and output currents for the complete N-stage rectifier circuit, using only the measured I-V and C-V characteristics of a single diode.

Also presented in this work is an experimental procedure to measure how the impedance modulation at the tag side affects the signal at the reader. The method allows the tag designer to efficiently predict the effect of a modulator design at the system level and gives a useful instrument to choose the most appropriate impedances.

Finally, the design of a fully-integrated, remotely powered and addressable RFID tag working at 2.45 GHz is described. The achieved operating range at a 4 W Effective Isotropically Radiated Power (EIRP) reader transmit power is at most 12 m. The Integrated Circuit (IC) is implemented in a 0.5 μm silicon-on-sapphire technology. A state-of-the-art rectifier design is embedded to supply energy to the transponder. Inductive matching and a folded-dipole antenna are key elements for achieving this performance.

1

Introduction

THE trend in the automated industry is to move towards fast and real-time identification, further improving the high level of accuracy needed to enable continuous identification and monitoring. Such a level of real-time knowledge is often called *ambient intelligence*. One of the technologies that made this concept viable is known as Radio Frequency IDentification or more simply RFID. Companies, individuals and states can benefit from such a technology. There are numerous applications including: logistics, access control, transportation, pet management, counterfeit struggle, e-documents (biometric passports), etc. As usual with new technologies, these benefits should be balanced with the impact on personal privacy. Like no other technology, RFID opens new application horizons but also introduces new topics of reflection for lawmakers.

Passive (without embedded electrical energy) RFID transponders are composed of an electronic Integrated Circuit (IC) that usually contains data and an antenna. The IC is powered by a reader that also communicates with the tag in order to get its data (usually on the order of a few hundreds bits). The general overview of such a system is shown in Fig. 1.1.

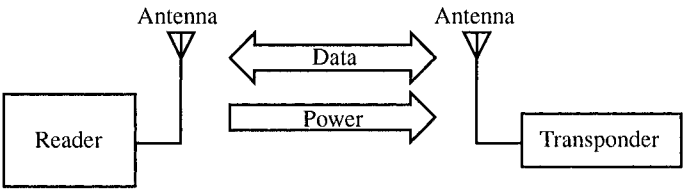

Fig. 1.1. RFID system overview.

1.1 Objective of this work

The goal of this work is to bring to light the trade-offs that occur in the optimization of passive Radio Frequency Identification systems operating at UHF and microwave frequencies. At these frequencies[1] (VHF: 433 MHz, UHF: 900 MHz or 2.45 GHz[2]), the identification transponder (called tag or transponder hereafter) is operating in the *far-field region* of an antenna. The far-field region is the region in which plane-wave propagation takes place. The beginning of the far-field region occurs at a distance from the antenna roughly equal to one wavelength of the emitted signal. At low frequencies (LF: 135 kHz and HF: 13.56 MHz or 27.12 MHz) where we find 95 % of the RFID market (2004 values [1]), the tag lies in the *near-field region* in which the inductive coupling phenomenon is used. LF and HF tags thus inherently reach a smaller operating range than their VHF, UHF and microwave counterparts. In this work, we consider only UHF and microwave systems. LF and HF systems are treated extensively in [2] and [3].

1.2 Organization of this book

There are three key issues in the development of a UHF or microwave system. First, we find the Wireless Power Transmission (WPT) issue. As will be presented in **chapter 2** and **chapter 3**, the choices of the *rectifier architecture*, the *antenna design* and the *integrated circuit process technology* are of central importance. These chapters are a developed version of [4].

Tag-to-reader communication is the second issue and will be addressed in **chapter 4 and chapter 5** where a complete study of the possible signal modulations will be proposed. **Chapter 6** presents an experimental method to quantify the backscattered power in phase and amplitude of any antenna. In **chapter 7**, we take advantage of the previous chapters to design a full integrated passive transponder operating from 900 MHz up to 5 GHz depending on the antenna size and achieving 12 m of reading range at 2.45 GHz. This chapter is an extended version of [5].

The third issue that limits the performance of an RFID system is the reader design. This aspect will be described in **chapter 8** where an architecture of both the RF and baseband system is proposed.

Finally, **chapter 9** concludes this work with the obtained results as well as new research ideas.

---

[1] LF: Low Frequency
HF: High Frequency
VHF: Very high frequency
UHF: Ultra-High Frequency

[2] Although the 2.45 GHz Industrial Scientific and Medical (ISM) band is part of the UHF spectrum according to the DIN40015 standard, it will be named "microwave" in this work.

2

Wireless Power Transmission

This chapter presents the history of Wireless Power Transmission (WPT) from Tesla to the rectenna. The basic rectifier, its building blocks and the full-wave modified Greinacher rectifier are then described [4]. The antenna and its issues for WPT illustrate the basic trade-offs that occur. Finally, a numerical example of WPT concludes this chapter.

2.1 History of Wireless Power Transmission

THE idea of Wireless Power Transmission (WPT) was first conceived and explored in 1899 by Nikola Tesla. During a conference, he announced that his personal dream of WPT was realized. He attempted to distribute ten thousand horse-power under a voltage of one hundred million volts. As said in his words: "This energy will be collected all over the globe preferably in small amounts, ranging from a fraction of one horse-power to a few horse-power. One of its chief uses will be the illumination of isolated homes."

Tesla conducted his experiments in Colorado Springs, Colorado, in 1899 (Fig. 2.1). Under a $30,000 (value in 1900!) grant from Colonel John Jacob Astor, owner of the Waldorf-Astoria Hotel in New York City, Tesla built a gigantic coil in a large square building over which rose a 60 m mast with a 1 m diameter copper ball positioned at the top. The coil was resonated at a frequency of 150 kHz and was fed with 300 kW of low-frequency power obtained from the Colorado Springs Electric Company. When the RF output was fed to the mast, an RF potential was produced on the sphere that approached 100, 000, 000 V, according to Tesla [6]. Some of his experiments were related by the journalists of his time. According to them, he succeeded in lighting two hundred 50 W incandescent lamps 42 km away from the base station.

Tesla not only thought that the globe was a good conductor but that the moderate altitude atmospheric layers were excellent conductors. Therefore, he wanted to prove it was possible to use these layers in order to transmit large amounts of electrical

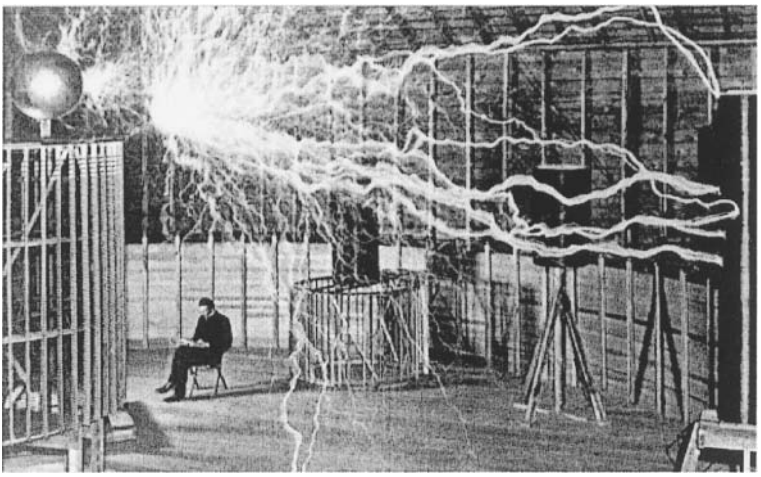

Fig. 2.1. Tesla in his Colorado Spring laboratory

energy over any distance. He proposed the idea (Fig. 2.2) but his sponsor, Morgan, retorted, "If everyone is able to draw energy from there, where would the electricity meter be?"

The work of Tesla was based on very long wavelengths and thus, the concept of radio wave focusing couldn't be used. The work of Heinrich Hertz demonstrated electromagnetic wave propagation in free space and its possible detection. Although theoretically possible, electromagnetic wave focusing was not feasible in practice, due to the lack of short wavelength generators. The klystron tube and the microwave cavity magnetron arrived in the late 30's [7]. Real interest in WPT began in the 50's and triggered the modern history of free-space power transmission. For an extensive historical presentation, the interested reader is referred to [6].

Since Tesla's experiments on WPT, there has been more than one century of research, with most progress made after 1958, on the topic of high-power beaming. Applications concerning high power transmission, like solar-powered satellite-to-ground systems (SPS) [6] and helicopter powering, have been developed. Typical efficiency of those systems is about 85% at lower microwave frequencies and less than this higher in the spectrum. The common point of these system is the *rectenna*.

2.2 The rectenna

In the work of Tesla, there was a need for an energy transducer. It was needed to convert one type of energy to another. For the WPT in this present work, the energy conversion from RF to DC is realized based on a *rectenna* circuit.

A rectenna is a rectifying antenna, a special type of antenna that is used to directly convert microwave energy into DC electricity. By connecting a Schottky diode to the access of a dipole antenna, we obtain a simple rectenna. The use of a Schottky diode is

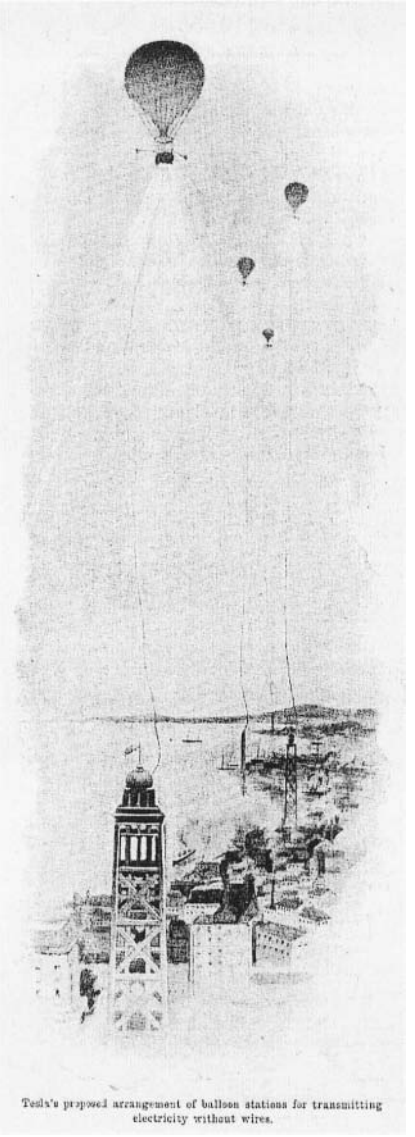

Fig. 2.2. Tesla's idea to transmit electrical energy from the atmosphere down to the earth. The use of a fire balloon would allow the electricity to flow along a conducting wire down to a base station. The city could then be "easily" energized.

necessary to achieve a high efficiency in the overall conversion process. A schematic of a typical rectenna circuit is shown in Fig. 2.3. The antenna captures the power from its surroundings (represented by the power density S) and generates a voltage

at the diode D access. The latter rectifies the voltage to a DC current that charges the capacitor C at the rate RC.

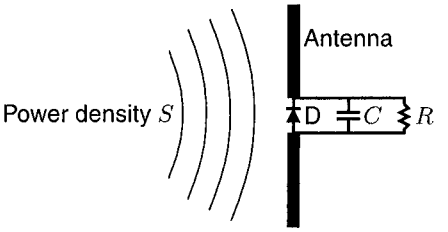

Fig. 2.3. A typical rectenna schematic.

William C. Brown was the first to succeed in demonstrating a microwave powered helicopter in 1964 using the rectenna [6]. The rectenna was thoroughly studied starting from the second half of the twentieth century resulting in high overall efficiency systems. With the advent of integrated circuits and low power technologies, new applications were made possible. In the mid 1980's [8], Radio Frequency IDentification Systems (RFID) appeared in which an inductive or electromagnetic coupling antenna was used for both power transmission and as a communication link. Other applications of WPT include biomedical implants with passive telemetry as a communication link [9]. More recently, the recycling issue of the ambient microwave energy was addressed [10]. The vast majority of these applications make use of a *rectifier* building block, similar to the basic rectenna of Fig. 2.3, to draw their energy.

2.3 Rectifier building blocks

The use of low threshold diodes (e.g. Schottky) and good quality capacitors allow a continuous voltage to be drawn out of a small amplitude pulsed signal (typically sinusoidal). The rectifier circuit is built out of two basic electrical circuits, the *clamping circuit* and the *envelope detector circuit.*

2.3.1 Clamping circuit

The goal of this circuit is to establish a DC reference for the output voltage by using a diode clamp as shown in Fig. 2.4.

By conducting whenever the voltage at the output terminal of the capacitor v_{out} goes negative, this circuit builds up an average charge on the terminal that is sufficient to prevent the output from ever going negative. Positive charge on this terminal is effectively trapped. If all elements are ideal, the residual negative voltage Δv_{r} is null and v_{out} is exactly equal to $\widehat{v_{\text{in}}} + v_{\text{in}}$ where $\widehat{v_{\text{in}}}$ is the peak amplitude of v_{in}.

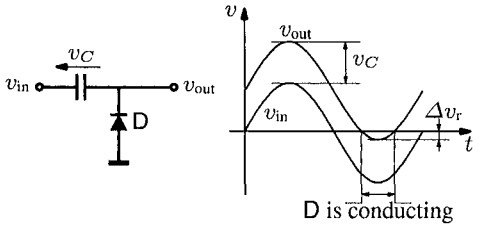

Fig. 2.4. Diode clamp circuit and its output waveform.

2.3.2 Rectifier circuit

When a voltage v_{in} is applied on the input of the circuit of Fig. 2.5, the capacitor charges until its voltage v_C is equal to the maximum of v_{in}. If no resistor is connected

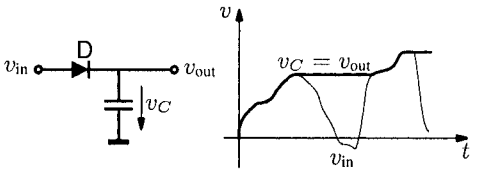

Fig. 2.5. Basic rectifier circuit and its output waveform.

in parallel with the output capacitor, the voltage v_{out} never reduces.

In practice, the leakage current of the capacitor induces an output voltage drop. If v_{in} is a sinusoidal signal, the capacitor will charge every time its voltage is near its peak value. Consequently, the mean output voltage $\overline{v_{out}}$ is slightly smaller than the peak amplitude of v_{in}.

In both cases, the threshold voltages of the diodes are not taken into account. But it should be mentioned that they further reduce the output voltage amplitude. All these effects are addressed later in this chapter.

2.3.3 The voltage doubler

The voltage doubler is obtained by cascading the blocks from sections 2.3.1 and 2.3.2. The result is shown in Fig. 2.6

As can be seen in Fig. 2.6, and from 2.3.1 and 2.3.2, the voltage doubler outputs a DC voltage. In the ideal case, v_{out} is twice the amplitude of v_{in}. This circuit is actually a half wave voltage doubler since only the positive peaks of the input signal are rectified. To take advantage of both positive and negative peaks, one must use the full-wave rectifier.

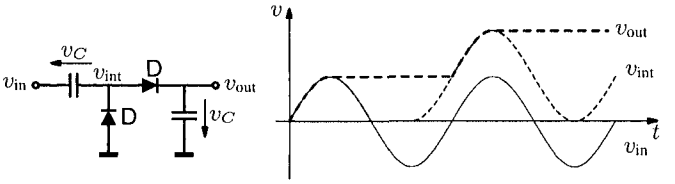

Fig. 2.6. Voltage doubler circuit and its waveforms.

2.3.4 Full-wave rectifier

In this case, the structure of Fig. 2.6 is mirrored with respect to the ground. The *full-wave rectifier* is obtained and is represented in Fig. 2.7. The waveforms shown are

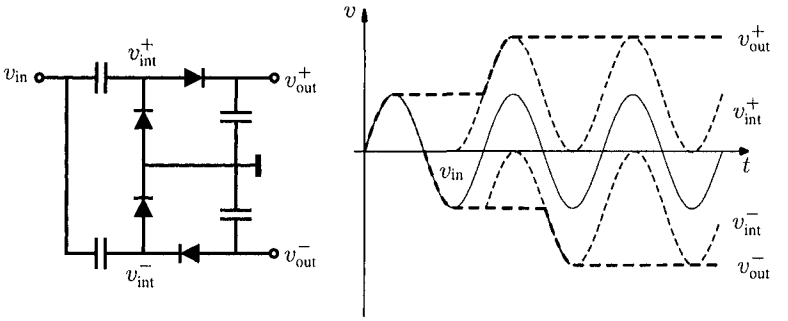

Fig. 2.7. Full-wave voltage doubler circuit and its waveforms.

only valid in the ideal case, i.e. zero leakage capacitors, no threshold voltage (0 V) and no reverse current in the diodes.

In practice, in low power applications, the voltage level at the input of a rectifier as in Fig. 2.7 is on the order of a few hundred millivolts. The non-idealities of real-life components noticeably affect the voltage multiplication factor between the output voltage and the input amplitude. The minimum supply voltage for today's RFID tags is typically 1.2 V. To achieve such an amplitude level, one has to cascade the circuit of Fig. 2.7. It results in the Greinacher cascade of Fig. 2.8(a).

2.3.5 Full-wave Greinacher rectifier

A little modification in the rectifier of Fig. 2.8(a) leads to the circuit of Fig. 2.8(b). The rectifier is first symmetrized and then the capacitors are rearranged so that every rectifying diode is excited with the same input signal amplitude. The resulting topology offers a nice symmetry. To reduce the number of capacitors, one could disconnect C_1 and C_2 from the ground and combine them to form only one "output or charging capacitor" per stage.

More importantly, its low power input impedance is smaller than in the non-modified version. This can be an advantage when the antenna-transponder matching issue is addressed. Another advantage of this structure is the lower capacitive losses along the RF path to the diodes. The capacitors act indeed as voltage dividers. Thanks to its symmetry, the modified structure reduces the reflected harmonic content.

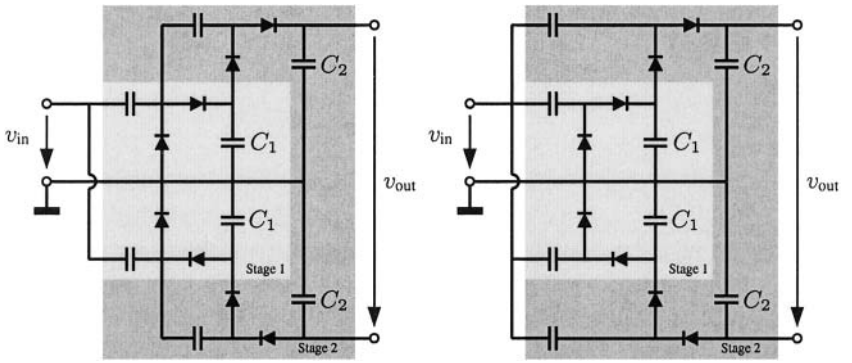

(a) Direct cascaded version.

(b) Capacitors path modified version.

Fig. 2.8. Full-wave modified Greinacher rectifiers.

The output voltage is equal to $4N\widehat{v_{in}}$ where N is the number of stages. But in both cases, the dynamic impedance issue, due to the output current consumption and the input voltage impedance (e.g. the antenna), deeply affects this simple result. As will be shown in the next chapter, the use of rectifiers at low power levels is a challenging task when both the power and operating range issues are taken into account.

2.4 Antenna

The antenna is the second building block of the rectenna (see Fig. 2.3). Its characteristics affect in many ways the overall efficiency of WPT systems. In general, an arbitrary antenna has a complex input impedance (related to the feeding point) which can be written in the form $Z_{ant} = R_A + jX_{ant}$, where $R_A = R_{loss} + R_s$ (see Fig. 2.9).

R_s is the radiation resistance of the antenna, R_{loss} is the loss resistance of the antenna, X_{ant} is the imaginary part of the antenna input impedance, S corresponds to the effective aperture of the antenna and P_{AV} is the available power that the antenna can deliver to a *matched* load.

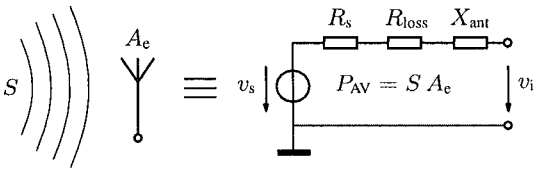

Fig. 2.9. Antenna equivalent electrical model.

2.4.1 Loss resistance

The loss resistance R_{loss} is due to the actual resistance of the elements that form the antenna (typically the copper in a patch antenna and the chosen dielectric), and to dielectric losses. Power dissipated in this manner is lost as heat. Although it may appear that the "DC" resistance is low, at higher frequencies the *skin-effect* δ is in evidence and only the surface areas of the conductor are used (see Fig. 2.10). As a result the effective resistance is higher than would be measured at DC for closed loop antennas (see Fig. 2.11). It is proportional to the circumference of the conductor and to the square root of the frequency (see Eq. (2.1)).

The resistance can become particularly significant in high current sections of an antenna where the effective resistance is low. Accordingly, to reduce the effect of the loss resistance it is necessary to ensure the use of very low resistance conductors.

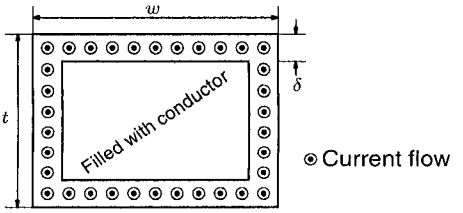

Fig. 2.10. Cross-section of a conductor. It shows the current near its surface.

The losses due to the skin-effect can be modeled by a resistance known as the high frequency resistance R_{HF} and its value can be calculated with the following approximation

$$R_{HF} \approx \frac{1}{\sigma\delta(\text{conductor perimeter})} = \sqrt{\frac{\mu_0 \pi f}{\sigma}} \frac{1}{(2w + 2t)} \tag{2.1}$$

where w and t are the width and the thickness of the conductor (see Fig. 2.10), σ is the material conductivity and μ_0 is the permeability of free space.

The losses are difficult to evaluate but, at UHF, R_{loss} is generally negligible compared with R_s. *In this work, the effect of R_{loss} is neglected.*

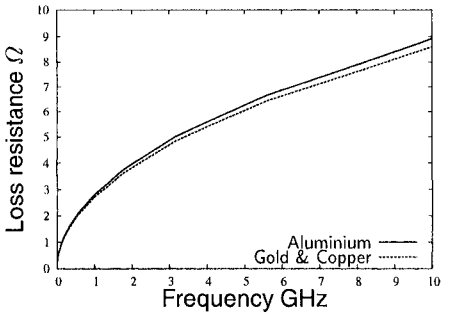

Fig. 2.11. High frequency resistance in different materials. These results are valid for a conductor whose cross-section size is 1 mm width×35 μm thickness.

2.4.2 Radiation resistance

The other resistive element is the "radiation resistance." This can be thought of as virtual resistor. It arises from the fact that power is "dissipated" when it is radiated. The aim, when designing an antenna, is to "dissipate" as much power in this way as possible. It varies from one type of antenna to another, and from one design to another. It is dependent upon a variety of factors. A typical half wave folded dipole operating in free space has a radiation resistance of around 300 Ω (see Table 4.5).

Note that the radiation resistance is not a real resistor, but simply a convenient form for representing a loss of energy from the antenna. In a real resistance, the lost energy is converted to heat. With respect to radiation resistance, *the energy isn't converted to heat, but simply radiated as radio waves.*

2.4.3 Antenna-Rectifier interface

The antenna is connected to the rectifier, which contains diodes that are sensitive to the voltage at their ports. In order for the diodes to transmit power (by reducing the real part of their impedance) the voltage level has to be sufficient. Moreover, it is necessary that the voltage applied to the diodes be greater than (or approaching) their threshold voltage. As will be described in the next chapter, the physical condition for the rectifier to deliver a growing output voltage is satisfied when the charge due to the direct current exactly compensates the charge due to the inverse current of a rectifying diode. The voltage source amplitude $\widehat{v_s}$ (see Fig. 2.9) is equal to

$$\widehat{v_s} = 2\sqrt{2R_s P_{AV}}. \tag{2.2}$$

$\widehat{v_s}$ is thus proportional to the square-root of the radiation resistance R_s. If the rectifier is modeled (zero order approximation) as a resistive load R_i (see Fig. 2.12), the input voltage v_{in} is equal to

$$\widehat{v_{in}} = \widehat{v_s}\frac{R_i}{R_i + R_s} = 2\sqrt{2R_s P_{AV}}\frac{R_i}{R_i + R_s} \tag{2.3}$$

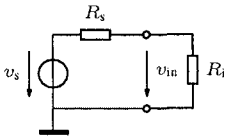

Fig. 2.12. First order model of the antenna connected to the rectifier.

Equation (2.2) shows that to increase $\widehat{v_s}$, a high radiation resistance R_s is mandatory. Furthermore, from (2.3), it is clear that the maximal transmitted power is obtained as antenna-rectifier matching is ensured, i.e. when the connected load impedance R_i is exactly equal to R_s (or $Z_{in} = Z_{ant}^*$ in the complex case). This result is very important to WPT because it says in essence that to design an optimal WPT system, it is necessary to have both *power-matching and a high radiation resistance at the receiving end of the system.*

2.4.4 Numerical example

To gain more insight into the WPT issues, a numerical example is presented in this section.

A typical WPT system is shown in Fig. 2.13. The effective isotropically radiated power P_{EIRP}, equal to $P_{RF}\, G_{PA}\, G_t$, is radiated in the direction of a battery-less device situated at a distance d. The power density S at the device antenna is

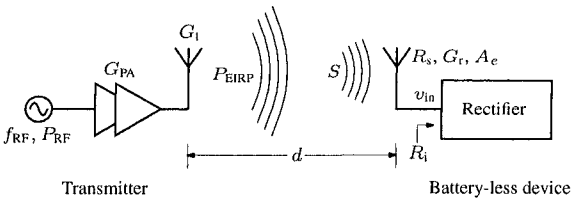

Fig. 2.13. Typical WPT system.

$$S = P_{EIRP} \frac{1}{4\pi d^2}.$$

The power P_r collected by the device antenna and transferred to the load is

$$P_r = A_e S$$

where A_e is the effective aperture of the antenna. In general, the maximal effective aperture is related to the antenna gain G_r and the wavelength λ_{RF} by

$$A_e = \frac{\lambda_{RF}^2}{4\pi} G_r \tag{2.4}$$

so that P_r is

$$P_r = S\frac{\lambda_{\mathrm{RF}}^2}{4\pi}G_{\mathrm{r}} = P_{\mathrm{EIRP}}\,G_{\mathrm{r}}\frac{\lambda_{\mathrm{RF}}^2}{(4\pi d)^2} \tag{2.5}$$

Eq. (2.5) is known as the *Friis relation*.

Using (2.3), the input voltage $\widehat{v_{\mathrm{in}}}$ at the rectifier is

$$\widehat{v_{\mathrm{in}}} = 2\sqrt{2R_{\mathrm{s}}P_{\mathrm{AV}}}\frac{R_{\mathrm{i}}}{R_{\mathrm{i}}+R_{\mathrm{s}}} \tag{2.6}$$

$$= 2\sqrt{2R_{\mathrm{s}}}\frac{R_{\mathrm{i}}}{R_{\mathrm{i}}+R_{\mathrm{s}}}\sqrt{P_{\mathrm{EIRP}}}\frac{\lambda_{\mathrm{RF}}}{4\pi d}\sqrt{G_{\mathrm{r}}}. \tag{2.7}$$

Substituting the typical values of Table 2.1, $\widehat{v_{\mathrm{in}}}$ is plotted for different values of R_{s} and R_{i} as a function of the distance d in Fig. 2.8.

Table 2.1. Typical values borrowed from the FCC regulations for a WPT system operating at 2.45 GHz.

λ_{RF}	12.24 cm
P_{EIRP}	4 W

Fig. 2.14 clearly shows that the main challenge for WPT applications is the ability to deal with less than a 100 mV input signal amplitude. Reaching distances of more than 10 m is particularly demanding since $\widehat{v_{\mathrm{in}}}$ is inversely proportional to the distance. The impedance arrangement also has a noticeable impact. In Fig. 2.14(a), there are no differences between the 300 Ω and the 900 Ω but from the four figures, it is clear that a high input resistance performs better. In Fig. 2.15, the input voltage $\widehat{v_{\mathrm{in}}}$ available at a distance of 10 m is represented for different values of R_{i} as a function of R_{s}. In order to maximize $\widehat{v_{\mathrm{in}}}$, it is necessary to have a high value for R_{i}. At high frequencies, such values are difficult to obtain because of parasitics; a 1 pF capacitance operating at 2.45 GHz represents $-j65\ \Omega$, limiting the real impedance level. Careful design and technology choices allow the overall input capacitance level presented to the antenna to be kept to a minimum. But values below 500 fF are not easily realized. As will be shown in chapter 3, R_{i} depends on the output current consumption. Consequently, the consumption of the WPT device has to be minimized.

2.4.5 WPT today and possible future applications

Considering today's typical regulations, the monolithic modified Greinacher rectifier is a viable candidate for short range micro-powered devices. RFIDs make extensive use of rectifiers as power supplies both in the low frequency range and in the UHF range. Working range of about 15 m is announced by industrials [11] for an emitted power of 30 W at 915 MHz (US licensed site). Wireless distributed sensor networks could also benefit from such a technology, e.g. for automatic tire temperature or pressure control [12]. Micro-batteries, e.g. thin film lithium ion cells, could store

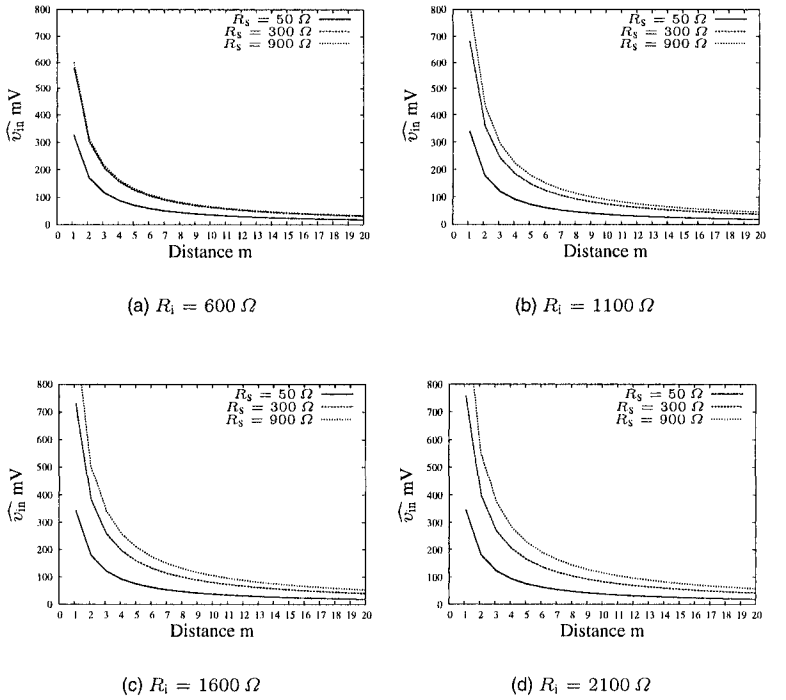

Fig. 2.14. Input voltage $\widehat{v_{in}}$ for different value of R_s and R_i as a function of the distance d.

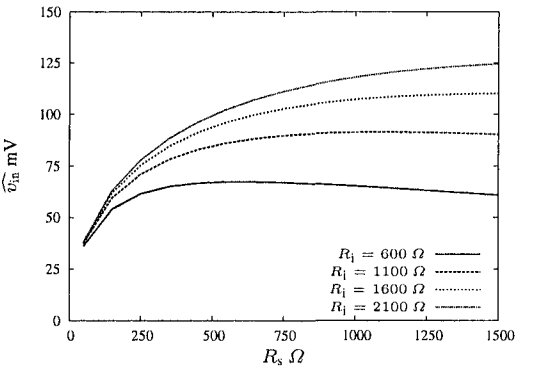

Fig. 2.15. Available voltage at 10 m of a 4 W transmitter in different impedance level conditions.

energy during idle time, or a dedicated frequency band could be used (as proposed by the ITU [13]) to supply the necessary power to a sensor when demanded. The data obtained could then be captured using typical RFID communication techniques, e.g. backscattering (see chapter 4).

2.5 Conclusion

The issues for wireless power transmission have been described. The possible circuit topologies that allow RF signal rectification have been presented. The modified-Greinacher structure constitutes a viable candidate for WPT devices. The antenna has also been identified to be a fundamental component of any WPT system. Finally, a numerical example gave some insight into the numbers involved. This concludes this chapter and opens the development of the modified-Greinacher structure model derived in the next chapter.

3

Analysis of the Modified-Greinacher Rectifier

As described in chapter 2, the use of low threshold voltage and low reverse current diodes and capacitors makes it possible to obtain a relatively high output voltage (1-2 V) given a sinusoidal input signal of about 200 mV. These values depend on the received power, the DC output current delivered to the load, and the impedance matching quality between the antenna and the rectifier's input. It is the purpose of this chapter to discuss all these issues in order to predict the performance of a modified-Greinacher full-wave rectifier in a given process technology [4].

3.1 Matching strategy

BEFORE starting the model development, the matching strategy is discussed in this section. The WPT application that is presented in this work is about RFID tags consisting of an antenna and an integrated circuit (IC). The antenna is responsible for capturing as much RF power as possible whereas the IC transforms the received RF power into a continuous DC voltage source for a given application (see Fig. 3.1).

In a traditional RF receiver, the matching strategy between the antenna and the front-end is often defined as a compromise between noise and power losses. As a result, the impedance level chosen is often in the neighborhood of 50 Ω.

In the case of RFID, the trade-off is more about power return losses, input voltage and backscattered power. The latter point is discussed in detail in chapter 5. For the moment, the goal is to maximize the operating (or powering) range.

From section 2.4.3, the voltage at the input of the rectifier is

$$\widehat{v_{\text{in}}} = 2\sqrt{2R_{\text{s}}P_{\text{AV}}}\frac{R_{\text{i}}}{R_{\text{i}}+R_{\text{s}}}. \tag{3.1}$$

The optimum in terms of absorbed power at the input is achieved when $R_{\text{i}} = R_{\text{s}}$. Furthermore, the voltage level $\widehat{v_{\text{in}}}$ is scaled up by the factor $\sqrt{R_{\text{s}}}$. For this reason, a *high*

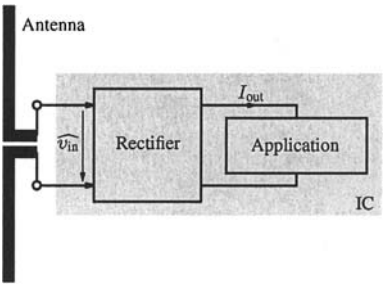

Fig. 3.1. Typical RFID tag building blocks.

radiation resistance antenna is desired to increase the powering range of the system. With this reasoning, the input capacitance C_i is neglected. Its effect is discussed later in this chapter (see section 3.5). For the moment, it should be mentioned that C_i reduces the real input impedance.

The available power from the antenna P_{AV} is fixed. If the application circuit asks for more output current I_{out}, the input current raises and R_i decreases. The power matching is thus dynamic and one could ask for *which value of* R_i *it is preferable to power-match* R_s *in order to keep* $\widehat{v_{in}}$ *as high as possible when mismatch occurs.* To answer this question, the ratio $\alpha = R_i/R_s$ is introduced. Furthermore, $\widehat{v_{in}}$ is normalized to $2\sqrt{2R_sP_{AV}}$ to obtain

$$\widehat{v_{in\,norm.}} = \frac{2\sqrt{2R_sP_{AV}}\frac{\alpha R_s}{\alpha R_s + R_s}}{2\sqrt{2R_sP_{AV}}} = \frac{\alpha}{\alpha + 1} \tag{3.2}$$

Equation (3.2) is represented in Fig. 3.2.

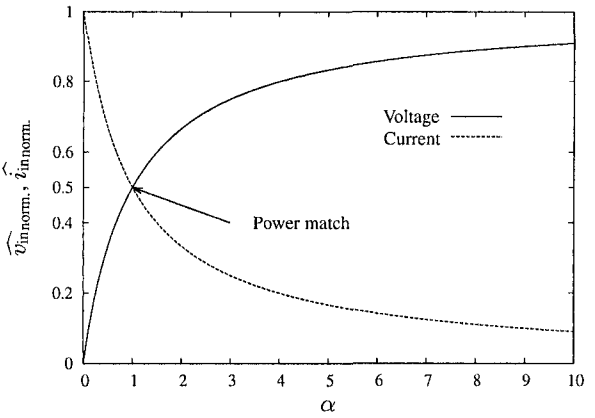

Fig. 3.2. Normalized input voltage and current.

Let's consider the antenna to be matched to the rectifier input impedance. In the graphic of Fig. 3.2 it corresponds to the point where $\alpha = 1$. Two cases arise

1. R_s is matched to $R_i|_{max}$, i.e. when $I_{out} = 0$;
2. R_s is matched to $R_i|_{min}$, i.e. when $I_{out} = I_{out\_max}$.

In the first case, R_i decreases since I_{out} can only increase. In Fig. 3.2, it means that α decreases. Consequently, $\widehat{v_{in}}$ also decreases which gives the advantage of an increasing current $\widehat{i_{in}}$. But the diodes that compose the rectifier need a sufficient voltage to be able to draw current. As a result, V_{out} quickly drops and the WPT device shuts down.

In the second case, R_i only increases and more importantly, $\widehat{v_{in}}$ increases. It is an interesting situation because the output power reduces when less power is available due to mismatch, and v_{in} increases, *simultaneously*. In other words, the necessary input voltage $\widehat{v_{in}}$ to operate the rectifier is guarantied as long as the absorbed power is sufficient.

As a summary, in order to keep $\widehat{v_{in}}$ at a sufficiently high level when mismatch between R_s and R_i occurs, it is more efficient to power-match R_s to $R_i|_{min}$, i.e. when the output current I_{out} is maximum.

3.2 Rectifier equivalent circuit

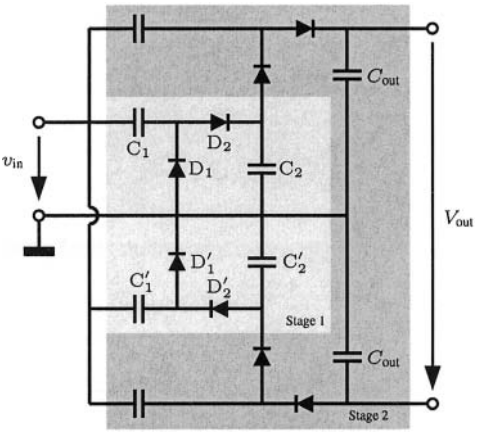

Fig. 3.3. 2-stage modified-Greinacher full-wave rectifier.

To achieve an optimal matching as described in the previous section, it is necessary to have a good knowledge of R_i. In order to do so, a model of the rectifier is developed in this chapter.

The modified-Greinacher rectifier (Fig. 3.3) is essentially non-linear in its nature due to the presence of diodes. It is thus a difficult task to analyze it in the time domain during its start-up. However, we model this circuit in the steady-state as a constant

input impedance (R_i and C_i for a constant input voltage amplitude $\widehat{v_{in}}$ and a constant output current I_{out}), a constant output resistance (R_{out} for a constant input voltage amplitude $\widehat{v_{in}}$ and a constant output current I_{out}) and an output voltage source V_0 (see Fig. 3.4).

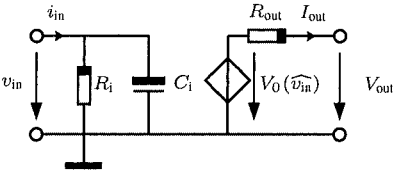

Fig. 3.4. Rectifier equivalent circuit model.

R_i , R_{out} and C_i are controlled, as will be demonstrated, by both the output current I_{out} and the input sinusoidal voltage amplitude $\widehat{v_{in}}$, whereas V_0 depends only on $\widehat{v_{in}}$.

3.3 Analysis strategy

The input impedance $R_i||C_i$ implies a linear input current $i_{in}(t)$. In reality, $i_{in}(t)$ has a pulsed shape (see Fig. 3.5) and of course, this doesn't look like a linear signal.

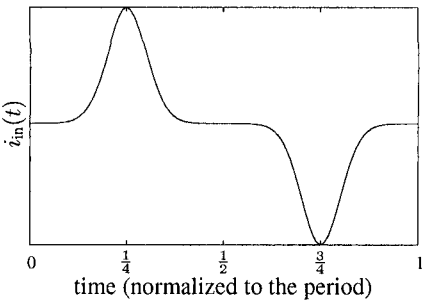

Fig. 3.5. Input current shape during one period of signal.

However, by respecting the power balance at the antenna-rectifier interface, the input current can be transformed into an equivalent sinusoidal input current. As a result, the input resistance is linearized and draws the same amount of power from the antenna (the source).

After the transient mode, the rectifier enters the steady-state mode during which the circuit operates in a very symmetrical fashion. As will be shown, in this mode, the rectifying diodes draw exactly the same amount of charge during a time period of the

input signal. This will greatly simplify the model since the electrical characteristics of only one diode will be necessary to derive all the model parameters.

As a first step, the ideal case where all elements are lossless is studied. Then the real case based on real world diodes is considered. Furthermore, for the present study, the following assumptions are made:

1. The rectifier operates in steady-state mode;
2. The output current is constant during the whole signal period;
3. All the diodes are identical;
4. The coupling capacitors are considered as short-circuits at the frequency of analysis (see section 3.7.2).

3.4 Ideal case

In this case, a 1-stage rectifier composed of ideal diodes is considered, i.e. 0 V threshold voltage, no reverse current and infinite conductance in forward mode. The working principle of the 1-stage rectifier of Fig. 3.6 is the following. Capacitor C_1 and diode D_1 shift the voltage $v_{in}(t)$ up at B, as C'_1 and D'_1 shift the voltage $v_{in}(t)$ down at B'. Diode D_2 and capacitor C_2 rectify the voltage at B (AC and DC components), as D'_2 and C'_2 rectify the voltage at B'. After the transient, equilibrium is reached and the circuit enters its steady-state mode. In this mode, the rectifier delivers a constant output current I_{out} and a constant output voltage V_{out} that is calculated in the next subsection.

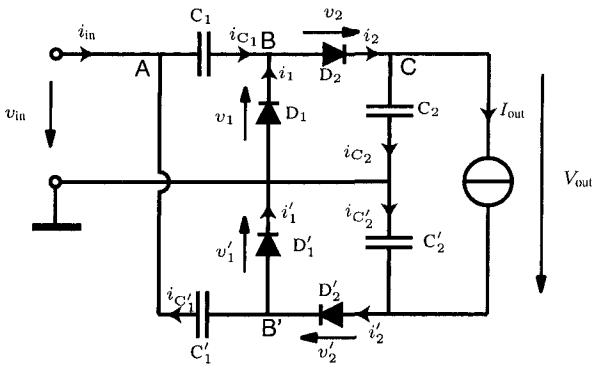

Fig. 3.6. 1-stage full-wave rectifier.

3.4.1 Steady-state solution of the ideal rectifier

For $I_{out} = 0$, the following steady-state analysis allows us to compute the values of R_i and C_i (see Fig. 3.4). In the case where the input voltage source v_{in} is an ideal

alternating voltage source, the continuous output voltage V_{out} is equal to $4\widehat{v_{\text{in}}}$. The circuit is indeed symmetrical, and since the output voltage is continuous, and the voltage applied to the diodes contains an alternative component, the only possible steady-state solution for the voltage on the diodes is

$$\boxed{\begin{array}{ll} v_1(t) = -\widehat{v_{\text{in}}} - v_{\text{in}}(t) & v_2(t) = -\widehat{v_{\text{in}}} + v_{\text{in}}(t) \\ v_1'(t) = -\widehat{v_{\text{in}}} + v_{\text{in}}(t) & v_2'(t) = -\widehat{v_{\text{in}}} - v_{\text{in}}(t) \end{array}} \tag{3.3}$$

so that the output voltage V_{out} is constant, i.e.:

$$V_{\text{out}} = -v_1(t) - v_2(t) - v_1'(t) - v_2'(t) = 4\widehat{v_{\text{in}}}. \tag{3.4}$$

In the case of the N-stage version, all the diodes are driven with the voltage expressed in (3.3). The output voltage for an N-stage configuration is thus

$$V_{\text{out}} = 4N\widehat{v_{\text{in}}}. \tag{3.5}$$

When an output current I_{out} is delivered to the load, it tends to discharge C_2 (and likewise C_2') which recharges rapidly through D_2 (and D_2') at every positive (and respectively negative) alternation of v_{in}. In steady-state, the charge quantity pulsed by the current $i_2[t]$ compensates exactly the one drawn off by I_{out}. We thus have at equilibrium (see node C on figure 3.6)

$$\begin{aligned} &\int_0^T i_2[t]\,\mathrm{d}t = \int_0^T I_{\text{out}}\,\mathrm{d}t + \underbrace{\int_0^T i_{C_2}[t]\,\mathrm{d}t}_{=0} \\ &\Rightarrow \int_0^T i_2[t]\,\mathrm{d}t = I_{\text{out}}T \end{aligned} \tag{3.6}$$

and for $i_2'[t]$

$$\int_0^T i_2'[t]\,\mathrm{d}t = I_{\text{out}}T.$$

During the recharge of C_2 (or C_2'), diode D_1 (or D_1') is reverse biased and the current $i_2[t]$ can only come from C_1 (or C_1'). This capacitor thus accumulates the same charge quantity $I_{\text{out}}T$ which is released at the next negative (or positive) peak through D_1 (or D_1'). We thus also have

$$\begin{aligned} &\int_0^T i_1[t]\,\mathrm{d}t = \int_0^T I_{\text{out}}\,\mathrm{d}t + \underbrace{\int_0^T i_{C_1}[t]\,\mathrm{d}t}_{=0} \\ &\Rightarrow \int_0^T i_1[t]\,\mathrm{d}t = I_{\text{out}}T \end{aligned} \tag{3.7}$$

and for $i_1'[t]$

$$\int_0^T i_1'[t]\ \mathrm{d}t = I_{\text{out}}T.$$

In (3.6) and (3.7), the second term of the integral is null. The reason is that V_{out} at the beginning of a signal period is the same at the beginning of the next period, i.e.

$$V_{\text{out}}[nT] = V_{\text{out}}[(n+1)T].$$

Hence, the charge balance on the capacitance C_{out} associated with V_{out} is null

$$Q_{\text{out}}[nT] = Q_{\text{out}}[(n+1)T],$$

which implies that

$$\int_0^T i_{C_1}[t]\ \mathrm{d}t = 0.$$

In steady-state, equations (3.6) and (3.7) are valid for all diodes of an N-stage rectifier. In order to sustain an output current I_{out}, every diode lets the charge quantity $I_{\text{out}}T$ flow over one period of signal. (They operate like a water-bucket chain.) As a result, the behavior of the rectifier in the steady-state mode is ruled by only one equation:

$$\int_0^T i_{\text{d}}[t]\ \mathrm{d}t = I_{\text{out}}T. \tag{3.8}$$

Expression (3.8) represents the equations of the rectifier that have to be used to compute the steady-state solution. The real case only differs in that the voltage on each diode at equilibrium $\overline{V_{\text{D}}}$ isn't equal to $\widehat{v_{\text{in}}}$ anymore. It is calculated as a function of $\widehat{v_{\text{in}}}$ for a given output current I_{out}. The next step is to determine R_{i} in order to address the antenna impedance matching issue.

3.4.2 Determination of R_{i}

Due to the non-linear behavior of the diodes, the current that enters the rectifier is pulsed. Thus we cannot talk about a *constant* input impedance. Nevertheless, as said before, our goal is to model the input impedance of the rectifier using a *time constant* input resistance R_{i} which represents the mean power $\overline{P_{\text{in}}}$ that enters the rectifier during one period of signal $v_{\text{in}}(t)$, i.e.

$$\overline{P_{\text{in}}} = \frac{1}{T}\int_0^T v_{\text{in}}(t)i_{\text{in}}(t)\ \mathrm{d}t. \tag{3.9}$$

By doing so, we convert the pulsed input current to a sinusoidal current

$$i_{\text{in,sin}}(t) = \frac{v_{\text{in}}(t)}{R_{\text{i}}} = \frac{\widehat{v_{\text{in}}}\sin\omega t}{R_{\text{i}}}. \tag{3.10}$$

In the ideal case, the rectifier is non-dissipative. As a consequence, the power that enters the network is equal to the DC power delivered to the load P_{DC}, i.e.

$$\overline{P_{\text{in}}} = P_{\text{DC}} = V_{\text{out}} I_{\text{out}}. \tag{3.11}$$

Using (3.5), we get for an N-stage ideal rectifier

$$\begin{aligned} \frac{\widehat{v_{\text{in}}}^2}{R_{\text{i}}} \int_0^T \sin^2 \omega t \, \mathrm{d}t &= 4N \widehat{v_{\text{in}}} I_{\text{out}} \\ \Rightarrow R_{\text{i}} &= \frac{\widehat{v_{\text{in}}}}{8N I_{\text{out}}}. \end{aligned} \tag{3.12}$$

As described earlier, the equivalent input resistance R_{i} is inversely proportional to the output current I_{out}. Due to the parallelism of the structure, R_{i} is also inversely proportional to the number of stages N. N is thus an important design parameter. The relationship between R_{i} and $\widehat{v_{\text{in}}}$ is explained later in section 3.5.

To take into account the imperfections of the diode, e.g. reverse current, threshold voltage, etc., we need to consider the real current-voltage characteristics of the diodes. Furthermore, the calculation of R_{out} and C_{i} makes more sense in the real case studied in the next section.

3.5 Real case

The preceding study shows that once the steady-state equilibrium is reached, every diode sees at its terminals the input signal $v_{\text{in}}(t)$ (or $-v_{\text{in}}(t)$) shifted up a constant voltage $\overline{V_{\text{D}}}$ equal to $\widehat{v_{\text{in}}}$ if all diodes are ideal. As a reminder, the steady-state voltage on the diodes of a one stage rectifier are

$$\boxed{\begin{array}{ll} v_1(t) = -\overline{V_{\text{D}}} - v_{\text{in}}(t) & v_2(t) = -\overline{V_{\text{D}}} + v_{\text{in}}(t) \\ v_1'(t) = -\overline{V_{\text{D}}} + v_{\text{in}}(t) & v_2'(t) = -\overline{V_{\text{D}}} - v_{\text{in}}(t). \end{array}} \tag{3.13}$$

3.5.1 Steady-state solution

In the real case, $\overline{V_{\text{D}}}$ is necessarily smaller than $\widehat{v_{\text{in}}}$ due to losses, which allows the crossing of the diodes' threshold voltage during every charge cycle in C_1 and C_2. Since the circuit operates in the steady-state mode, the balance of charge entering and leaving the capacitor C_2 equals zero. The latter remark is also valid for C_1. Equations (3.6) and (3.7) are thus still valid and the output voltage V_{out} stabilizes at

$$V_{\text{out}} = 4N\overline{V_{\text{D}}}. \tag{3.14}$$

The value of $\overline{V_{\text{D}}}$, trivial in the ideal case, is obtained in the real case by solving the following equation

$$\int_0^T i_{\text{D}}[v_{\text{D}}(t)] \, \mathrm{d}t = I_{\text{out}} T \tag{3.15}$$

where $v_D(t) = \overline{V_D} \pm \widehat{v_{in}} \sin \omega t$ is the voltage that appears on every diode of the network at equilibrium and i_D is the current that flows through each diode.

There is no sufficiently accurate continuous model to cope with every operating mode of the diode, i.e. from the reversed bias mode up to the weak and strong inversion conditions. Furthermore, experiments we have conducted have shown that only extracted current-voltage characteristics (simulations or measurements) are able to predict the behavior of rectifiers at low input power levels. The problem has to be addressed using a numerical method based on the DC current-voltage characteristics (I-V) extracted from measurements or simulations of a real world device. Typical

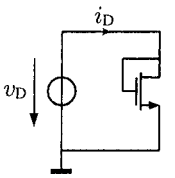

Fig. 3.7. Measurement setup for the I-V curve extraction of the diode-mounted transistor.

measured I-V curves (Fig. 3.7) are shown in figure 3.8 for a diode-mounted low threshold voltage transistor fabricated in the SOS fully depleted UTSi process (Ultra-Thin Silicon) [14]. In the calculations that follow, we use the $10\,\mu\text{m} \times 0.5\,\mu\text{m}$ diode which offers better performance.

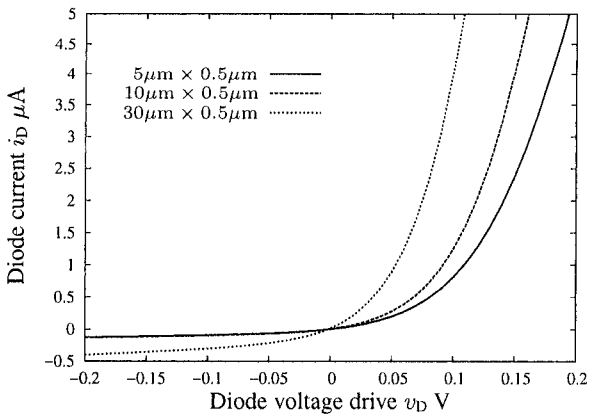

Fig. 3.8. Current-voltage characteristics of typical measured devices.

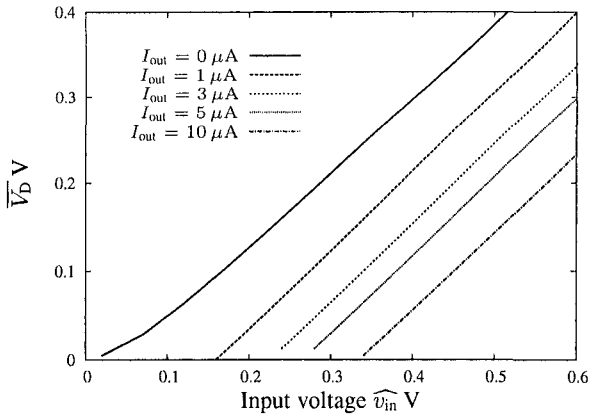

Fig. 3.9. $\overline{V_D}$ for different output currents for the 10 μm × 0.5 μm diode.

The steady-state voltage $\overline{V_D}$ that appears on each diode as a function of $\widehat{v_{in}}$ for typical values of I_{out} is obtained using (3.15) and is plotted in figure 3.9 for a diode realized in the aforementioned process. The output voltage can then be calculated using (3.14).

3.5.2 Determination of C_i

Parasitic capacitances of real devices are of importance at high frequency. A poor IC layout design can lead to significant input capacitance. And without proper impedance matching, the performance can be dramatically altered. There are two sources of capacitance in a diode-mounted transistor: the extrinsic part due to the layout geometry of the device, and the intrinsic part due to the channel formation. Source-bulk and drain-bulk capacitances were negligible in our process but should be taken into account in typical bulk CMOS or partially depleted SOI technology [15]. Although capacitor models exist [16], these are not easily mathematically integrable. Hence, we measured the input capacitance of a single diode as a function of its bias voltage and performed a numerical analysis. The C-V curves for different transistor geometries are shown in figure 3.10.

At high frequency, the equivalent capacitor seen at the input of the rectifier reduces the input voltage amplitude. This has in turn an unfavorable impact on the output voltage. It is also the reason that we cannot cascade too many rectifying stages. Every device appears in parallel at the input where we must sum up their capacitances (see Fig. 3.6). If the input impedance drops too low, the voltage swing on each diode is too small to charge up the capacitors thus leading to an efficiency drop.

Our approach to calculate the equivalent capacitor is to compute the mean capacitance over one period of signal using the steady-state voltage solution and the measured C-V curves $C_D[V_D]$.

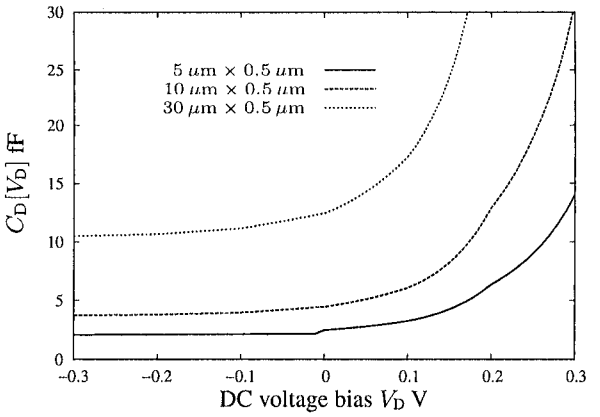

Fig. 3.10. C-V curves for different diode-mounted transistors.

$$C_{\text{i, rectifier}} = \frac{4N}{T} \int_0^T C_D[\overline{V_D} + \widehat{v_{in}} \sin \omega t] \, dt \tag{3.16}$$

The found capacitor $C_{\text{i, rectifier}}$ finally appears in parallel with R_i.

The sum of the RF input pad capacitors and layout capacitors (line to line, etc.) constitutes an unpredictable capacitor C_{added}. It can be estimated using existing CAD parasitics extraction tools. Particular care during layout is necessary to keep all added input capacitors in the RF front end circuit to a minimum.

The total input capacitor is finally

$$C_i = C_{\text{i, rectifier}} + C_{\text{added}}.$$

3.5.3 Determination of R_i

As in the ideal case, we compute the mean power that enters the circuit and we find the *equivalent* input resistance R_i that induces the same amount of power in identical conditions. The DC I-V characteristics of the diodes are used since we are interested in the *absorbed active power.*

The mean power that enters the circuit during one period of signal is calculated as

$$\overline{P_{in}} = \frac{1}{T} \int_0^T v_{in}(t) i_{in}(t) \, dt. \tag{3.17}$$

From node A, B, B' and due to the symmetry of the circuit (Fig. 3.11), we get

$$\overline{P_{in}} = \frac{2}{T} \int_0^T v_{in}(t) i_2(t) - \frac{2}{T} \int_0^T v_{in}(t) i_1(t). \tag{3.18}$$

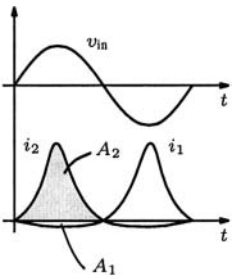

Fig. 3.11. Internal diode current.

Furthermore, the phase shift between signals $i_1[t]$ and $i_2[t]$ is equal to half a period (Fig. 3.11). We can thus simplify equation (3.18) to

$$\overline{P_{in}} = \frac{4}{T}\int_0^T v_{in}(t) i_D(t)\,\mathrm{d}t \tag{3.19}$$

which can be generalized for the N-stage case

$$\overline{P_{in}} = \frac{4N}{T}\int_0^T v_{in}(t) i_D(t)\,\mathrm{d}t. \tag{3.20}$$

We note here that the characteristics of only one diode are sufficient to compute $\overline{P_{in}}$ (if they are all identical).

With the value of $\overline{P_{in}}$, obtained using a numerical method, we can calculate the *equivalent time constant resistance* R_i that satisfies the power equivalence

$$\begin{aligned} \overline{P_{in}} &= \frac{1}{T}\int_0^T \frac{\widehat{v_{in}}\sin^2\omega t}{R_i}\,\mathrm{d}t = \frac{\widehat{v_{in}}^2}{2R_i} \\ \Rightarrow R_i &= \frac{\widehat{v_{in}}^2}{2\overline{P_{in}}}. \end{aligned} \tag{3.21}$$

A typical input resistance curve as a function of the input voltage for a varying output current I_{out} is shown in figure 3.12.

The equivalent input real part R_i increases with $\widehat{v_{in}}$. This behavior can be explained since the output current is maintained at a constant value, and due to equation (3.12), R_i has to rise with an increasing $\widehat{v_{in}}$. R_i decreases dramatically with an increase in the output current. The higher the output current, the smaller the difference between the ideal and the real case (Fig. 3.12).

R_i as a function of I_{out} for different $\widehat{v_{in}}$ is shown in Fig. 3.13. As expected, R_i is very high for low values of output current. For higher values of I_{out}, R_i approaches a short-circuit. However, for a typical application that draws about 10 μA, R_i is about 5 kΩ.

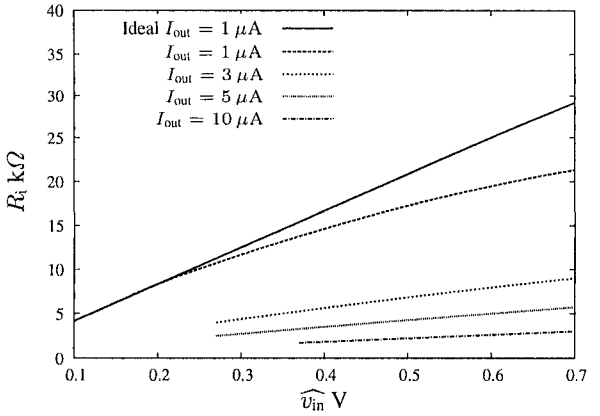

Fig. 3.12. R_i as a function of $\widehat{v_{in}}$ for a 3-stage rectifier.

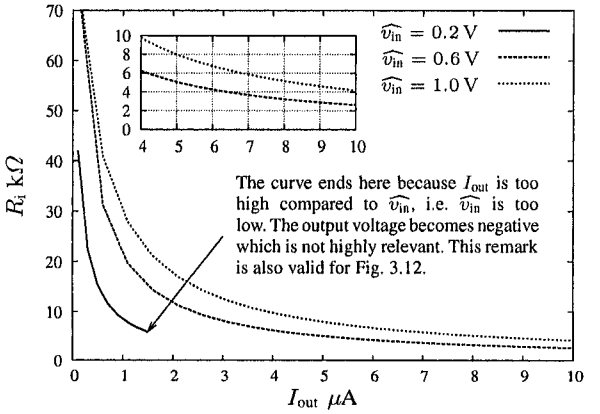

Fig. 3.13. R_i as a function of I_{out} for a 3-stage rectifier.

3.5.4 Determination of R_{out}

From figure 3.4 we can write for the output resistance R_{out}

$$V_{out} = V_0 - I_{out}R_{out} \quad \Rightarrow \quad R_{out} = \frac{V_0 - V_{out}}{I_{out}} \tag{3.22}$$

where $V_0 = 4N\overline{V_D}|_{I_{out}=0}$ is the output voltage with no output current $I_{out} = 0$ (see Fig. 3.9 for this particular case). R_{out} as a function of I_{out} for different values of v_{in} is computed using equations (3.14) and (3.15) for $I_{out} = 0$, and equations (3.14), (3.15) and (3.22) for $I_{out} > 0$, and plotted in figure 3.14.

As can be seen in Fig. 3.14, R_{out} is very big compared to a typical voltage source where the output resistance approaches 0 Ω. R_{out} calculated here corresponds to the *static output resistance* of a voltage source, i.e. it is valid for the average value of I_{out}.

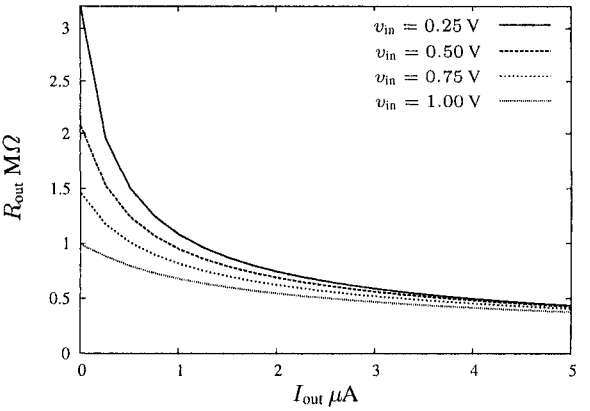

Fig. 3.14. R_{out} as a function of I_{out} for a 3-stage rectifier.

For the spikes of I_{out}, there exists a *dynamic output resistance* whose value diminishes as the output capacitance increases.

3.5.5 Rectifier efficiency

The *conversion efficiency* η_c is defined as [17], [18]

$$\eta_c = \frac{\text{DC Output Power}}{\text{Incident RF Power-Reflected RF Power}} \tag{3.23}$$

whereas the *overall efficiency* η_o is equal to

$$\eta_o = \frac{\text{DC Output Power}}{\text{Incident RF Power}}. \tag{3.24}$$

As we have seen before, the power that enters an N-stage rectifier is given by (3.20). The DC Output Power P_{DC} is simply

$$P_{DC} = V_{out} I_{out} = 4N\overline{V_D} I_{out}. \tag{3.25}$$

Using (3.20) and (3.25) we compute the conversion efficiency for any rectifier. As an illustration, the conversion efficiency for a 3-stage rectifier based on three different diode-mounted transistors (see legends on Fig. 3.15 and Fig. 3.8) is shown in Fig. 3.15.

The overall efficiency for the 10 μm × 0.5 μm diode is also calculated and shown in figure 3.16 for different output currents.

3.6 Results and comparisons

A 3-stage rectifier was designed and fabricated in the aforementioned process (Fig. 3.18). Diode-mounted transistors were also integrated to extract both current-voltage and capacitance-voltage characteristics. The measurements were done in a

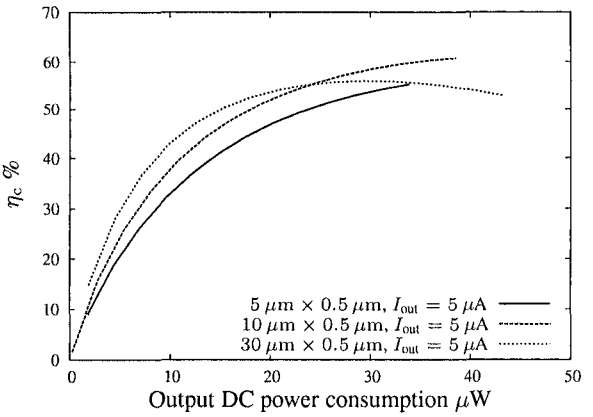

Fig. 3.15. Conversion efficiency for a 3-stage rectifier.

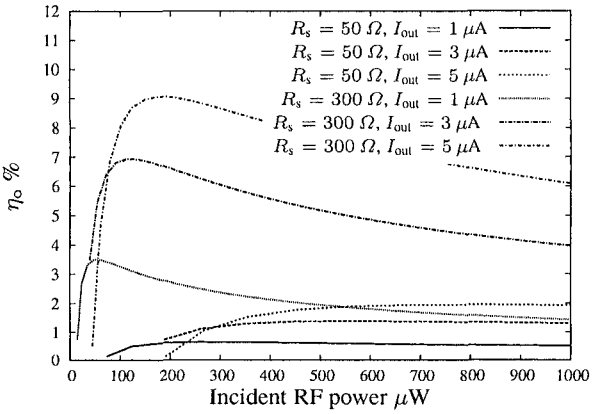

Fig. 3.16. Overall efficiency of the 3-stage rectifier at 915 MHz.

traditional 50 Ω system. Based on these device measurements, R_i, C_i, given the design variables I_{out} and the 50 Ω generator impedance (which corresponds to R_s in the model), we compute the output voltage of the rectifier V_{out} as a function of the generated power P_{AV}. The obtained results are compared with the measurements of the fabricated rectifier and are presented in Fig. 3.17 for different values of output current I_{out}. *Model-based calculations* and *measurements* are in excellent agreement and thus validate both the assumptions and the model. Furthermore, this also validates the efficiency curves of Fig. 3.15 and 3.16, as these can be derived from the values plotted in Fig. 3.17.

As shown before, a high impedance level R_s is desirable in order to optimize the circuit's performance. The case of a $R_s = 300\ \Omega$ antenna is illustrated in Fig. 3.19 using *transistor-based simulations*. In this particular case, the results given by the model using a *simulated I-V curve* are compared to transistor level simulation results. Here also the results are in excellent agreement.

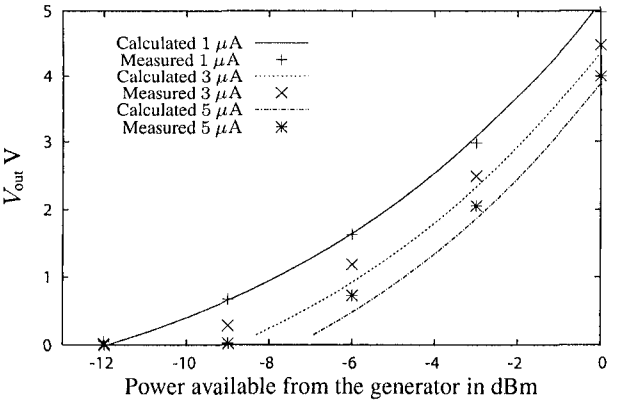

Fig. 3.17. V_{out} measured at 915 MHz for $R_s = 50\ \Omega$.

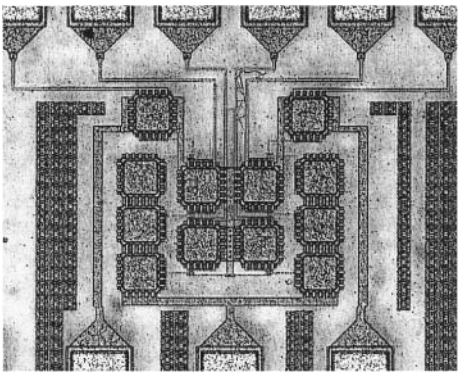

Fig. 3.18. Chip micro-photograph of the 3-stage rectifier

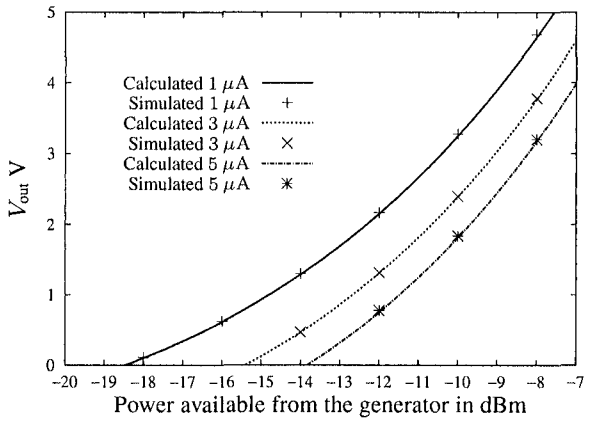

Fig. 3.19. V_{out} simulated at 915 MHz for $R_s = 300\ \Omega$.

3.7 Design

3.7.1 Trade-offs

The design of the rectifying device, i.e. the diode or the diode-mounted transistor in our case, involves a trade-off between three fundamental factors: the reverse current, the direct current (threshold voltage and slope), and the capacitance behavior. To increase the direct current slope to achieve a higher efficiency, one should increase the width of the transistor. Unfortunately, increasing the width increases the reverse current and hence, the losses (see Fig. 3.8 for an illustration). Furthermore, the capacitance is proportional to the transistor size (the extrinsic part at least, see Fig. 3.10), thus limiting the number of stages we can cascade. In that sense, the use of Schottky diodes, if well controlled at the process level, would improve the overall performance. When cascading stages, one should notice that in order to produce an output current I_{out}, every diode of the rectifier has to integrate a charge quantity of $I_{\text{out}}T$ (see equations (3.6) and (3.7)). Since the charge quantity is limited by the received power in the complete system case (rectifier and antenna), the number of stages is also limited. Furthermore, the optimal number of stages may vary with respect to the received power. The only sure way to improve the circuit is to use minimal length transistors. Although increasing the length usually reduces the reverse current, the forward current and the parasitic capacitances degrade more rapidly.

3.7.2 Capacitor design

A good starting point to design the capacitors consists of choosing the maximal admissible voltage ripple ΔV_{max} at the output of one rectifier (see Fig. 3.20). The necessary output capacitance C_{out} that insures a voltage ripple lower than ΔV_{max} is then equal to

$$C_{\text{out}} \geq \frac{I_{\text{out}}T}{\Delta V_{\text{max}}}\left(\frac{1}{k} - \frac{\delta}{2\pi}\right) \tag{3.26}$$

where k is the number of rectifying alternations per rectifier circuit (1 in the present

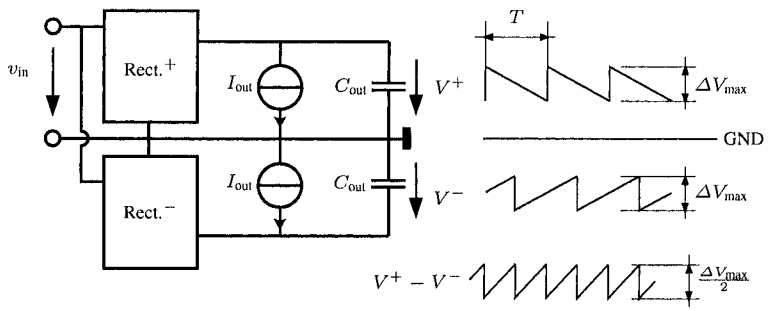

Fig. 3.20. Calculation of the output ripple

case), I_{out} is the output current of the rectifier, T is the period of the RF signal and δ corresponds to the conducting angle [19]. The conducting angle δ can be calculated based on the steady-state solution and its value is given by

$$\delta = \frac{1}{2} - \frac{\arcsin(\widehat{V_{\text{D}}}/\widehat{v_{\text{in}}})}{\pi}. \tag{3.27}$$

It should be mentioned that the ripple of the output voltage $V_{\text{out}} = V^+ - V^-$ is equal to[1] $\frac{\Delta V_{\text{max}}}{2}$. Furthermore, its frequency is doubled.

Concerning the "intermediate capacitors", i.e. all the capacitors except C_{out} (see Fig. 3.3), their values don't significantly affect the output ripple. The only necessity is to keep their corresponding impedance as small as possible compared to the impedance of the diodes in order to not decrease the conversion efficiency. These capacitors act like voltage dividers and thus, it is preferable that they represent a short-circuit at the frequency of interest.

In the case where these "intermediate capacitors" cannot be considered as short-circuits, it can be shown that the overall input capacitance C_{i}' is approximately[2] equal to

$$C_{\text{i}}' = C_{\text{i, rectifier}} \frac{\gamma(1+2\beta)}{2(1+2\beta+\gamma+\gamma\beta)} \tag{3.28}$$

where $\beta = \text{C}_2/\text{C}_\text{d}$, $\gamma = \text{C}_1/\text{C}_\text{d}$ are the normalization factors with respect to the diode's overall capacitance C_d, and $C_{\text{i, rectifier}}$ corresponds to the input capacitance with the "intermediate capacitors" shorted. The second term on the right hand side of (3.28) tends towards 1 as β and γ increases. To satisfy assumption 4 of section 3.3, a value of 30 for both β and γ is sufficient. In the design of Fig. 3.18, the "intermediate capacitors" are equal to 900 fF, rounded up to 1 pF in the design of Fig. 3.18.

3.7.3 Antenna and matching issues

As we have seen before, power matching between the antenna and the rectifier at a high impedance level is essential. In figure 3.21, the impedance level is equal to 2 kΩ, which is optimal for the 3-stage rectifier of this work when delivering an output current $I_{\text{out}} = 1\mu\text{A}$. Both topologies of figure 3.21 are equivalent at one frequency (915 MHz in this case) and result in the same performance (see Fig. 3.22 where the calculated curves using the present model and the transistor level simulated points correspond respectively to topology 1 and topology 2). By introducing the LC matching circuit we introduce a degree of freedom in the design of the antenna. In fact, one can choose a realistic value for the antenna and design the matching circuit in order to achieve a given impedance level. When choosing the impedance level, one should notice that *the higher this level is, the more selective the system becomes.* Furthermore, parasitics also limit the maximal achievable value. In the case where I_{out} is not constant, it is preferable to choose the worst case value, i.e. when I_{out} is maximum. Finally, it is the application that defines the constraints for the antenna and the matching circuit design.

[1] In Fig. 3.20, the electrical signals are simplified to sawtooth signals for the explanation.

[2] The approximation is to consider a diode impedance with a large real part, which is generally the case.

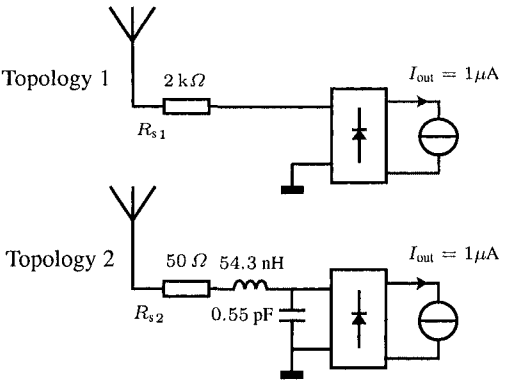

Fig. 3.21. Equivalent topologies at 915 MHz.

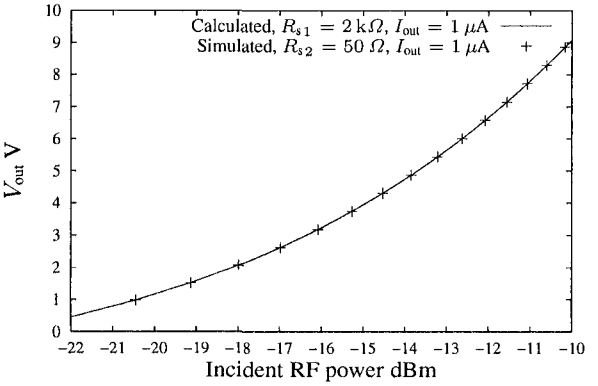

Fig. 3.22. Output voltage of the 3-stage rectifier at 915 MHz

3.8 Conclusion

The study of the modified-Greinacher μ-power rectifier has been made possible by transforming the input pulsed current into a sinusoidal one. The circuit input is thus modeled as a simple resistor R_i. We have also shown that the parasitic capacitors associated with each diode can be modeled with the help of an equivalent input capacitor C_i. Finally, a voltage source controlled by the input signal amplitude $\widehat{v_{in}}$ and an output resistor R_{out} complete the model. The resistor R_i respects the power transmitted to the rectifier and allows the prediction of its conversion and overall efficiency.

A 3-stage rectifier was integrated in an SOS CMOS 0.5 μm process and the measurement results validate the model. A complete study of rectifiers in the framework of μ-power applications is made possible using the presented model.

4

Introduction to RFID

This chapter describes shortly the different types of RFID technologies available today. The issue of standardization is discussed for UHF and microwave frequencies. A section reports the power and frequency regulations around the world. The physical principles at UHF and microwave frequencies are presented for the passive case only. An overview of the environmental impacts is given and the data integrity issue is discussed.

4.1 Introduction

RADIOFrequency IDentification (RFID) is an automatic identification method, relying on storing and remotely retrieving data using devices called RFID tags or transponders. An RFID tag is a small object that can be attached to or incorporated into a product, animal, or person. RFID tags contain antennas to enable them to receive and respond to radio-frequency queries from an RFID reader or interrogator. Passive tags require no internal power source, whereas active tags require a power source.

It has been suggested that one of the first known devices was the IFF (Identification Friend or Foe) transponder. It was invented by the British in 1939, and was routinely used by the allies in World War II to identify airplanes as friends or foes.

Another early work exploring RFID is the landmark 1948 paper by Harry Stockman, entitled "Communication by Means of Reflected Power." Stockman predicted that "...considerable research and development work has to be done before the remaining basic problems in reflected-power communication are solved, and before the field of useful applications is explored." It required thirty years of advances in many different fields before RFID became a reality.

RFID has become very popular in many areas such as purchasing and distribution logistics, automation, manufacturing companies and even the wine industry where it is used as an anti-fraud system [20]. Moreover, wireless sensing applications could

also benefit from this technology, in which an ultra low-power IC design, a wide system operating range and a small transponder size are among the most important design parameters.

Passive transponders operating at low frequencies (typically 135 kHz or 13.56 MHz) are limited in distance for physical reasons [2]. The magnetic field strength at these frequencies is indeed inversely proportional to the third power of the distance between the radiating antenna and the tag. At UHF, wireless power transmission [6] is more suitable for long range operations since the field strength decreases "only" with the first power of the distance. Furthermore, the backscattering principle [2] offers a reliable communication link (see chapter 5).

4.2 Transponder types

RFID transponders are either active or passive. Passive RFID transponders do not have their own power supply; the tiny electrical current induced in the antenna by the incoming RF signal provides enough power for the transponder to send a response. Due to power and cost concerns, the response of a passive RFID transponder is necessarily brief: typically just an ID number.

Active RFID transponders, on the other hand, must have a power source, and may have longer ranges and larger memories than passive transponders, as well as the ability to store additional information sent by the transceiver. At present, the smallest active transponders are about the size of a coin. Many active transponders have practical ranges of tens of meters, and a battery life of up to several years. In this work, only passive transponders are considered.

As passive transponders are much cheaper to manufacture and do not depend on a battery, they constitute the vast majority of RFID transponders available today. According to [21], a transponder's average cost is US$0.50 as of 2004. The aim is to produce transponders for less than US$0.05 to make widespread RFID tagging commercially viable. However, chip manufacturers' supply of integrated circuits is not sufficient and demand is too low for prices to come down soon. Analysts from independent business research companies agree that a price level of less than US$0.10 is only achievable in 6-8 years (2004 case).

There are countless variants of transponders in terms of forms, system operations (Full Duplex or Sequential), memory, etc. However, the frequency chosen to operate the system is probably what affects the most both the overall performance and the design.

4.3 Low frequency systems

Low frequency systems offer (at the time of writing) an operating range between 0 and 1 m. The main reason for this is due to the nature of the physical principle used both for the power supply and the data communication, i.e. *near-field coupling*. There are two types of coupling, *capacitive* and *inductive* coupling. Capacitive coupling enables

the transfer of energy from one circuit to another by means of the mutual capacitance between the circuits whereas in inductive coupling, the transfer of energy from one circuit to another is obtained by virtue of the mutual inductance between the circuits.

With capacitive coupling, the antenna's resistance is no longer a critical factor, so antennas can be constructed from materials of considerably higher resistance than the metals used in inductive technology. In particular, this means that conductive inks, which have a moderate resistance, can be used to form the antenna [22]. Capacitive coupled systems operates at ranges between 0 and 1 cm. The frequency can be chosen between DC and 30 MHz because no power is radiated. Such a system also offers greater amounts of available power, which allows the use of a microprocessor. They are primarily used in high security applications with a very low operating range like electronic door locking systems or contact-less smart cards with payment functions [2].

Fig. 4.1. Inductive transponder examples. (Reproduced by permission of SOKYMAT)

Systems that operate up to 1 m are inductively coupled (see Fig. 4.1). At least 90% of all RFID systems purchased are of this type. Inductively coupled transponders are almost always operated passively. This means that all the energy needed for the operation of the micro-chip is provided by the reader. For this purpose, the reader's antenna coil generates a strong, high frequency electromagnetic field, which

penetrates the cross-section of the coil area and the area around the coil. Because the wavelength of the frequency range used (<135 kHz: 2400 m, 13.56 MHz: 22.1 m and 27.125 MHz: 11.05 m) is several times greater than the distance between the reader's antenna and the transponder, the electromagnetic field may be treated as a simple magnetic alternating field with regard to the distance between transponder and antenna. As for the capacitive case, we deal here with *near-field coupling*. In this region, the magnetic field strength attenuates according to the relationship $\frac{1}{d^3}$, where d is the distance between the reader and the transponder. It corresponds to a power damping characteristic of $60 \log d$ or 60 dB per decade (of the distance), i.e. the magnetic field intensity decays rapidly as the inverse cube of the distance between the reader antenna and the transponder. This rapid attenuation of the energizing and data communication field with increasing distance is the fundamental reason why low frequency passive RFID systems have a maximum reading distance of about 1 m.

To communicate with the reader, the transponder modulates its input impedance, which translates to a current variation in the reader coil; this process is called *load modulation*. Since this work only deals with high frequency systems, low frequency systems will not be discussed further.

4.4 High frequency systems

To achieve a higher operating range, it is necessary to raise the system frequency in order to take advantage of the *far-field* propagation characteristics. The electromagnetic field strength attenuates according to the relationship d^{-1} and corresponds to a power damping factor of $20 \log d$. The transition between the *near-field* and the *far-field* occurs at about $\frac{\lambda}{2\pi}$ meters from the reader antenna, where λ is the wavelength of the RF carrier. Considering this relation and the power decay as a function of the distance, possible working frequencies start at a few hundreds of MHz, e.g. the ISM bands at 433 MHz, 900 MHz, 2.45 GHz, 5.8 GHz and 24.125 GHz. A similar communication principle to that described in section 4.8 called *radar cross section modulation* or *backscattering modulation* is used at high frequencies. The technology used is similar, although, as we'll see in chapter 7, the IC design can severely affect the performance at microwave frequencies if not carefully carried out.

4.5 Standards

As in many technological sectors, many standards exist. For UHF RFID, no standard is universally accepted. There are solutions at many levels, e.g. international, national, industry or trade association. The goal is to make it easier to implement an RFID solution and to support it. Transponder format, communication protocols, frequency of operation and the code or ID can be part of the standard.

The largest driver today is the supply chain management where real time inventory is desired. The available standards at the time of writing are the EPC Global initiative [23] and the ISO 18000 standard [24]. The ISO only deals with the air interface whereas EPC also includes the data structure of the ID.

4.5.1 The EPC standard

The auto-ID center has proposed a new Electronic Product Code (EPC) to identify products just like the bar-code does. It is principally intended for supply chain management. Its structure is based on the Global Trade Item Number (GTIN), a group under which all existing bar-codes fall. There are 5 class types that offer different features (see table 4.1).

Table 4.1. EPC transponder classes

EPC class	Feature	Transponder type
Class 0	Read only	Passive (64 bits only)
Class 1	Write Once, Read Many (WORM)	Passive (96 bits min.)
Class 2	Read/Write	Passive (96 bits min.)
Class 3	Read/Write with embedded energy to enhance the operating range	Passive (96 bits min.)
Class 4	Read/Write active transmitter	Passive (96 bits min.)

These classes are not interoperable (although the UHF class 2 should merge with the class 0 and class 1 standards) and thus, the RFID reader has to be multi-standard.

An example of an EPC code structure is the 96-bit general identifier (GID-96) [23]. The General Identifier is composed of three fields - the General Manager Number, Object Class and Serial Number. Encodings of the GID include a fourth field, the header, to guarantee uniqueness in the EPC namespace, as shown in table 4.2.

Table 4.2. EPC data structure for the GID-96

	Header	General Manager Number	Object Class	Serial Number
bits	8	28	24	36
Example	00110111	282,636,865	12,564,328	32,684,786,459

4.5.2 The ISO standard

The ISO is based in Geneva, and its standards carry the weight of law in some countries. It is active in the development of RFID standards for supply chain management. Among these we find the ISO14443 for "proximity" cards and the ISO15693 for "vicinity" cards. They both recommend to use an RF carrier of 13.56MHz.

Closer to the UHF and higher frequencies, the ISO18000 part 4 to part 7 standards are a set of RFID specifications for item management. They define the forward and

return link parameters for technical attributes including, but not limited to, operating frequency, operating channel accuracy, occupied channel bandwidth, maximum EIRP, spurious emissions, modulation type, duty cycle, data coding, bit rate, bit rate accuracy, bit transmission order, and where appropriate operating channels, frequency hop rate, hop sequence, spreading sequence, and chip rate. They further define the communications protocol used in the air interface.

As of today, no particular standard dominates at the UHF and microwave level. It is probably the application (e.g. supply chain management, airport luggage, international freight, etc.) that will impose the standard in the near future.

4.6 Regulations

There are many ISM bands that can serve the RFID world. However, only a few of them are in use today. In the low frequency arena the two widely used bands are situated from 9 kHz to 135 kHz, and at 13.56 MHz. At higher frequencies, the emerging ISM bands are situated at 433 MHz, around 900 MHz (UHF) and at 2.45 GHz (microwave). The 433 MHz band is a viable candidate for high frequency RFID applications but the corresponding wavelength could be too long in terms of antenna size. In supply chain management, the UHF band seems to have become the standard although the microwave band offers a higher bandwidth and a form factor advantage (lower wavelength). Furthermore, at equal overall antenna dimensions, the microwave band leads to a higher directivity which can be an advantage in warehouse management applications. It should be mentioned that the 2.45 GHz microwave frequency is heavily attenuated by the presence of water. From now on, only the UHF and microwave cases are discussed.

4.6.1 Power regulations

In terms of power, the situation heavily depends on the country. In the US, 4 W EIRP as emitted power is allowed at both UHF and microwave bands by the FCC. In Europe, the situation is slightly different. In the 869.4 - 869.65 MHz band the available power is 0.5 W ERP. A future CEPT/ETSI regulations proposal could raise this value to 2 W ERP. In the microwave band, 0.5 W EIRP is allowed and for indoor applications 4 W EIRP can be radiated. In many other countries regulations are either similar to FCC or CEPT/ETSI. Table 4.4 summarizes the current situation in terms of countries, frequency bands and maximal power emission for the UHF and microwave cases [25]. A more detailed presentation of both the low and high frequency ranges is available in [2].

4.7 Radar Cross Section (RCS)

The RCS of an object is an expression of the extent to which it reflects radar pulses, usually with respect to their point of origin. It depends on factors such as the form of

Table 4.3. Regulations summary at UHF and microwave frequencies

Region	Frequency range	Available power
Europe[a]	869.4 - 869.65 MHz	0.5 W ERP
Europe[a]	2.400 GHz - 2.4835 GHz	0.5 W EIRP in. and outdoor
Europe[a]	2.400 GHz - 2.4835 GHz	4 W EIRP indoor
Europe[b]	865.5 - 867.6 MHz	2 W ERP
America[c]	902 - 928 MHz	4 W EIRP
America[c]	2.400 GHz - 2.4835 GHz	4 W EIRP
Others[d]	860 - 930 MHz	-
Other[d]	2.400 GHz - 2.4835 GHz	-

[a]Current CEPT/ETSI regulations: CEPT REC 70-03 Annex 1, ETSI EN 330 220-1
[b]Proposal for future CEPT/ETSI regulations
[c]FCC regulations, Part 15 Section 247
[d]In many other countries regulations either similar to FCC or CEPT/ETSI may apply

the object, the material, the wavelength of the signal and its polarization. The RCS is a function of the reflection coefficient at the interface between the antenna and the transponder. In that sense, the RCS can take any value between a minimum when the antenna is power matched to its load and a maximum when the antenna is either shorted or opened. It can be shown [2], [26] that these two limits are equal to

$$\sigma_{\max} = \frac{\lambda^2 G_t}{4\pi}\Big|_{R_{ant,t}\to 0}^{R_{ant,t}\to\infty} \tag{4.1}$$

$$\sigma_{\min} = 0 | R_{ant,t} \to R_s \tag{4.2}$$

where $R_{ant,t}$ is the resistance (radiation and losses) of the transponder antenna and R_s the antenna overall resistance.

4.8 Backscattering modulation technique

The backscattering technique or modulated Radar Cross Section (RCS or σ) allows the establishment of a communication between a reader and a transponder. This principle is based on the reflection of electromagnetic waves. It takes advantage of the reflection coefficient variation at the interface between the tag antenna and the tag input circuit. The latter coefficient is a complex value and can thus be changed both in amplitude and phase. This limits the possible RF modulation types to AM and PM or ASK and PSK when dealing with binary data. To describe it we consider a transponder composed of an antenna connected to a load impedance (Fig. 4.2). If the antenna impedance is matched to the load, no reflection occurs at the interface (4.2(a)). On

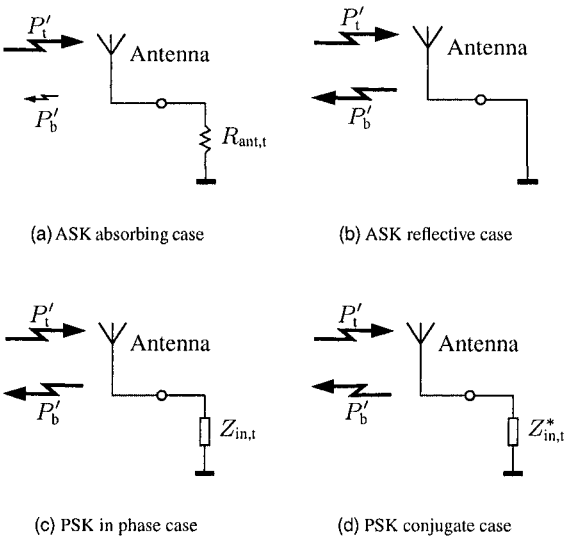

Fig. 4.2. Possible backscattering techniques

the contrary, if the load is shorted (or opened) (4.2(b)), total reflection occurs and the power P'_b is re-radiated by the antenna. Thus by switching between these two states, the received power P'_t is modulated in an ASK fashion. In terms of the antenna, it is its RCS or effective aperture that is modulated. The latter modulation is based on the module of the reflection coefficient. By varying the reflection coefficient phase, we obtain the PSK modulation scheme. In this case it is the imaginary part that is changed (4.2(c) and 4.2(d)). The modulation quality thus depends heavily on the impedance control at the process level. These cases are discussed in detail with both theoretical and practical issues in chapter 7.

4.9 Link budget

To calculate the power available to the reader P_r, we start from the end, i.e. from the power P_r back to the emitted power P_{EIRP} (see Fig. 4.3). Furthermore, polarization losses are not taken into account and a Line-Of-Site (LOS) communication is admitted.

Because of the reader antenna gain G_r, P_r is equal to $G_r P'_r$. Considering the transponder antenna gain G_t and the tag-reader path losses, P_r becomes

$$P_r = G_r P'_r = G_r P'_b \left(\frac{\lambda}{4\pi d}\right)^2 \tag{4.3}$$

$$= G_r G_t P_b \left(\frac{\lambda}{4\pi d}\right)^2 . \tag{4.4}$$

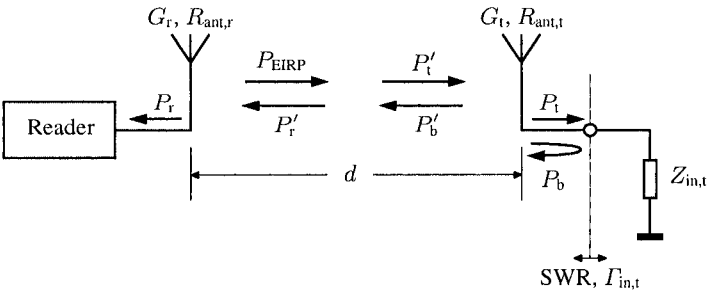

Fig. 4.3. Link budget calculation

The matching quality at the interface between the tag antenna and the tag input impedance can be expressed using the SWR at this point. We obtain

$$P_b = P_t \left(\frac{\text{SWR} - 1}{\text{SWR} + 1} \right)^2 . \tag{4.5}$$

Equation (4.5) can also be expressed using the reflection coefficient at the interface $\Gamma_{in,t}$

$$P_b = P_t \, |\Gamma_{in,t}|^2 . \tag{4.6}$$

The effective isotropic radiated power P_{EIRP} is attenuated by the reader-tag path loss and thus, the following relation holds

$$G_t P_t = P_{EIRP} \left(\frac{\lambda}{4\pi d} \right)^2 \tag{4.7}$$

Finally, substituting the values of equations (4.5), (4.6) and (4.7) into (4.3), we obtain the link power budget equation between the reader and the transponder

$$P_r = G_r G_t^2 \left(\frac{\lambda}{4\pi d} \right)^4 \left(\frac{\text{SWR} - 1}{\text{SWR} + 1} \right)^2 P_{EIRP} . \tag{4.8}$$

In term of the reflection coefficient, equation (4.8) becomes

$$P_r = G_r G_t^2 \left(\frac{\lambda}{4\pi d} \right)^4 |\Gamma_{in,t}|^2 \, P_{EIRP} . \tag{4.9}$$

The read distance d of a backscattering RFID system is thus proportional to the fourth root of the reader transmission power P_{EIRP}. Doubling the distance implies a multiplication by 16 of the transmission power. The read range is calculated more precisely, considering the antenna and the tag input impedances in the transponder design, in chapter 7.

4.10 Environmental impacts

The environmental issues are difficult to cope with. At UHF and especially at microwave frequencies, the signal is quasi-optical. For that reason multi-path phenomena occur and both constructive and destructive interference can take place. These effects can be reduced (or controlled) by using high directivity antennas, which are for equal dimensions better for high frequencies, e.g. microwave and beyond. Based on the operating frequency used and the material in which the signal propagates (air, cardboard, plastic, etc.), the attenuation factor may vary. The surroundings of the tag antenna heavily affect its choice and design. Wet cardboard can considerably reduce the efficiency of both the communication and the power transmission. The choice of an RFID antenna consists mainly of its type, its input impedance, its polarization, its RF performance when applied to the object and its performance degradation due to its surroundings. A non-exhaustive list of possible antennas to be used for transponders is shown in table 4.5.

Antenna	Radiation pattern	Bandwidth % of f_0	Impedance Ω
$\lambda/2$-Dipole	Omnidirectional	10-15	73
λ-Dipole	Omnidirectional	10-15	200
Folded dipole	Omnidirectional	15-20	300
Patch	Directional	2-3	30-100

Table 4.5: Possible antennas for use in RFID systems [27]

There is no perfect antenna for all environments. It is the application that defines the antenna specifications. There is a high probability that many types of transponders will share the same IC but will connect to different antenna types. The antenna issues are discussed in more detail in chapter 7.

4.11 Data integrity

In RFID applications, there is generally one reader and many tags. The task of the reader is to orchestrate the communication. As can be imagined, if two or more tags "talk" at the same time, collision occurs and the transaction has to be started again. This issue is typically solved using Time Domain Multiple Access (TDMA) techniques in which the entire available channel capacity (between the tags and the interrogator) is divided between the participants chronologically [2]. There are two possible procedures: *transponder-driven* or *interrogator-driven*.

4.11.1 Transponder-driven procedure

In the transponder-driven procedure, the tag controls the time of the data transfer. It thus functions asynchronously. For example, this is the case in the ALOHA procedure which was developed in the 1970s for ALOHANET, a radio network for data

transmission in Hawaii. As soon as a data packet is available it is sent from the tag to the reader. This procedure is used exclusively with read-only transponders, which generally transmit only a small amount of data. The transponder sends its data cyclically. The data transmission time is only a fraction of the repetition time. The pauses between transmission are thus relatively long. Moreover, the repetition times for the individual tags differ slightly. There is therefore a certain probability that two or more transponders can transmit their data packets at different times without collision. The necessary time, for which a given number of transponders containing a certain amount of information is read, can be calculated with a given reliability (e.g. a probability of 99.9%). The typical time to read 5 tags with a 99.9% reliability is 1250 ms [28]. Transponder-driven procedures are naturally very slow and inflexible. Most applications use the reader as the master (interrogator-driven).

4.11.2 Interrogator-driven procedure

In interrogator-driven procedures we differentiate between *polling* (or addressing) and *binary search*. These procedures can be considered synchronously since every step in the communication transaction is reader-controlled. A tag is first selected from a group of tags in the interrogating zone using a certain algorithm. Then the communication takes place between the selected tag and the reader.

Addressing procedure

The addressing procedure requires a list of all serial numbers that can occur in a given application. As a result, every serial number has to be polled in a certain interrogating zone. This can be quite time consuming and inefficient as the number of tags increases. It is meant for applications where only a "small" number of tags exist in a finite set. Here, "small" depends on the data-rate D at which the communication takes place. If one needs T_R seconds to read one serial number among N, the maximal duration T_{max} of a successful communication session is equal to

$$T_{max} = T_R \cdot N. \tag{4.10}$$

Considering the amount of information in bits I contained in a tag, T_R is given by

$$T_R = \frac{I}{D}$$

so that Eq. 4.10 becomes

$$T_{max} = \frac{I}{D} \cdot N. \tag{4.11}$$

From Eq. 4.11 it is clear that the worst-case read time decreases proportionally as the data-rate increases. This procedure is thus only suitable for applications with few *known* transponders in the field. To reduce the implementation complexity of this work, the addressing procedure has been chosen (see section 7.4).

Binary search procedure

Binary search procedures are by far the most flexible. In this case, a tag is selected from a group by intentionally causing a data collision in the serial number transmitted to the reader. To succeed, the reader should be able to determine exactly the bit position at which a collision occurred. This places a stringent design constraint on the tag side where the bit rate has to be well controlled. Ideally, every transponder should have the same bit rate which can be obtained at the circuit level by using a switched capacitor bank. A comprehensive description of this procedure is available in [2].

4.12 Conclusion

This chapter presented an overview of the RFID world. This technology is already implemented at different levels, e.g. logistics, automation, etc. At present, we find mostly LF and HF systems but UHF devices will surely be used in the near future where long operating ranges and high data-rates are a necessity. The ISO and EPC standards will probably pave the way to harmonization.

Secondly, the phenomenon and communication techniques used in UHF RFID systems have been described. The environmental impacts on communication will bring a myriad of antenna designs. Different techniques to immunize the antenna against surrounding influences have been proposed[1]. Finally, an interrogator-driven addressing procedure has been chosen for the transponder design detailed in chapter 7. Before presenting the design of the tag, a thorough analysis and comparison of possible modulation techniques are discussed in the next chapter.

[1] See for example US2005197074.

5

Backscattering architecture and choice of modulation type

The input impedance of an RF transponder is mainly influenced by the rectifier. As seen in chapter 3, it is possible to compute the impedance coming from the rectifier. To enable the communication from the tag to the reader there are two backscattering modulation choices: Amplitude Shift Keying (ASK) and Phase Shift Keying (PSK). A thorough comparison of these two modulation types in the light of the backscattering issue is presented in this chapter.

5.1 Modulation types

THE backscattering modulation technique is based on the variation of the reflection coefficient Γ at the input of a transponder (see Fig. 5.1). Γ can vary either in amplitude or in phase. As a result, two modulation types are possible: ASK and PSK.

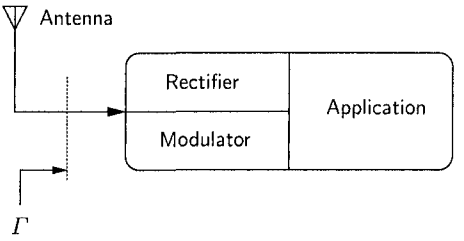

Fig. 5.1. Passive transponder system architecture.

To implement ASK, the reflected power is switched between two or more values at a given rate. In the case of passive tags and considering the amount of data to transmit, a Binary Amplitude Shift Keying (BASK) is sufficient.

PSK backscattering modulation relies on the relative phase variation between the incoming and the reflected waves at the antenna. The transponder switches its input impedance between two values, ensuring the widest modulation angle between the power waves being reflected in the two modulation states (Binary Phase Shift Keying or BPSK is considered here).

5.2 Modulator architectures

The electrical equivalent of Fig. 5.1 is shown in Fig. 5.2. At resonance, the antenna is equivalent to a radiation resistance R_s (see chapter 2) and a voltage source v_s in series. The amplitude $\widehat{v_s}$ is given by

$$\widehat{v_s} = 2\sqrt{2P_{AV}R_s}, \tag{5.1}$$

where P_{AV} is the available power from the antenna. P_{AV} can be determined using the Friis equation (see section 2.4.4). As seen in chapter 3, the rectifier is modeled by a

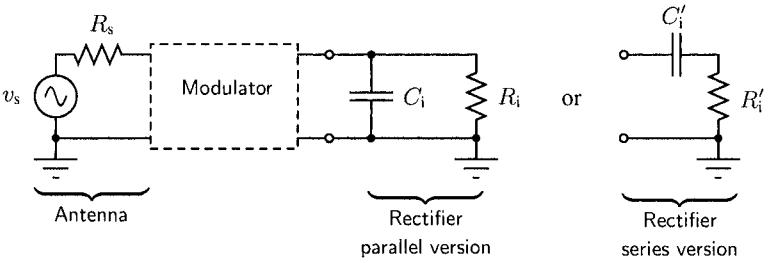

Fig. 5.2. Schematic of a remotely powered device.

capacitance C_i in parallel with a resistance R_i. At a given frequency, a series equivalent circuit is also possible and is represented in Fig. 5.2. Both rectifier equivalent circuits can be used and the choice depends on the analysis type.

5.3 ASK modulator

ASK modulators can be realized using one of the four configurations of Fig. 5.3. There are thus four possible integrated circuit architectures (the inductance L is considered off-chip) that are to be analyzed.

In the ideal backscattering ASK modulator, the reflected power switches between complete absorption and complete reflection. In this case, a perfect On-Off Keying (OOK) modulator is obtained. Complete reflection is ensured by setting the input impedance either to a short-circuit or to an open-circuit state. In practice, a short-circuit is easier to implement and more reliable at high frequencies. Complete absorption is

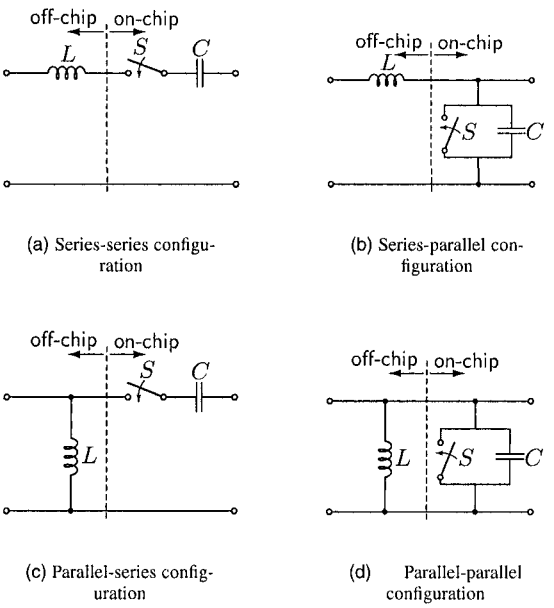

(a) Series-series configuration

(b) Series-parallel configuration

(c) Parallel-series configuration

(d) Parallel-parallel configuration

Fig. 5.3. Possible backscattering ASK modulator schematics.

less trivial because in this case, the purpose of the modulator is to match R_s to the load while the switch is open. The simplest networks that allow power matching between a real source and a complex load are shown in Fig. 5.4. At first sight, the topology of Fig. 5.4(b) and 5.4(d) are incompatible with an off-chip inductor.

Secondly, series-series (Fig. 5.3(a)) and parallel-parallel (Fig. 5.3(d)) modulator configurations are topologically incompatible with the networks of Fig. 5.4. They are thus unable to match R_s to R_i (or R_i'). Consequently, there are only two possible configurations, which are Fig. 5.3(b) and Fig. 5.3(c).

Before going further in the analysis, certain practical constraints cannot be neglected. In the first place, the diodes used to realize the rectifier have a low threshold voltage V_t, but always greater than zero. This translates to an input resistance that cannot be lowered to zero. It can approach zero for high input amplitudes but not for low power devices. In this work, this resistance is on the order of 1 kΩ (see chapter 3). As a result, the available power from the antenna cannot be *completely absorbed* unless a lossy matching network is used. In practice, this can be a tedious task at high frequency. Secondly, a real integrated modulator switch S is far from perfect. It introduces parasitics that lead to a certain extent to performance degradation depending on the architecture (typically when set up in series with the rectifier).

R_s is thus smaller than R_i (or R_i' if C_i' is small enough) and to ensure a positive loaded quality factor of the complete circuit and realistic element values in practice, only Fig. 5.3(b) is relevant to the present analysis. Moreover, the capacitance C that

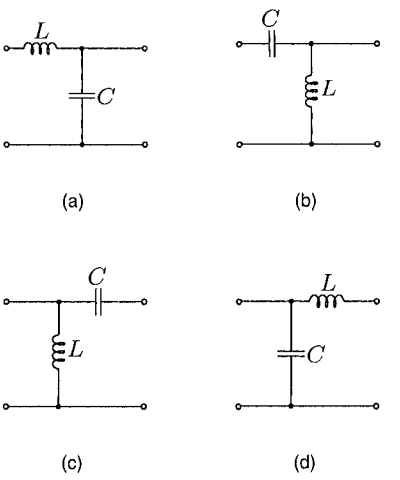

Fig. 5.4. Possible matching networks for the ASK modulation.

appears in parallel with the switch, which is a rather small value (few tenths of femto-Farad), is inherently present when the switch is open.

The topology of Fig. 5.3(b) is thus the most appropriate to implement ASK. In this case, the tag input voltage can be maximized and the communication Bit-Error Rate (BER) can be minimized (see section 5.6.1 and 5.6.3). The other configurations can be implemented but lead to poorer performance.

5.4 PSK modulator

For PSK, information is carried in the phase difference between the two modulation states (see section 5.1). Ideally, the impedances presented to the antenna have to be complex conjugates so that the modulation angle can be maximized. To achieve complex conjugate impedances, an inductive part is necessary. In IC technology it is well known that such a device is a big die-area consumer and should be avoided where possible. Fortunately, at high frequencies, the necessary series or parallel inductive part can be achieved by antenna design. Every antenna carries either an inductive or capacitive part depending on the operating frequency; except at resonance where it is completely resistive. The integrated modulator circuit task is thus to vary the capacitance that the inductive antenna sees. It is shown in section 5.7 what value these parameters should have.

Practically, the four architectures shown in Fig. 5.5 are possible. To ensure a constant available power to the tag, the impedances Z_1 and Z_0 seen by the radiation resistance of the antenna during the two modulation states must have a constant modulus, i.e.

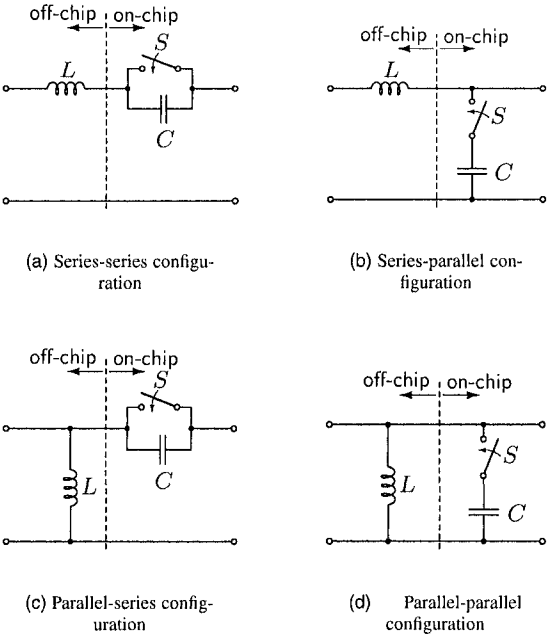

(a) Series-series configuration

(b) Series-parallel configuration

(c) Parallel-series configuration

(d) Parallel-parallel configuration

Fig. 5.5. Possible backscattering PSK modulator schematics with an off-chip inductor.

$$|Z_1(L_{\text{ant}}, C_{\text{in},1}, R_{\text{i}}|_1)| = |Z_0(L_{\text{ant}}, C_{\text{in},0}, R_{\text{i}}|_0)|. \tag{5.2}$$

The series-parallel and the parallel-series of Fig. 5.5(b) and Fig. 5.5(c) do not fulfill this requirement as depicted in the impedance chart of Fig. 5.6. X_L, $R_{\text{i}}|_1$, $R_{\text{i}}|_0$, $X_{C,1}$ and $X_{C,0}$ are, respectively, the impedances of the antenna inductance, the resistive parts and the capacitive parts in the two modulation states. As can be seen, even if capacitance values can be found to ensure constant argument impedances, the real parts are not constant. This results in a variation of the reflection coefficient modulus and thus, amplitude modulation occurs. This is also valid for the dual parallel-series configuration of Fig. 5.5(c). The two other schematics, i.e. Fig. 5.5(a) and Fig. 5.5(d), fulfill Eq. (5.2) and are potential candidates for the implementation. To restrict the analysis length and remain general, only the series-series PSK architecture is analyzed in section 5.7.

5.5 Analysis strategy

In remotely powered applications that take advantage of the backscattering communication technique, there are three aspects that should be taken into account. The *voltage amplitude* at the rectifier input is one of them. It is of importance because the diodes

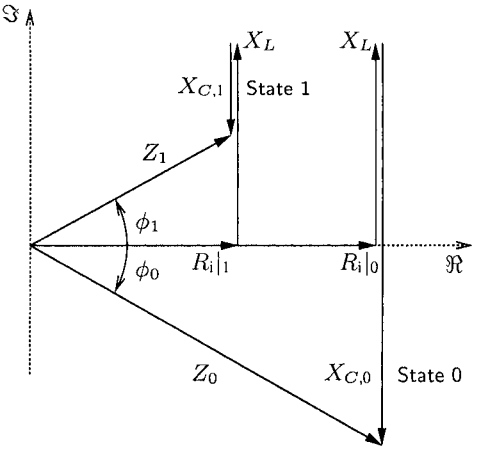

Fig. 5.6. Impedance chart of the series-parallel PSK modulation.

that compose the rectifier are sensitive to the voltage at their ports. Without a sufficient level, no RF power can be absorbed. The *power* is thus another important issue since part of it is available to the circuit itself whereas the rest enables tag-to-reader communication.

Last but not least, the *communication quality* measured in terms of Bit Error Rate (BER) is to be analyzed. To simplify and make the study consistent with the voltage and power analysis, the reflection coefficient approach is preserved. But, as will be shown in chapter 6, backscattering modulation is so closely related to the antenna properties that it cannot be quantitatively analyzed without taking the antenna into account. But since the underlying electromagnetic phenomenon is linear [29], [30], the reflection coefficient approach is still valid for comparison purposes. As will be seen, the choice of modulation type is a trade-off between these three parameters.

5.6 ASK series-parallel case

The circuit of Fig. 5.7 implements series-parallel backscattering ASK modulation. The capacitance C in parallel with the switch is neglected in the following since it only slightly affects the matching issue when considering the component values. If the switch is closed, the impedance seen at point B toward the right is a shorted inductor. Consequently, the reflection coefficient modulus is equal to 1 and total power reflection occurs. Conversely, when the switch is open, the available power from the antenna is ideally completely absorbed by the load R_i' if power matching occurs.

5.6.1 Voltage considerations

With reactive matching, i.e. $\omega^2 L C_i' = 1$, the input voltage amplitude $\widehat{v_{in}}$ at point A in the absorbing case ("0") is equal to

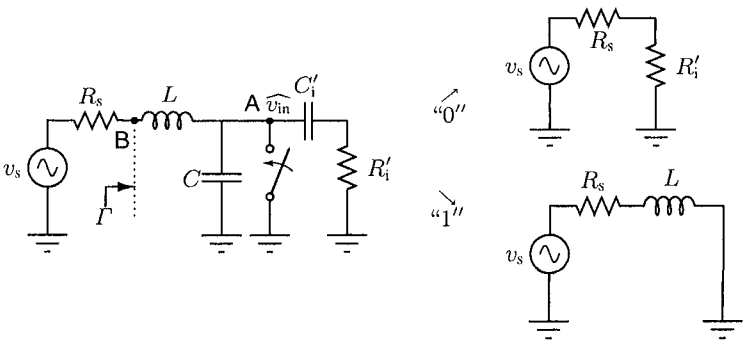

Fig. 5.7. Schematic for the series-parallel ASK modulation analysis.

$$\widehat{v_{in}} = \widehat{v_s}\alpha\sqrt{\frac{1+Q_{in}^2}{Q_{in}^2(\alpha-1)^2+(\alpha+1)^2}} \tag{5.3}$$

where $\widehat{v_s}$ is the antenna voltage source amplitude, $\alpha = \frac{R'_i}{R_s}$ is defined as the mismatch figure between R'_i and R_s and $Q_{in} = \frac{1}{\omega R'_i C'_i}$ is the input series quality factor. *The input voltage in the reflective state ("1") is simply 0 due to the short-circuit.*

Power matching occurs when $\alpha = 1$. In this case, Eq. (5.3) becomes

$$\widehat{v_{in}} = \widehat{v_{in}}_{max} = \frac{\widehat{v_s}}{2}\sqrt{1+Q_{in}^2}$$

which simplifies for large values of Q_{in} to

$$\widehat{v_{in}}_{max} \approx \frac{\widehat{v_s}}{2}Q_{in}. \tag{5.4}$$

The input voltage amplitude is thus proportional to Q_{in} and only the quality factors of the elements that compose the tag limit the value of $\widehat{v_{in}}$. As can be seen from Eq. (5.4), Q_{in} can boost the input voltage amplitude significantly.

$\widehat{v_{in}}$ normalized to its maximal value $\frac{\widehat{v_s}}{2}\sqrt{1+Q_{in}^2}$ versus α is equal to

$$\widehat{v_{in}}_{norm.} = \frac{\widehat{v_{in}}}{\widehat{v_{in}}_{max}} = 2\alpha\frac{1}{\sqrt{Q_{in}^2(\alpha-1)^2+(\alpha+1)^2}}. \tag{5.5}$$

It is plotted in Fig. 5.8. As can be seen in Fig. 5.8, the greater the quality factor Q_{in}, the more sensitive to α the input voltage is. In practice, Q_{in} is on the order of 1 to 10.

5.6.2 Power considerations

With the backscattering modulation technique, the communication relies on the amount of power that is (re-)radiated or backscattered in the direction of the reader. It

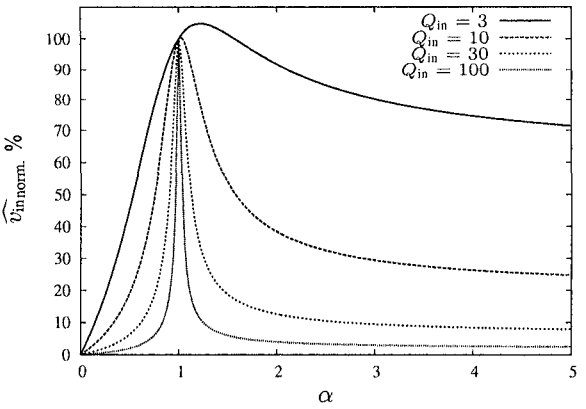

Fig. 5.8. Normalized input voltage $\widehat{v_{in}}_{norm.}$ versus α.

is thus the power burnt in the antenna radiation resistance R_s that has to be analyzed. In order to do so, we compute the reflection coefficient Γ at point B (see Fig. 5.7). The impedances seen at this point are:

$$Z_l = R_s \quad \text{and} \quad Z_r = R'_i + j\left(\omega L - \frac{1}{\omega C'_i}\right) \tag{5.6}$$

where Z_l is the impedance seen toward the left and Z_r is the impedance seen toward the right. Using Eq. (5.6), Γ is given by

$$\Gamma = 1 - \frac{2j}{Q_{in}(\alpha - 1) + j(1 + \alpha)}. \tag{5.7}$$

The reflected power in the reflection state $P_{r,r}$ is equal to the power available from the antenna P_{AV} since the tag's input antenna is shorted. In the absorption state, the reflected power $P_{r,a}$ depends on the input quality factor Q_{in} and the ratio α. Using 5.7, it is given by :

$$P_{r,a} = P_{AV}|\Gamma|^2 = P_{AV}\frac{\left(1 + Q_{in}^2\right)(\alpha - 1)^2}{(1 + \alpha)^2 + Q_{in}^2(1 - \alpha)^2}. \tag{5.8}$$

If $\alpha = 1$, $P_{r,a} = 0$ and the complete available power is absorbed. Eq. (5.7) is plotted in Fig. 5.9 for different quality factors. Here again, a small mismatch between R'_i and R_s with relatively high quality factors leads to a dramatic increase of $P_{r,a}/P_{AV}$. The modulation depth is thus very dependent on the factor α for moderately high quality factors.

In wireless power transmission systems, power management is of paramount importance. The power devoted to the communication is not available to supply the remote circuit energy and vice versa. In Fig. 5.10, the reflected power during standard ASK modulation is plotted. In order to increase the absorbed power during communication, the Duty-Cycle DC is introduced. The DC allows a more efficient power

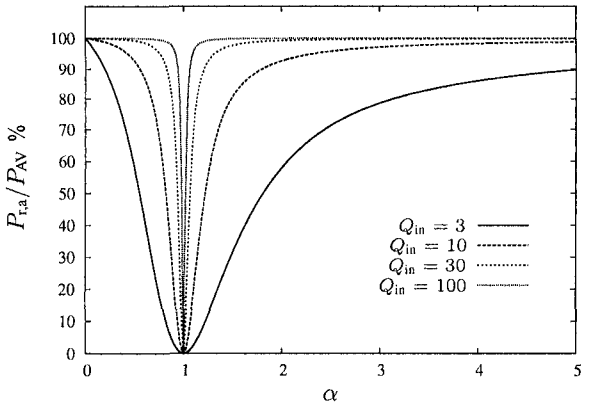

Fig. 5.9. Normalized reflected power versus α.

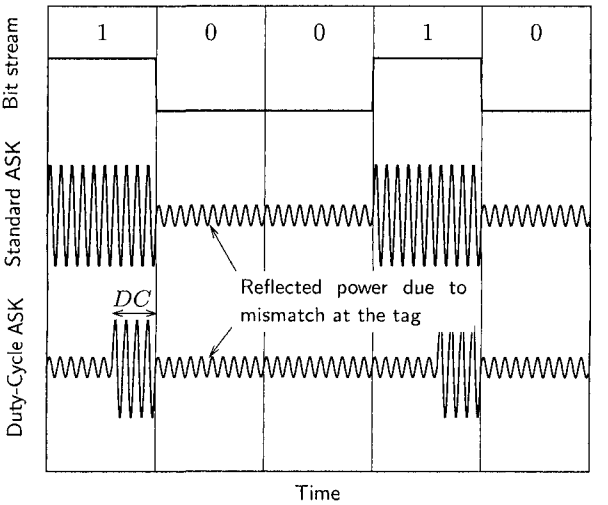

Fig. 5.10. Bit stream and the corresponding (reflected) ASK modulated signals illustrating the duty-cycle power management approach.

distribution at the remote side (the tag in the present case). To compare the modulation types, we compute the average reflected and absorbed power of bits "0" and "1."

The average reflected power $\overline{P_r}$ is given by:

$$\begin{aligned}\overline{P_r} &= \underbrace{DC\frac{P_{AV}}{2}}_{\text{Power due to short-circuit reflection}} + \underbrace{\frac{(2-DC)P_{AV}}{2}|\Gamma|^2}_{\text{Power due to mismatch in the absorption state}} \\ &= \frac{P_{AV}}{2}\left(DC + |\Gamma|^2(2-DC)\right).\end{aligned} \tag{5.9}$$

In the same manner, the power absorbed by the transponder P_a is 0 in the reflection state and in the absorption state, it is equal to:

$$P_{a,a} = P_{AV}\left(1 - |\Gamma|^2\right). \tag{5.10}$$

Consequently, the average absorbed power $\overline{P_a}$ becomes

$$\overline{P_a} = \frac{P_{AV}}{2}\left((2-DC)\left(1-|\Gamma|^2\right)\right). \tag{5.11}$$

Eq. (5.9) and (5.11) are plotted in Fig. 5.11 and 5.12.

As shown in Fig. 5.11 and Fig. 5.12, the power devoted to supply energy and the reflected power that enables the communication are complementary. As a result, they cannot both be maximized to P_{AV}. If more power is necessary to power the tag, less power is backscattered and the communication quality is (intuitively) deteriorated. This issue is analyzed in the next subsection.

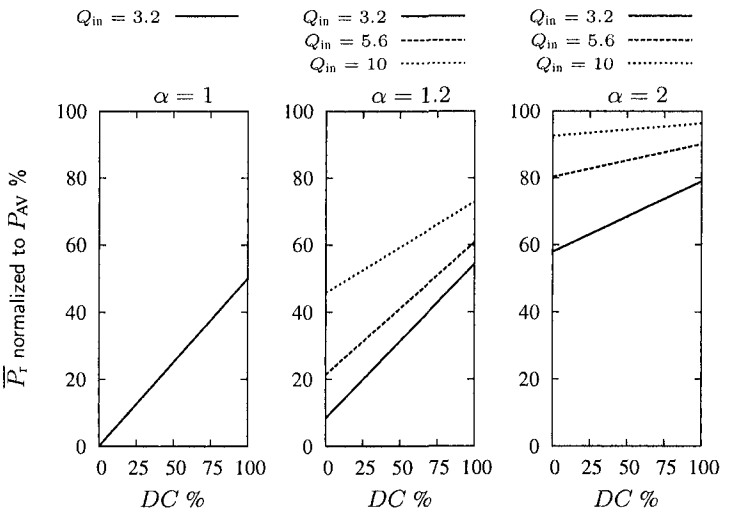

Fig. 5.11. Average reflected power $\overline{P_r}$ normalized to P_{AV} versus the modulation signal Duty-Cycle DC.

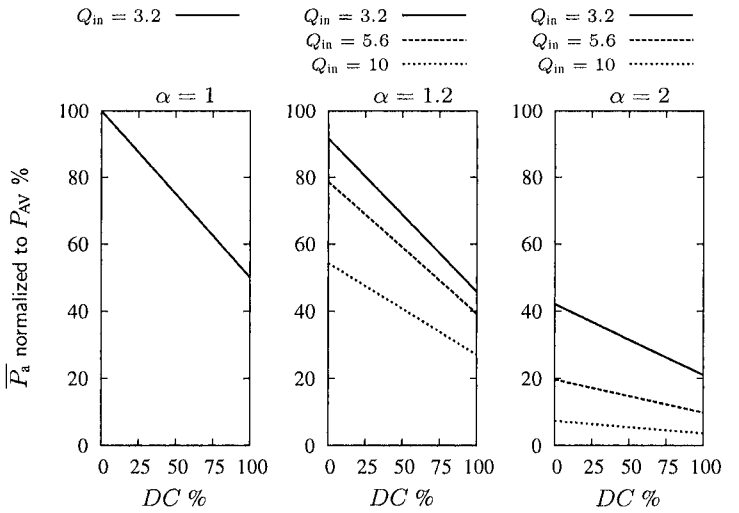

Fig. 5.12. Average absorbed power $\overline{P_a}$ normalized to P_{AV} versus the modulation signal Duty-Cycle DC.

5.6.3 Communication considerations

Digital modulations are compared in terms of their Bit Error Rate BER. Similarly to analog modulations where the Signal-to-Noise-Ratio SNR is used, the BER is evaluated as a function of the Energy per bit E_b over the noise level N_0. Both E_b and N_0 are determined at the receiver input [31].

For the present analysis, we consider the performance of a *matched-filter*[1] receiver and *white Gaussian noise corruption*. Thus, for binary signaling using the optimal threshold setting (for "mark" or "space" decision), the BER is

$$BER = Q\left(\sqrt{\frac{E_d}{2N_0}}\right) \tag{5.12}$$

where E_d is the difference signal energy at the receiver input. Q is a function defined by

$$Q(z) = \frac{1}{2}\,\mathrm{erfc}\left(\frac{z}{\sqrt{2}}\right) \tag{5.13}$$

and erfc is the complementary error function (see appendix A.1).

[1] A matched-filter is the linear filter that maximizes its instantaneous output signal power (see [31] page 477-478).

In the present case of ASK modulation (which is independent of the series/parallel configuration), the energy in the difference signal at the receiver input is

$$\begin{aligned} E_{\mathrm{d}} &= \int_0^T \left(A_1 \cos(\omega t + \theta) - A_0 \cos(\omega t + \theta)\right)^2 \mathrm{d}t \\ &= \frac{1}{2}(A_0 - A_1)^2 \end{aligned} \tag{5.14}$$

where T is the bit period signal, ω its frequency, θ its phase and A_0 and A_1 the amplitudes of bit 0 and bit 1.

The amplitudes A_0 and A_1 depend on the communication link, and using the Friis relation (with 0 dB antenna gain and no polarization loss), their values can be calculated as:

$$\begin{aligned} A_1 &= \underbrace{\frac{\lambda_{\mathrm{RF}}}{d}\sqrt{2P_{\mathrm{AV}}R_{\mathrm{ant,r}}}}_{\substack{\text{Amplitude } A \text{ in case of total reflec-} \\ \text{tion on the tag side}}} = A \\ A_0 &= |\Gamma| A \end{aligned} \tag{5.15}$$

where P_{AV} is the power available from the tag antenna, $R_{\mathrm{ant,r}}$ is the reader antenna radiation resistance, λ_{RF} is the RF carrier wavelength and d is the distance between the tag and the reader. Using (5.12) and (5.15), the BER for the ASK backscattering modulation is

$$BER = Q\left(\sqrt{\frac{E_{\mathrm{b}}}{N_0} \cdot \underbrace{\left(-1 + \sqrt{\frac{(Q_{\mathrm{in}}^2+1)(\alpha-1)^2}{(\alpha+1)^2 + Q_{\mathrm{in}}^2(1-\alpha)^2}}\right)^2}_{\text{Losses due to } Q_{\mathrm{in}} \text{ and } \alpha \neq 1}}\right) \tag{5.16}$$

where $E_{\mathrm{b}} = \frac{A^2 T}{4}$ is the average energy per bit for ASK.

At the communication level, the BER is also affected by the DC. The power of bit "1" (see Fig. 5.13) is scaled down by the DC factor. Hence, the bit energy is reduced and the BER increases compared to standard ASK and becomes

$$BER = Q\left(\sqrt{\frac{E_{\mathrm{b}}}{N_0} \cdot DC \cdot \left(-1 + \sqrt{\frac{(Q_{\mathrm{in}}^2+1)(\alpha-1)^2}{(\alpha+1)^2 + Q_{\mathrm{in}}^2(1-\alpha)^2}}\right)^2}\right). \tag{5.17}$$

Eq. (5.17) is plotted in Fig. 5.13 for different combinations $\{Q_{\mathrm{in}}, \alpha, DC\}$ as a function of the $\frac{E_{\mathrm{b}}}{N_0}$ ratio.

The power management approach that consists of a reduction of the duty-cycle has a relatively small influence compared to an α factor variation (see Fig. 5.13). A quality factor of 5 boosts significantly the voltage level at the tag input on one hand but on the other hand, if a small α mismatch occurs, the BER is dramatically degraded.

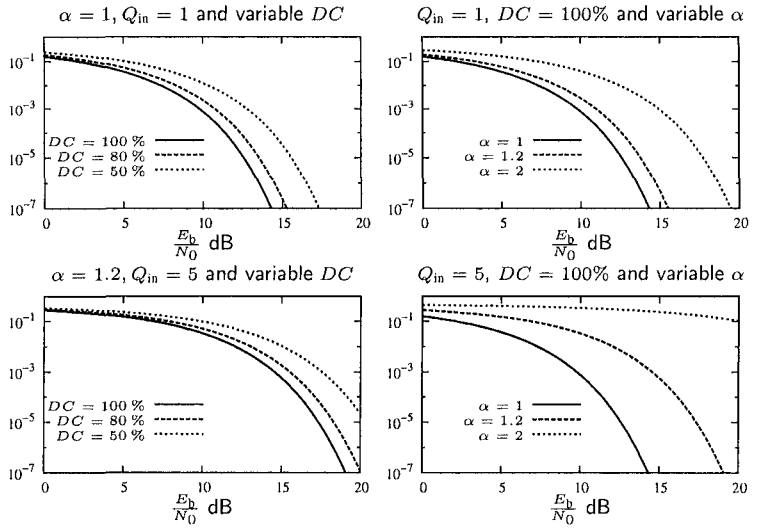

Fig. 5.13. BER versus $\frac{E_b}{N_0}$ for different Duty-Cycle DC, quality factors Q_{in} and α ratio in the ASK modulation case.

This shows clearly that voltage boosting using high Q elements is very much prone to BER degradation unless excellent matching is achieved. As the carrier frequency rises, this strategy can be tedious and risky to implement.

5.7 PSK series-series case

The PSK modulator circuit implementation is shown in Fig. 5.14. The backscattering PSK modulator switches the capacitance C on and off so that the impedance seen at point B toward the right alternates between a positive and negative reactance value (see Z_0 and Z_1 in Fig. 5.15). If the reflection coefficient modulus $|\Gamma|$ is kept constant

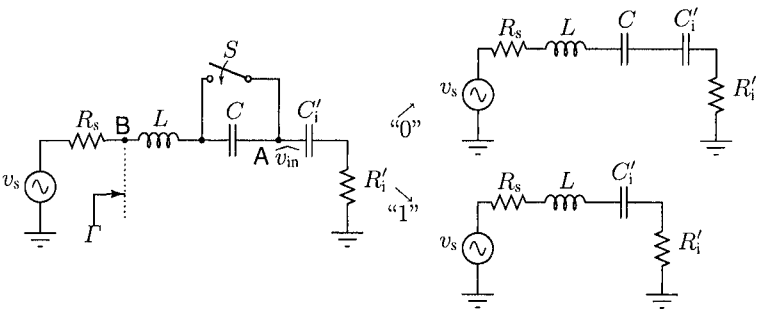

Fig. 5.14. Schematic for the series-series PSK modulation analysis.

in both states, only the phase of the reflected power wave changes. The impedance chart normalized to $R_s = R'_i = R$ in Fig. 5.15 illustrates the principle.

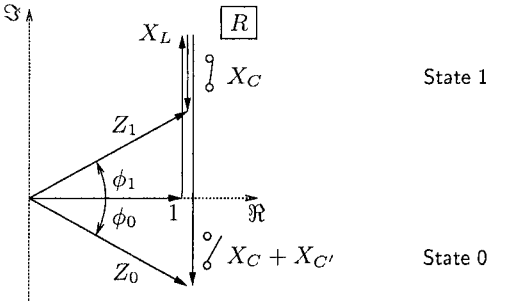

Fig. 5.15. Impedance chart of the series PSK modulation.

A representation of Fig. 5.14 using impedances is shown in Fig. 5.16 where X_L, X_C and X_i are, respectively, the impedances of the inductance L and the capacitances C and C'_i.

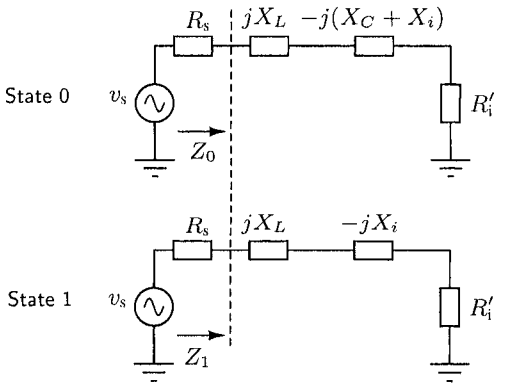

Fig. 5.16. Impedance representation of the series-series PSK modulation.

In order to ensure a constant reflected (or absorbed) power during both modulation states, the impedances Z_0 and Z_1 have to be complex conjugates. From Fig. 5.16, it means that the following relation for the inductance value has to be fulfilled:

$$X_L = X_i + \frac{X_C}{2}. \tag{5.18}$$

In this case, the impedances seen in both states become

$$\begin{aligned} Z_0 &= R_i' - j\frac{X_C}{2} \\ Z_1 &= R_i' + j\frac{X_C}{2} \end{aligned} \tag{5.19}$$

Using Eq. (5.19), we derive, as in the ASK case, the voltage considerations in the next subsection.

5.7.1 Voltage considerations

The voltage amplitude at point A $\widehat{v_{in}}$ is equal to

$$\widehat{v_{in}} = \hat{v}_s \sqrt{\frac{1+Q_{in}^2}{\left(1+\frac{1}{\alpha}\right)^2 + \left(\frac{Q_{in}\beta}{2}\right)^2}} \tag{5.20}$$

where $Q_{in} = \frac{X_i}{R_i'}$ is the input quality factor, $\alpha = \frac{R_i'}{R_s}$ is defined as the mismatch figure between R_i' and R_s and $\beta = \frac{X_C}{X_i}$ is the ratio between the two capacitances' impedances. The maximum of Eq. (5.20) occurs when $\alpha = 1$ and $\beta = 0$ and is given by

$$\widehat{v_{in}}_{max} = \frac{\hat{v}_s}{2}\sqrt{1+Q_{in}^2}. \tag{5.21}$$

Here again, $\widehat{v_{in}}$ can be boosted by choosing a high Q_{in}. Eq. (5.20) can be normalized to $\widehat{v_{in}}_{max}$, i.e.

$$\widehat{v_{in}}_{norm} = \frac{\widehat{v_{in}}}{\widehat{v_{in}}_{max}} = \frac{2}{\sqrt{\left(1+\frac{1}{\alpha}\right)^2 + \left(\frac{Q_{in}\beta}{2}\right)^2}} \tag{5.22}$$

The total capacitance seen at point A depends on the modulation state. Consequently, $\widehat{v_{in}}_{norm}$ varies with the modulation state and its respective values are given by

$$\begin{aligned} \widehat{v_{in}}_{norm}\big|_{State\ 0} &= \frac{2}{\sqrt{\left(1+\frac{1}{\alpha}\right)^2 + \left(\frac{Q_{in}\beta}{2}\right)^2}} \\ \widehat{v_{in}}_{norm}\big|_{State\ 1} &= \frac{2}{\left(1+\frac{1}{\alpha}\right)}. \end{aligned} \tag{5.23}$$

The amplitude difference depends on the $Q_{in}\beta$ product. When the real parts match, i.e. when $\alpha = 1$, the amplitude difference becomes

$$\Delta\widehat{v_{in}}_{norm} = \left| 1 - \frac{2}{\sqrt{4+\left(\frac{Q_{in}\beta}{2}\right)^2}} \right| \tag{5.24}$$

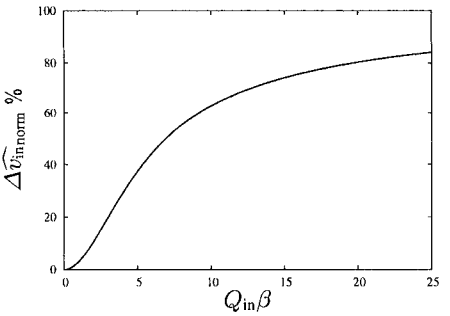

Fig. 5.17. Normalized input voltage amplitude difference versus the $Q_{\text{in}}\beta$ product.

and is plotted in Fig. 5.17. As can be seen, when the product $Q_{\text{in}}\beta$ is equal to 10, the amplitude difference between the two modulation states is about 70% of $\widehat{v_{\text{in}}}_{\text{max}}$. The voltage at the rectifier's output can thus significantly drop. This effect is emphasized as the difference between R_{s} and R_{i} increases. *The available power to the tag remains constant during both states, but the voltage at the rectifier input changes.*

To enable PSK, the input impedance has a reactive mismatch that necessarily leads to an input voltage amplitude smaller than $\widehat{v_{\text{in}}}_{\text{max}}$. This is a major difference when compared to ASK where $\widehat{v_{\text{in}}}_{\text{max}}$ can be achieved during one modulation state. In terms of operating range, this could be an advantage for ASK.

5.7.2 Power considerations

In phase shift keying, the power available to the transponder is constant during the two modulation states if the impedances Z_0 and Z_1 are complex conjugates. The reflection coefficient at point B (see Fig. 5.14) is equal to

$$\Gamma = 1 - \frac{4j}{2j + \alpha(Q_{\text{in}} + 2j)}. \tag{5.25}$$

As seen in Eq. (5.25), the reflection coefficient is independent of β and thus doesn't vary during the two modulation states. The power available[2] to the tag is equal to

$$P_{\text{a}} = P_{\text{AV}} \frac{16\alpha}{4(1+\alpha)^2 + Q_{\text{in}}^2\alpha^2} \tag{5.26}$$

and is plotted in Fig. 5.18 for different α.

In PSK modulation, the information is contained in the phase of the reflected signal. The modulation angle $\Delta\Phi$ is thus of importance and is equal to the difference of the reflected power argument between the two states. It is given by

$$\Delta\Phi = 2\arctan\left(\frac{4\,Q_{\text{in}}\alpha}{-4 + \alpha^2(4 + Q_{\text{in}}^2)}\right). \tag{5.27}$$

[2]Which is also equal to the average power.

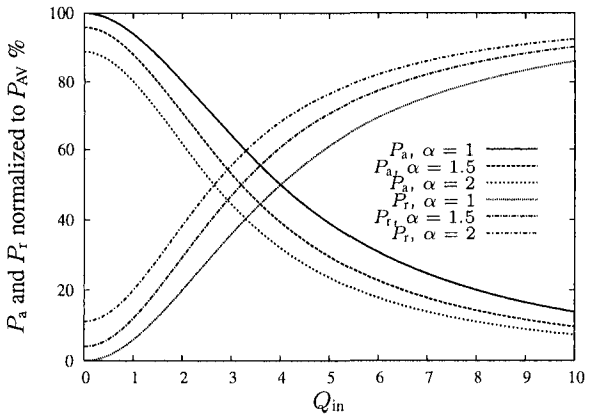

Fig. 5.18. Absorbed power P_a and reflected power P_r normalized to P_{AV} versus Q_{in} for PSK.

Eq. (5.27) is plotted in Fig. 5.19. Interestingly, the modulation angle increases, reaches a maximum and decreases with Q_{in} for $\alpha > 1$. Moreover, if α varies only a little bit from its nominal value 1, $\Delta\Phi$ is dramatically reduced.

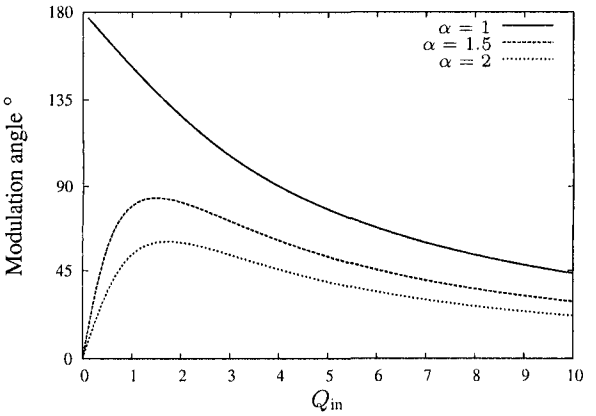

Fig. 5.19. Modulation angle for PSK.

From Fig. 5.18 and 5.19, we can see that it is not possible to have simultaneously the widest modulation angle (180 °) and backscattered power. It will be shown in the next subsection that an optimal trade-off exists between the power available to the tag and a reliable communication with the reader.

5.7.3 Communication considerations

As in section 5.6.3, we determine the performance of a *matched-filter* receiver and *white Gaussian noise corruption*. The information energy at the receiver input is

$$\begin{aligned} E_{\mathrm{d}} &= \int_0^T \left(2A\sin(\Delta\Phi)\cos(\omega t+\theta)\right)^2 \\ &= 2A^2T\sin\left(2\arctan\left(\frac{4\,Q_{\mathrm{in}}\alpha}{-4+\alpha^2(4+Q_{\mathrm{in}}^2)}\right)\right)^2 \end{aligned} \tag{5.28}$$

where T is the bit period signal, ω its frequency, θ its phase and A the amplitude of bit 1 and bit 0 ($|\Gamma|$ is considered constant during the two states). The amplitude A is computed using the Friis relation:

$$A = \frac{\lambda_{\mathrm{RF}}}{d}\sqrt{2P_{\mathrm{AV}}R_{\mathrm{ant,r}}}\,|\Gamma|. \tag{5.29}$$

where P_{AV} is the power available from the tag antenna, $R_{\mathrm{ant,r}}$ is the reader antenna radiation resistance, λ_{RF} is the RF carrier wavelength and d is the distance between the tag and the reader. Using (5.12) and (5.29), the BER for the PSK backscattering modulation is

$$BER = Q\left[\sqrt{2\frac{E_{\mathrm{b}}}{N_0}\cdot\frac{4+\alpha\left(-8+\alpha\left(4+Q_{\mathrm{in}}^2\right)\right)}{4+\alpha\left(8+\alpha\left(4+Q_{\mathrm{in}}^2\right)\right)}\sin\left(2\arctan\left(\frac{4Q_{\mathrm{in}}\alpha}{-4+\alpha^2\left(4+Q_{\mathrm{in}}^2\right)}\right)\right)^2}\right] \tag{5.30}$$

where $E_{\mathrm{b}} = \frac{A^2T}{2}$ is the average energy per bit for PSK. Eq. (5.30) is plotted in Fig. 5.20 for different α and Q_{in} as a function of the $\frac{E_{\mathrm{b}}}{N_0}$ ratio.

In Fig. 5.20, it can be seen that there is an optimal Q_{in} for a given BER and α. Its value depends both on Q_{in} and α (see Fig. 5.21). The overall minimal $\frac{E_{\mathrm{b}}}{N_0}$ is achieved for $\alpha = 1$ and $Q_{\mathrm{in}} \approx 5.6$. At this point, the power available to the tag is about 50% of P_{AV}.

5.8 ASK and PSK comparison

The optimal BER curves for both modulation types are shown in Fig. 5.22. As shown in this figure, the PSK modulation is superior to ASK by a factor of 0.74 dB which is a rather small difference at the cost of a more complex implementation. The impedances necessary to implement PSK induce a smaller available voltage at the rectifier input compared to ASK (during one modulation state). This results in a lower sensitivity for PSK. This affects the maximal operating range and in that sense, ASK can be advantageous. Furthermore, the average power available to the tag is the same in both cases (50%) when considering optimal parameters. This shows that *there is no clear advantage to implementing PSK rather than ASK in the framework of passive tags.*

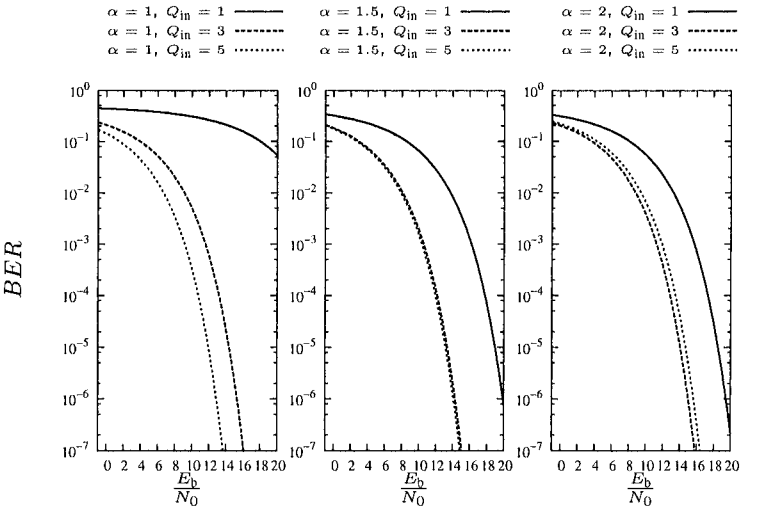

Fig. 5.20. BER versus $\frac{E_b}{N_0}$ for different reactive mismatch ΔQ in the PSK modulation case.

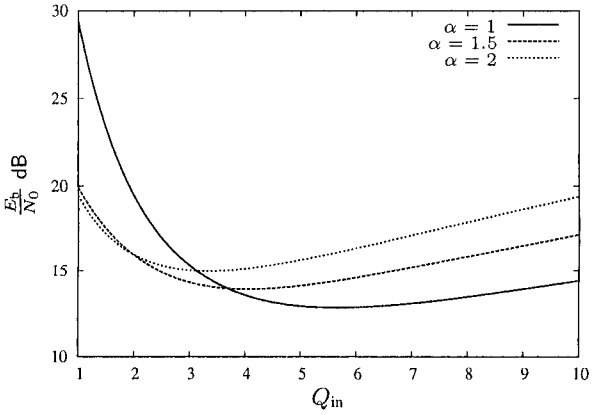

Fig. 5.21. $\frac{E_b}{N_0}$ versus Q_{in} for a BER of 10^{-6}.

5.9 PSK based on ASK or pseudo-PSK

The PSK modulation scheme described in the preceding sections is based on the reactive mismatch that varies the phase of the reflected wave at the tag. *It has been shown that it is not possible to have simultaneously* 180° *of modulation angle and reflected power.* As a result, there is a trade-off between the reflected power and the achievable BER.

In ASK, the modulation is based on the amplitude variation of the reflected wave. It has been seen before that to obtain a reliable communication, *the reflected power*

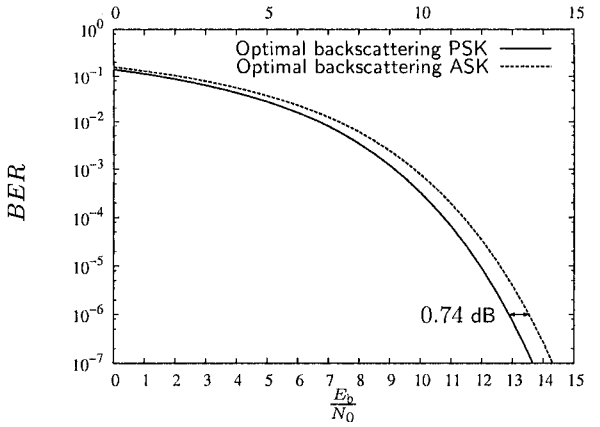

Fig. 5.22. Optimal ASK and PSK BER comparison (ASK: $DC = 100\%$, $\alpha = 1$ and PSK: $\alpha = 1$, $Q_{\text{in}} = 5.6$).

should be maximized and one can tune the BER using the duty-cycle power management approach.

In chapter 3, it has been shown that the input resistance is related to the output current consumption of the rectifier. In order to ensure a sufficient ASK modulation depth, the modulator should switch between a short-circuit and a close-to-power-matched impedance. In this case, the power wave will look like the one drawn in Fig. 5.23. But if the output current is small (a few μA), the input resistance is rather

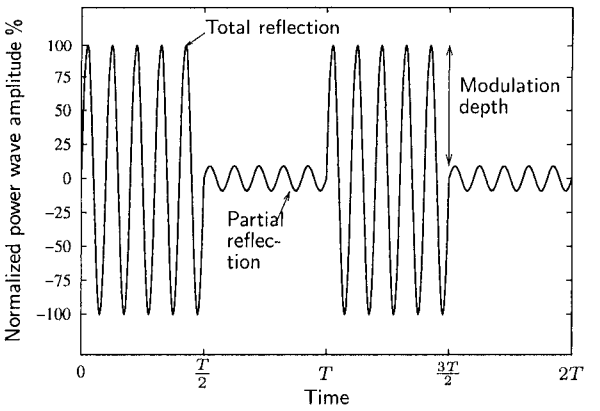

Fig. 5.23. Reflected power waves for the ASK modulation scheme.

large (a few kΩ). And to obtain a good ASK modulation, the antenna should be tuned to this high impedance level, which can be tedious in practice. This is also the case for PSK and thus both modulation types can be hard to implement when the operating

range is to be maximized. For this reason, pseudo-PSK is introduced in the next section. The idea of pseudo-PSK is to take advantage of the high input impedance as well as to offer a reliable communication based on phase modulation.

5.10 Pseudo-PSK

Without reactive losses, the antenna sees alternatively a short-circuit and a high impedance whose level is set by the tag output power consumption. If the real part of the antenna impedance is smaller than the real part of the input impedance, the reflection coefficient jumps from the $\Delta\phi = 0°$ region to the $\Delta\phi = 180°$ region in Fig. 5.24. The power wave that results in this case is shown in Fig. 5.25. The amplitude

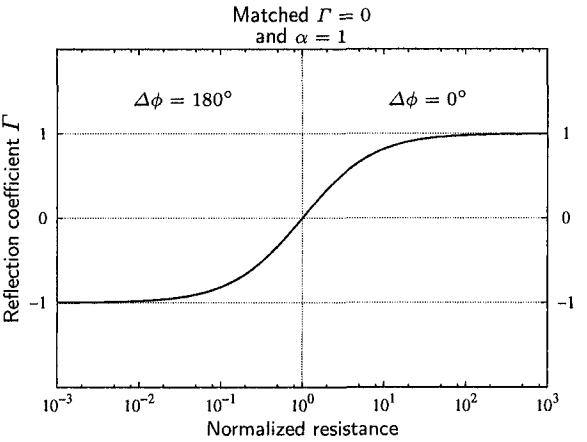

Fig. 5.24. Reflection coefficient amplitude.

difference between the two states represents the power absorbed by the tag during the high impedance state. In this configuration a poor ASK modulation is obtained. But the phase shift between the two modulation states is a stable 180°. An excellent and easy to implement BPSK modulator is thus obtained under the condition that the tag output current consumption is kept to a value that ensures a "sufficiently high" input impedance when the modulator switch is open.

The voltage and power analysis gives identical results to the series-parallel ASK cases (without the Duty-Cycle and reactive losses) found in section 5.6. But the communication considerations change significantly and are studied in the next section.

5.10.1 Communication considerations

The communication analysis is similar to section 5.7.3 except that the modulated signal envelope isn't constant. The signal amplitude received during the bit having

0° phase depends on the $\alpha = \frac{R_i}{R_s}$ ratio, which is necessarily greater than 1 to allow a 180° phase shift (see Fig. 5.24 and 5.26).

Its value is given by

$$A_0 = A_1 \left| \frac{\alpha - 1}{\alpha + 1} \right| \qquad \alpha > 1 \tag{5.31}$$

where A_1 is the signal amplitude during bit 1 (short-circuit). Therefore, the BER is equal to

$$BER = Q\left(\sqrt{2 \left| \frac{\alpha - 1}{\alpha + 1} \right| \frac{E_b}{N_0}} \right) \qquad \alpha > 1. \tag{5.32}$$

Eq. (5.32) is plotted in Fig. 5.27 for different $\alpha > 1$ together with standard PSK, optimal ASK and PSK curves.

As seen in Fig. 5.27, a value of $\alpha = 5$ offers superior performance than optimal PSK and ASK. For $\alpha = 20$ the BER is almost identical to standard PSK. In this case, the mean available power drops to 9% of the available power at the antenna. For a 300 Ω antenna ($\lambda/2$ folded dipole), the input resistance should be 6 kΩ. This impedance level is difficult to reach in practice and the BER improvement is only 1 dB better than the case where $\alpha = 5$. Such a design goal maybe isn't worth it. One

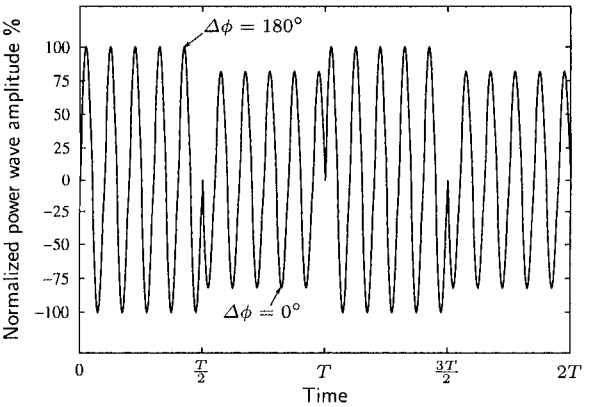

Fig. 5.25. Reflected power waves for the pseudo-PSK modulation scheme.

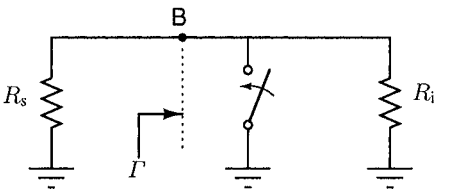

Fig. 5.26. Schematic for the series pseudo-PSK modulation analysis.

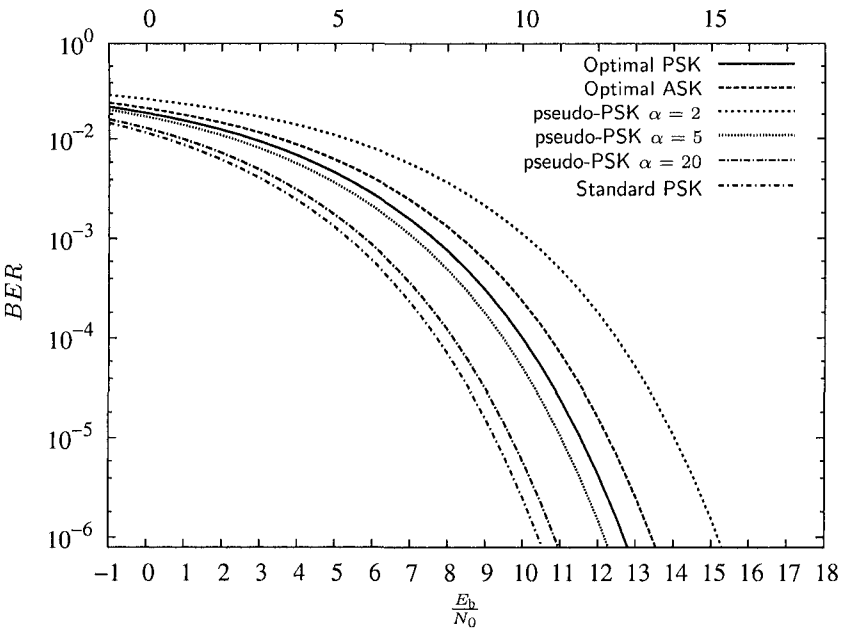

Fig. 5.27. BER versus $\frac{E_b}{N_0}$ for different α ratio in the pseudo-PSK case alongside the other modulation scheme.

could use a 73 Ω antenna ($\lambda/2$ dipole) to lower the necessary input impedance to 1.46 kΩ. But the drawback in this case is a reduction of the available input voltage. Compared to the 300 Ω antenna this reduction is equal to

$$1 - \frac{\sqrt{73}}{\sqrt{300}} = 51\%.$$

The rectifier sensitivity is thus dramatically affected.

5.11 Wireless power transmission and communication optimization

The achievable operating range is an important figure of merit in a WPT system. As shown in chapters 2 and 3, the impedance level at the tag input determines the voltage level at the rectifier's input and as a result, the operating distance. When the tag is modulating, two impedances are successively connected to the antenna and as shown in this chapter, the input voltage level can vary significantly. The maximal operating range during modulation (ASK, PSK or pseudo-PSK) is thus affected. The choice of these two impedances is thus fundamental. What has been found is that impedance matching at a high impedance level during one modulation state is optimal to achieve a

long range system. But it should be recalled that the output power consumption of the tag (as well as input parasitics) limits the maximal impedance level. The consequence of this for backscattering modulation is that a pseudo-PSK can turn out to perform better if the impedance level is higher than standard PSK during one modulation state. Then, by trimming the output rectifier charging capacitance, an optimum can be reached. This remark is also valid for the ASK case although the communication quality is usually worse.

5.12 Conclusion

As described in this chapter, the trade-offs in terms of power dedicated to the communication and the power dedicated to the voltage supply of the tag is not a simple fifty/fifty power distribution. There are three key aspects that should be taken into account when choosing the modulation scheme for a remotely powered device that communicates using the backscattering technique. These are the voltage sensitivity of the rectifier, the necessary power to the application and the Bit Error Rate.

In terms of input voltage amplitude, the series configuration has shown superior performance when compared to its parallel counterparts. The amplitude can be raised with the Q factor of the RF front-end. In practice, the series input resistance $R_{\text{in,s}}$ and capacitance $C_{\text{in,s}}$ are quite sensitive to the output current consumption. As a consequence, the output power consumption should be regulated in order to ensure a small variation of the input rectifier impedance.

As described in sections 5.6.2 and 5.7.2, the absorbed and reflected power do not depend on the configuration. Their average values are mainly determined by the modulation scheme. Standard ASK modulation allows a maximum of 50% of the received power to be used. The duty-cycle power management approach can further scale up this value (see section 5.6.2). In PSK, the power available to the circuit is constant during the modulation states, which is an advantage compared to ASK and pseudo-PSK. In the latter scheme, a maximum of 50% of absorbed power is possible (see Fig. 5.28).

The last key point (considered in this study) is the communication consideration. There are two basic possible approaches, phase and amplitude modulation of the reflection coefficient. Only digital modulations were analyzed in this chapter. It is well known that BPSK is superior to BASK in terms of BER, but in remotely powered applications where backscattering modulation is used, there exists a strict trade-off between the power part given to the application and the part dedicated to the communication. Fig. 5.27 summarizes pretty well the situation. As can be seen, there is not a big difference between the optimal ASK and PSK cases. ASK is advantageous in terms of available power to the application while PSK performs better when comparing the BER.

As shown in section 5.9, the optimum is a modulation trade-off or a trade-off between ASK and PSK. Indeed, the pseudo-PSK presented here offers a BER almost equal to standard PSK. Furthermore, the power management issue is also adequately addressed. Rectifiers have inherently a large real part of their input impedance and if

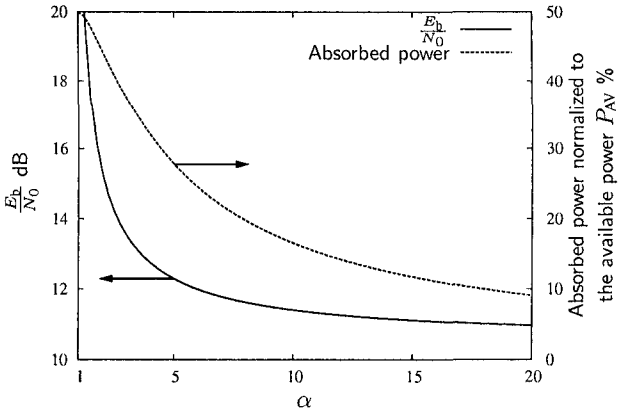

Fig. 5.28. Necessary $\frac{E_b}{N_0}$ to achieve a BER of 10^{-6} and absorbed power versus the α factor in the pseudo-PSK modulation scheme.

the reactive part is compensated by proper antenna design, pseudo-PSK is certainly the modulation scheme of choice. With pseudo-PSK, both the operating range and the communication quality are maximized.

As mentioned in section 5.5, a reflection coefficient analysis was conducted in this chapter. The backscattering phenomenon is tightly related to the antenna geometry [29] and to the impedance connected to it. As shown in [32], an analysis based on the Thevenin or Norton equivalent circuit of the antenna cannot lead to satisfying results. An approach based on [29], [30] and [32] to analyze *quantitatively* the backscattering phenomenon is the purpose of the next chapter.

6

Backscattering modulation analysis

In this chapter, we analyze the backscattering phenomenon from a quantitative point of view. The theoretical background is described first. As a second step, a practical approach to quantify the effect of the tag loading at the reader side is derived. The impact on the RFID system and more particularly on the reader architecture is also studied. Finally, a graphical interpretation of the complex transformations that occur as well as the impact on the wireless power transmission issue conclude this chapter.

6.1 Introduction

THE communication link between the tag and the reader is based on the backscattering phenomenon [2]. The tag antenna reflects the impinging power with a certain amplitude and/or phase variation depending on the antenna geometry and also on the load impedance (see Fig. 6.1). This impedance is generally implemented at the integrated circuit level [5], [33], [34]. The impedance presented by the tag when no modulation takes place is dominated by the rectifier [4]. The antenna is generally designed to match the complex conjugate impedance of the rectifier in order to optimize the operating range.

There is a degree of freedom in the choice of the modulator impedances. To limit the integrated circuit layout size, only resistive and capacitive elements are used. The impact of the impedance values is to vary both the phase and the modulus of the backscattered electric field. It is shown in [32] that limitations exist for the Norton and Thevenin equivalent circuits for a receiving antenna. As a consequence, the determination of the phase and amplitude of the reflected signal using the equivalent antenna circuit approach cannot lead to satisfying results. This chapter proposes a method based on [29] and [35] to determine the amplitude and phase of the received signal at the reader antenna from a backscattering tag (see Fig. 6.2). Using this method,

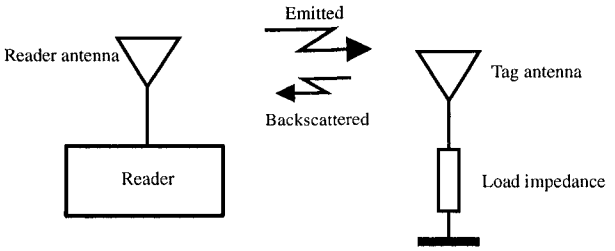

Fig. 6.1. Backscattering phenomenon

the circuit designer can predict the phase or amplitude modulation depth of a given impedance connected to the tag antenna.

6.2 Theoretical analysis

It is well known [29] that electromagnetic waves backscattered by any antenna depend both on antenna geometry and antenna load. For a given antenna in free space, the electric field at a particular point in space and at a particular frequency can be expressed as:

$$E_{scat}(Z_L) = E_{scat}(Z_{ANT}) - \Gamma_{L,Z_{ANT}} \frac{E_t I_s}{2I_t} \tag{6.1}$$

where $E_{scat}(Z_L)$ is the scattered field when the antenna is loaded with impedance Z_L, $E_{scat}(Z_{ANT})$ is the same field when the antenna is loaded with Z_{ANT}, I_s is the current flowing in the antenna when short-circuited, E_t is the electric field generated by the antenna as a radiator when the current I_t flows in its terminals, Z_{ANT} is the antenna impedance and Γ_L is defined as

$$\Gamma_{L,Z_{ANT}} = \frac{Z_L - Z_{ANT}}{Z_L + Z_{ANT}} \tag{6.2}$$

In the following we adopt the convention that Γ_{X,Z_y} is the reflection coefficient related to the impedance indicated by X and normalized to Z_y, as is clear from (6.2).

Dividing both sides of (6.1) by E_{sent}, which is the field corresponding to the wave impinging on the antenna, and observing that the system composed of the antenna and the load is linear, we can write:

$$\frac{E_{scat}(Z_L)}{E_{sent}} = \frac{E_{scat}(Z_{ANT})}{E_{sent}} - \Gamma_{L,Z_{ANT}} \frac{E_t}{2I_t} \frac{I_s}{E_{sent}} \tag{6.3}$$

where $\frac{E_{scat}(Z_{ANT})}{E_{sent}}$ and $\frac{E_t}{2I_t} \frac{I_s}{E_{sent}}$ are complex constants depending on the particular antenna and on the position at which the field is calculated.

From Eq. (6.3), it is clear how the load affects the backscattered wave. It should be noted that this field is not directly proportional to the reflection coefficient. This is due

to the presence of a *structural* component of the scattered wave, which is embedded in the $\frac{E_t}{2I_t}\frac{I_s}{E_{sent}}$ coefficient in Eq. (6.3).

In order to quantify at the reader side the effects of load modulation at the tag side, we model the tag-reader system of Fig. 6.1 as a two-port network characterized by its scattering matrix S as shown in Fig. 6.2.

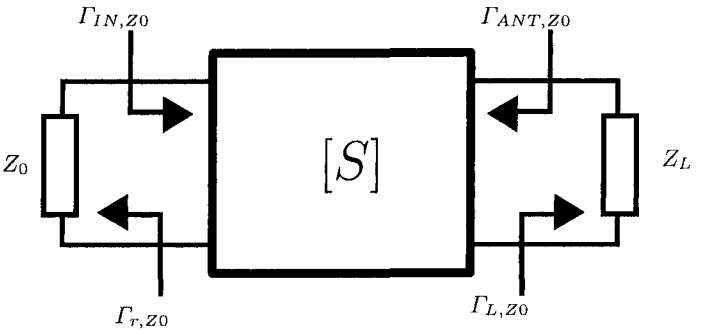

Fig. 6.2. Model of the tag-reader system

The characteristics of the modulation can be extrapolated by analyzing Γ_{IN,Z_0}, the reflection coefficient at the reader antenna input normalized to the impedance of this antenna. Assuming that the reader antenna is terminated by a Z_0 load [1], the reflection coefficient is equal to the ratio of the transmitted voltage wave to the received voltage wave. The variations in phase and amplitude normalized to the transmitted signal, which is also used at demodulation, can be directly observed from the behavior of Γ_{IN,Z_0}. The usual formula can be applied to get

$$\Gamma_{IN,Z_0} = S_{11} + \frac{S_{12}S_{21}}{1 - S_{22}\Gamma_{L,Z_0}}\Gamma_{L,Z_0} \tag{6.4}$$

A good approximation for the present problem is to assume that the impedance of the tag antenna, i.e. the impedance seen from the tag port, is constant and equal to the free space antenna impedance. Using this approximation we can say that $\Gamma_{ANT,Z_0} \approx S_{22}$; if we normalize the scattering matrix to the impedance Z_{ANT} and indicate the obtained s-parameters with an apostrophe, we have

$$S'_{22} \approx \Gamma_{ANT,Z_{ANT}} = 0$$

and Eq. (6.4) becomes:

$$\Gamma_{IN,Z_{ANT}} = S'_{11} + S'_{12}S'_{21}\Gamma_{L,Z_{ANT}} \tag{6.5}$$

$$= A + B\Gamma_{L,Z_{ANT}}. \tag{6.6}$$

[1] This is the usual situation in which a 50 Ω antenna is terminated with a 50 Ω impedance in order to get the maximum power transfer both in transmission and in reception.

Eq. (6.4) states that the knowledge of two complex constants A and B is enough to completely characterize the modulation performance. It is clear that these constants are changing as the tag moves relative to the reader; this causes an amplitude and absolute phase variation of the received signal.

Once the two coefficients are known, the whole Smith chart (normalized to Z_{ANT}) can be transformed to the plane of $\Gamma_{IN,Z_{ANT}}$ using Eq.6.5. At this point it is possible to transform the reflection coefficient to the Smith chart normalized to Z_0 and the modulation performance can be analyzed. As all the transformations cited are bilinear transformations, the Smith chart of the load (which is a circle) will be mapped to another circle in the Γ_{IN,Z_0} plane, as will be clear in the following.

6.3 Experimental characterization

6.3.1 Practical procedure

In order to obtain the two coefficients needed in using (6.5), the following procedure has been adopted.

1. the tag antenna impedance is measured with a network analyzer, obtaining Γ_{ANT,Z_0};
2. a series of different impedances which could be attached to the tag antenna are prepared: this consists of the measurements of the reflection coefficient Γ_{L,Z_0} of each impedance;
3. the tag/reader system is placed in an anechoic environment and a list of values for Γ_{IN,Z_0} are measured at the reader antenna for each different load, previously prepared;
4. the reflection coefficient for the loads and for the input are normalized to Z_{ANT} and the resulting data are used to fit (6.5) with the Least Mean Square (LMS) method;
5. the coefficients resulting from the fitting can be used to plot Γ_{IN,Z_0} with Γ_{L,Z_0} as a parameter, using the known transformation formulas.

It should be noted that the value of the two coefficients needed for the evaluation of (6.5) can be extracted using only two different load conditions. The use of a greater numbers of loads and the consequent LMS fitting are used to reduce the effects of noise and errors in measurements. Moreover, in the following the use of more than two terminations provides the proof that expression (6.5) is a good approximation.

The procedure described above was repeated using the following combination of reader-tag antennas: two 8 dBi flat patch 900 MHz antennas from HyperLink Technologies; two 2.4 GHz 15.5 dBi WLAN planar array antennas from the same manufacturer; one of the 2.4 GHz antennas just described for the reader and the printed folded dipole used in [5] for the tag. All the measurement were made with an HP8753D network analyzer which has a 50 Ω input impedance. The high directivity antennas show a 50 Ω impedance (consequently $Z_0 = Z_{ANT}$) and coaxial connector input: the impedances used for the fitting were built using standard termination (short-circuit,

load) and coaxial cable of different lengths. For the folded dipole antenna, a balun such as the one in [36] was designed for the conversion from balanced antenna input to the coaxial input of the network analyzer. The same balun was used to measure the four impedances used in this case (0 Ω, 300 Ω, 9.1 kΩ SMD resistors and a 0.3 pF SMD capacitor); in this way it is possible to measure the impedances of the components in the same conditions as when they are connected to the antenna. To de-embed the effect of connectors and of the balun the TRL calibration method [37] was used. The first two setups were used in order to show that the procedure described is very general and can be used for each antenna. The setup with the folded dipole is much more interesting because it shows how good measurement results can be obtained in a usual case, in which a printed antenna is present. It is clear that all the parameters of (6.4) can be obtained from a full 2-port measurement of the S matrix of Fig. 6.2. However it can be difficult to connect a printed antenna for the tag side and to de-embed the results. The procedure just described is much more practical and it requires only the availability of a network analyzer.

6.3.2 Results

In Fig. 6.3, Fig. 6.4 and Fig. 6.5, the experimental data are compared to the data obtained from the fitting procedure. For each setup four different loads were used; we avoid reporting the measurement of the load reflection coefficients for the sake of brevity. The magnitude of the error vectors between measurement and fitting are less than -25 dB, -36 dB and -40 dB respectively for Fig. 6.3, Fig. 6.4 and Fig. 6.5[2]. It can be observed that the fitting appears more precise in the case of the high gain antennas relative to the folded dipole case; this is due to the larger error involved in the measurement of printed components. For them it is necessary to use baluns if a fully-differential network analyzer is not available. The data analysis shows that the model is descriptive of the backscattering phenomenon and can be used to design RFID systems.

6.4 Impact on RFID Systems

The calculated coefficients A and B can be used to predict the modulation performance for every pair of loads at the tag side, assuming a binary alphabet. This is done for the dipole antenna and the results are shown in Fig. 6.6, in which the reader reflection coefficient at various frequencies is shown with the tag load as a parameter; the Smith circle of the load is mapped for each frequency to one of the *modulation circles* shown in the figure. The circle with dots is the locus of the reflection coefficient for every pure reactive load, i.e. the Smith chart boundary, at 2.4 GHz and the other circles sweep in frequency from right to left until 2.5 GHz with a 20 MHz step. At 2.4 GHz

[2]The error is reported in absolute terms and not in relative ones because some of the reflecting coefficients shown are very near to the origin; this causes a large increase of the relative error without indicating a loss of accuracy.

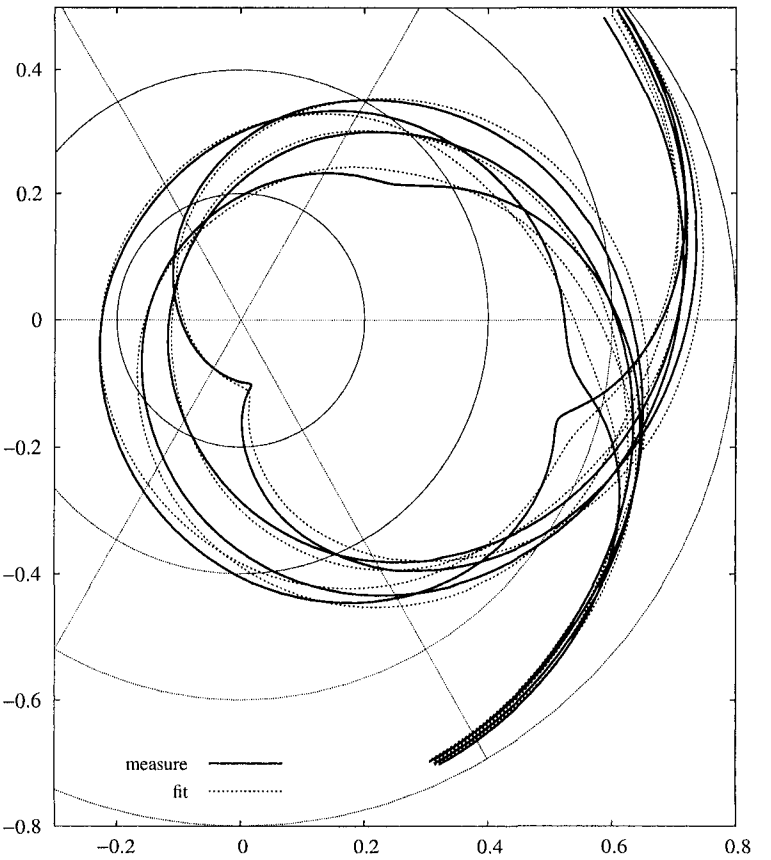

Fig. 6.3. Experimental data and fitting of Γ_{IN,Z_0} for the 900 MHz antennas

the dots show the impedances which should be used to achieve optimum PSK and optimum ASK. These impedances are calculated at each frequency point and the resulting modulation performance is presented in Fig. 6.7; for phase modulation the maximum phase difference between two points on the same circle is used and for amplitude modulation the maximum modulation index[3] is used.

Fig. 6.6 can be used to choose the modulation impedances together with the constraints for the tag realization by taking into account the relative performances. It should be noted that a modulation angle of 180° cannot be achieved unless the modulation circle contains the origin. The shift of the Smith chart from the origin is due to the structural scattering of the antenna, which causes the presence of a component of the scattered signal *not depending on the load.* In the real case, other

[3]The modulation index is defined as the ratio of the amplitude difference in the two modulation states to the maximal amplitude.

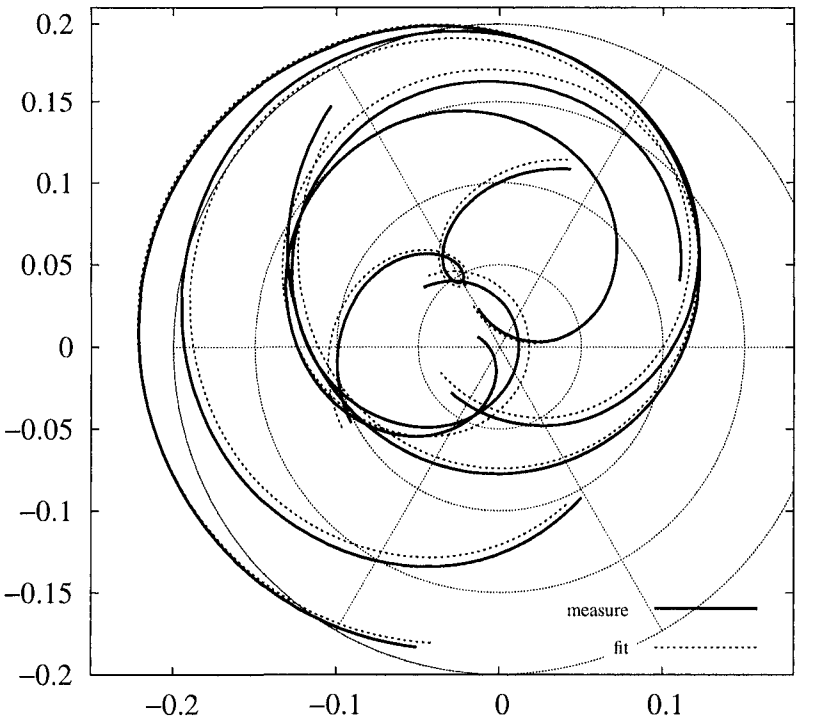

Fig. 6.4. Experimental data and fitting of Γ_{IN,Z_0} for the high gain 2.4 GHz antennas

effects cause the circle to be shifted from the origin: the leakage in the reader from the transmitting path to the receiving path, the reflection of the transmitted wave from the environment, and the reflection of the reader output signal at the reader antenna input due to imperfect matching. These effects should be taken into account even if very small because the backscattered signal is several orders of magnitude smaller than the sent signal.

To have some insight we can consider $Z_{ANT} = Z_0$ for which the center of the modulation circle is A, while B gives a scaling and a rotation of the circle. In this case, considering A constant with frequency, the bigger effect of a frequency change is the rotation of the modulation circle due to B. This effect is given by the variation of the ratio of tag-reader distance to wavelength and is clearly recognizable in Fig. 6.8 for the dipole antenna, in which typical ASK and PSK modulation are shown. (Note that the dipole impedance is 300 Ω.) From this analysis it is clear that a simple amplitude or phase demodulator cannot be used to reach the maximal performance, such as 180° PSK modulation. To achieve better performance one should use architectures which cancel the effect of the terms independent from load modulation, such as low-IF systems [5] or I/Q demodulators [34], or systems which allow a rotation of the

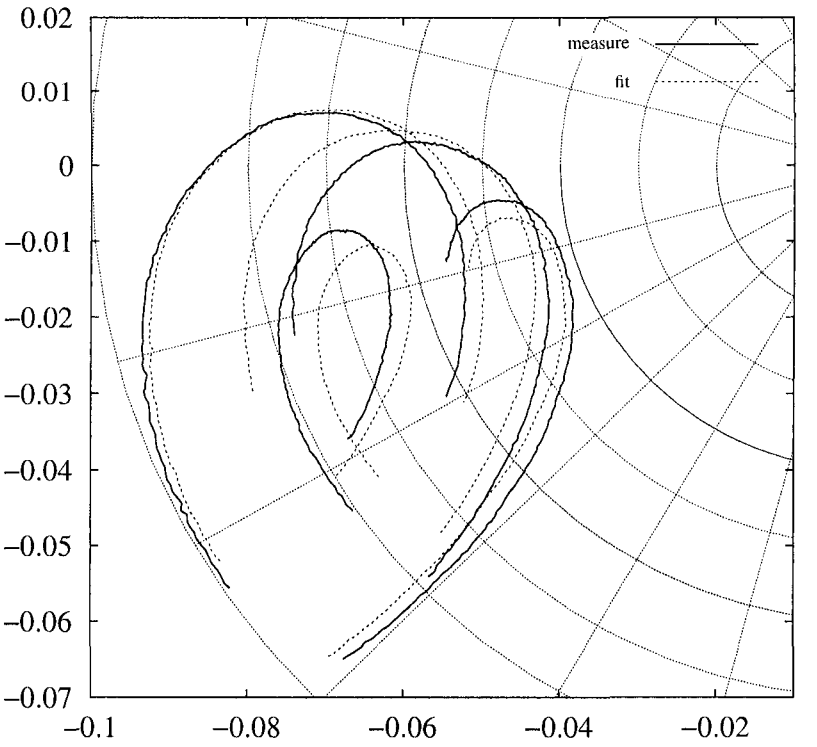

Fig. 6.5. Experimental data and fitting of Γ_{IN,Z_0} for the folded dipole

modulation circles to move the constellation points to the optimal position, such as frequency sweeping loops (see section 8.9). However, to correctly design and predict the final performance, the proposed approach must be used in order to map each tag load to its corresponding constellation point in the plane of Γ_{IN,Z_0}.

6.5 Graphical Interpretation

The mathematical transformations described in section 6.2 are of two types. The first and last (or third) are *bilinear* transformations whereas the second is a *linear* transformation. The bilinear operation transforms circles into circles. As a result, the Smith chart described by Γ_L of the tag load impedance Z_L (the impedance practically responsible for backscattering modulation) normalized to Z_0 is first re-normalized to Z_{ANT} using a bilinear transformation:

$$\Gamma_{L,Z_{ANT}} = \frac{\Gamma_{L,Z_0}(Z_0 + Z_{ANT}) + Z_0 - Z_{ANT}}{\Gamma_{L,Z_0}(Z_0 - Z_{ANT}) + Z_0 - Z_{ANT}}. \tag{6.7}$$

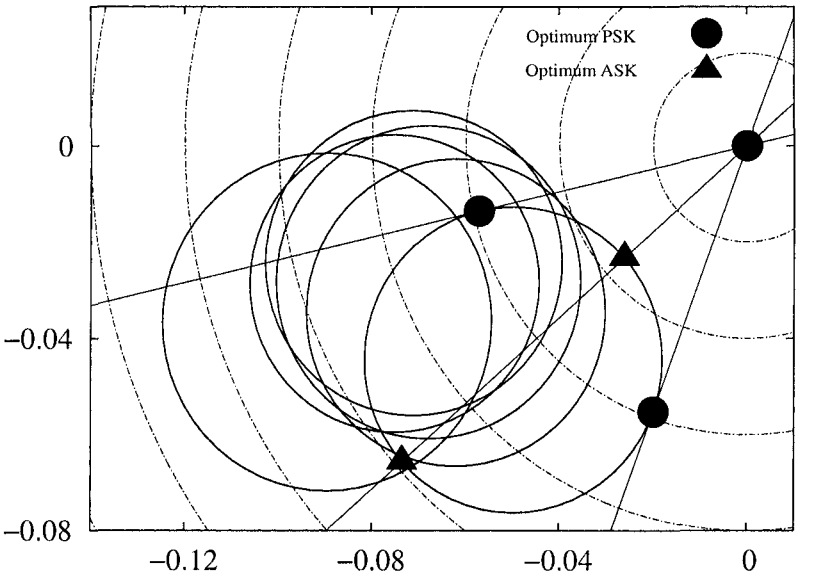

Fig. 6.6. Modulation circles in the reflection coefficient space for folded dipole antenna.

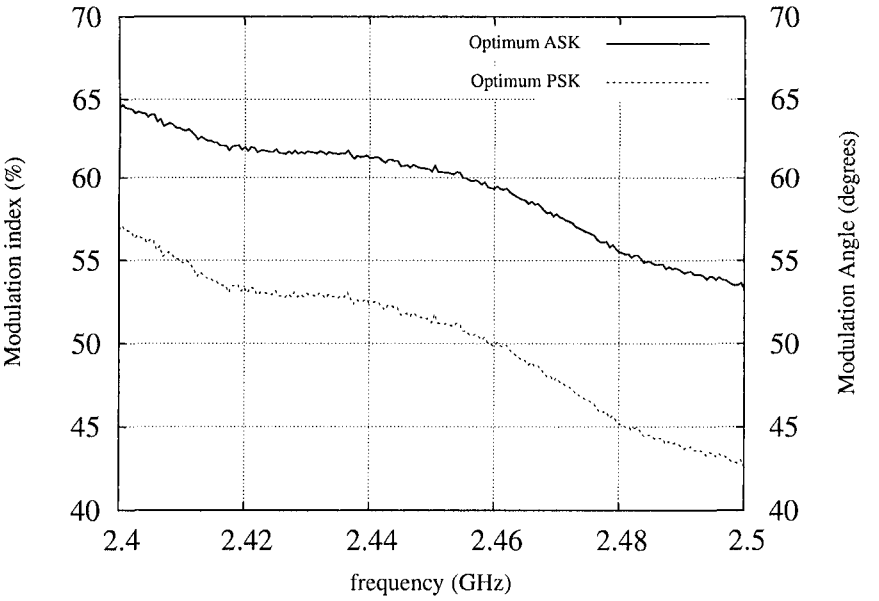

Fig. 6.7. Modulation performance for folded dipole antenna.

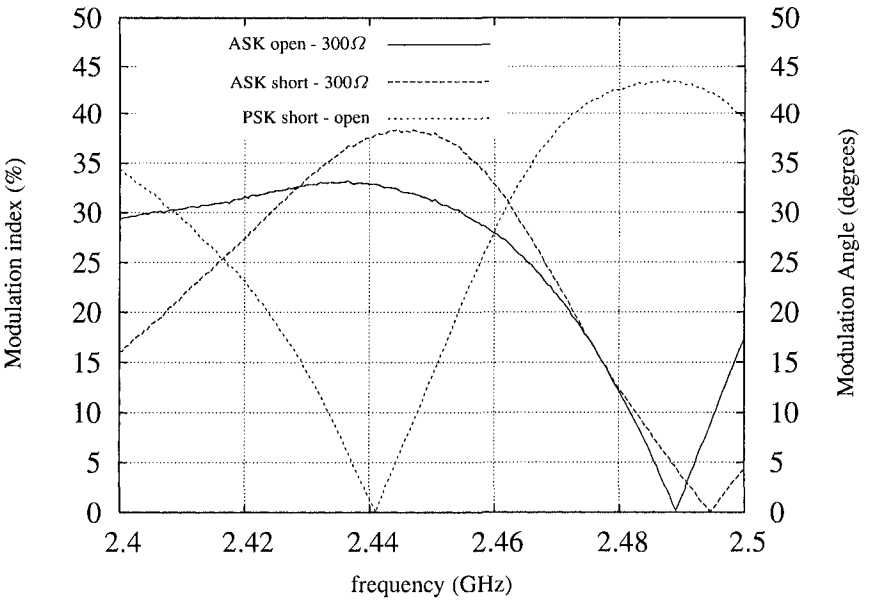

Fig. 6.8. Modulation performance for particular impedances

Graphically, it corresponds to the transformation of Fig. 6.9 into the polar chart of Fig. 6.10 for $Z_0 = 50\,\Omega$ and $Z_{ANT} = 290 - j180\,\Omega$.

The second step is obtained using Eq. (6.5). The A and B values depend on the antenna. As proposed by Hansen [29], A corresponds to the *structural* Radar Cross Section (RCS) and B is the *antenna* RCS. From Eq. (6.5) we have for $\Gamma_{IN,Z_{ANT}}$:

$$\Gamma_{IN,Z_{ANT}} = A + B\Gamma_{L,Z_{ANT}}. \tag{6.8}$$

Eq. (6.8) corresponds graphically to shrinking the modulus of $\Gamma_{L,Z_{ANT}}$ as well as a rotation if $\Im(B) \neq 0$. The graphical effect of A is a translation in the complex plane of $\Gamma_{IN,Z_{ANT}}$. Fig. 6.11 is the result of the transformation of the polar chart of Fig. 6.10 through Eq. (6.8) using the practically obtained value (see Section 6.3) $A = -0.11278 - j\,0.0037419$ and $B = -0.08041 + j\,0.079831$. Due to the reflection coefficient definition (6.7) and that $Z_{ANT} \notin \Re$, $\Gamma_{L,Z_{ANT}}$ has no physical meaning in terms of power reflection. As a result, $|\Gamma_{L,Z_{ANT}}|$ can be bigger than 1 [38].

The $\Gamma_{IN,Z_{ANT}}$ chart of Fig. 6.11 still has to be normalized to $Z_0 = 50\,\Omega$, i.e. the impedance of the network analyzer used for the measurements. The result is shown in Fig. 6.12.

Using this method, one can see the transformation of any passive impedance at the tag side to the reader side. It is then possible to choose the optimal impedance values for backscattering modulation (see Section 6.4).

The chart of Fig. 6.11 is valid at one frequency and at a given distance between the tag and the reader. The distance d has an effect on the magnitude and argument

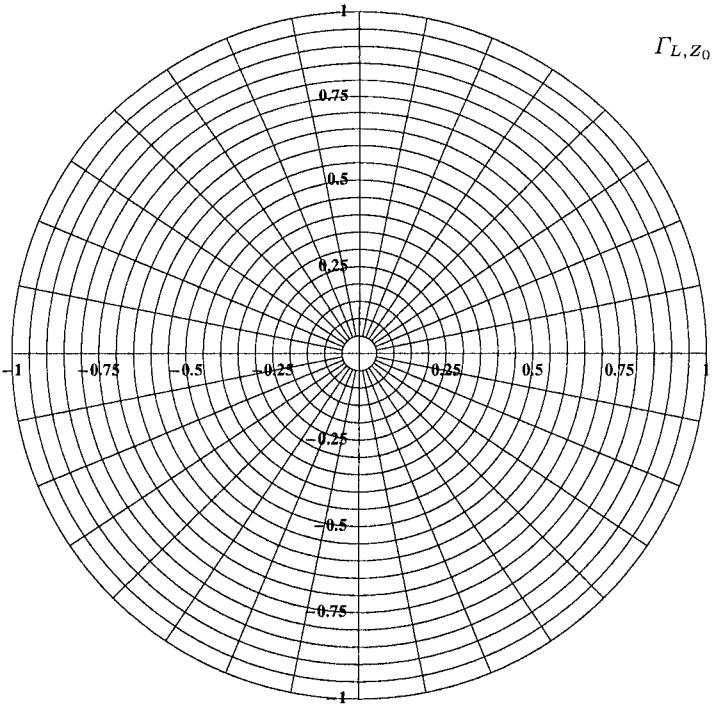

Fig. 6.9. Γ_{L,Z_0} polar chart

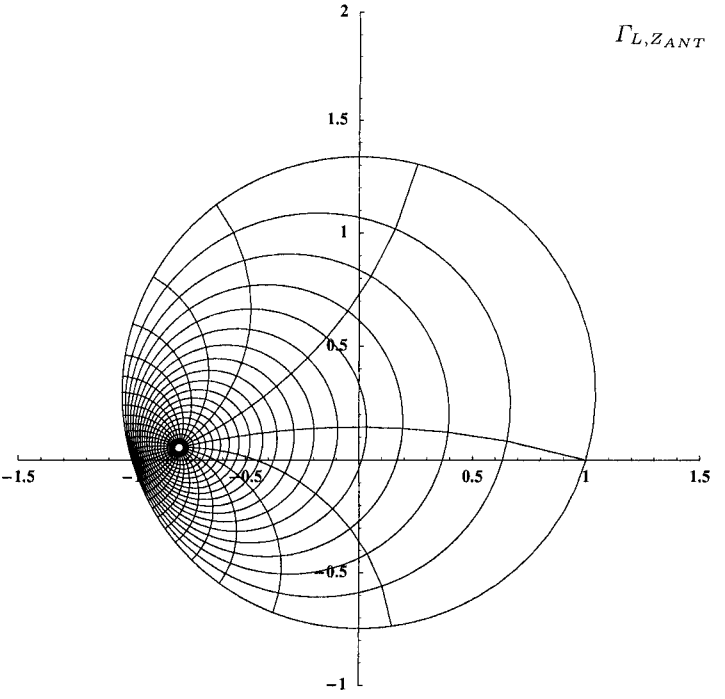

Fig. 6.10. $\Gamma_{L,Z_{ANT}}$ polar chart

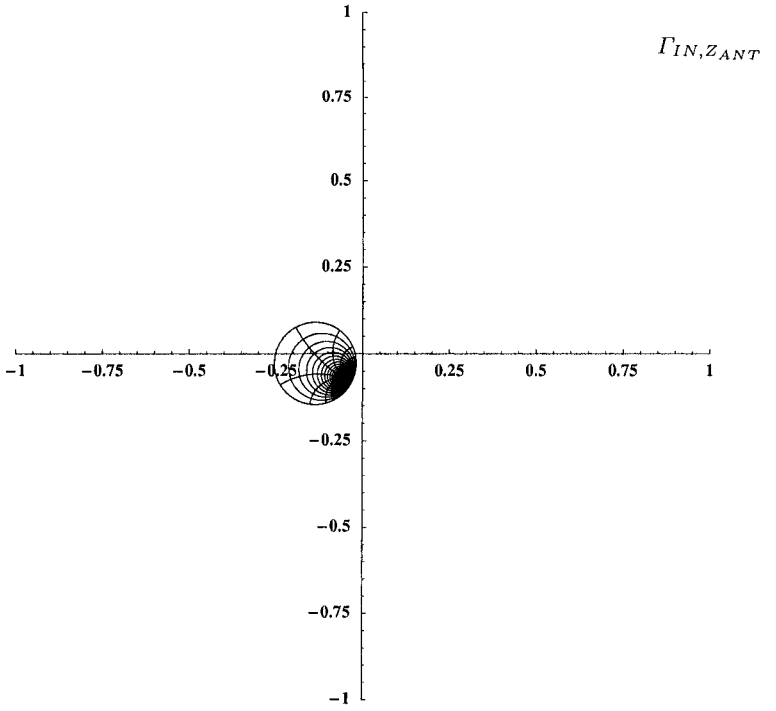

Fig. 6.11. $\Gamma_{IN,Z_{ANT}}$ polar chart

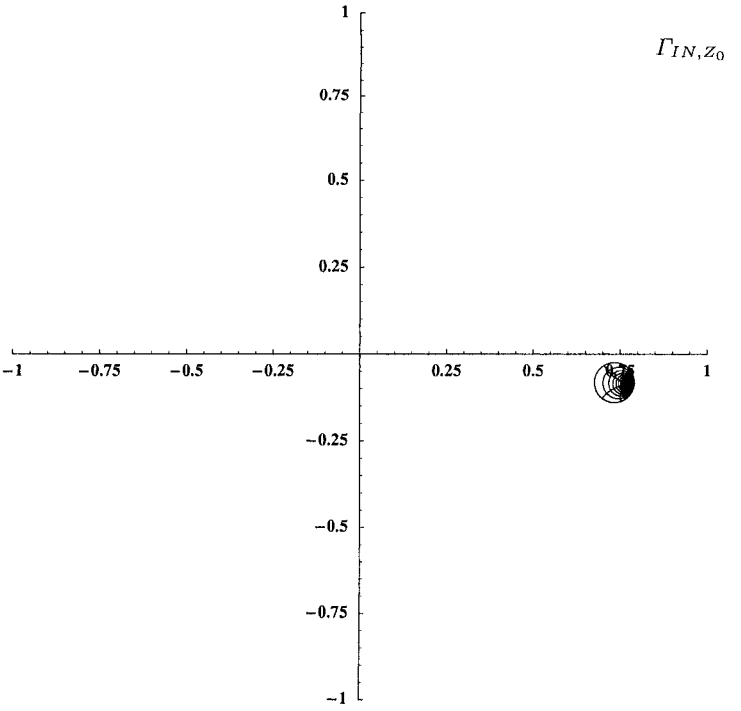

Fig. 6.12. Γ_{IN,Z_0} polar chart

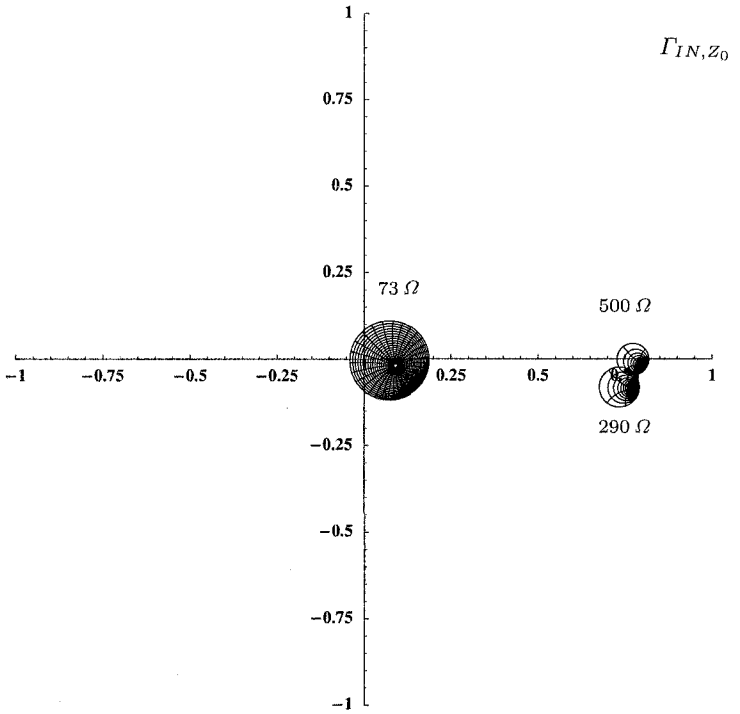

Fig. 6.13. Γ_{IN,Z_0} polar chart with the usual parameters except the tag impedance antenna set to 73 Ω, 290 Ω and 500 Ω.

of both A and B. The magnitude diminishes with d^{-2} and the argument varies with respect to the wavelength over distance ratio.

6.6 Impact on Wireless Power Transmission

In chapters 2 and 3 it was shown that the tag antenna impedance should have a high radiation resistance in order to maximize the input voltage amplitude at the rectifier. The method obtained in this chapter allows the analysis of the impact of this radiation resistance on communication quality.

In Fig. 6.13, we can see that the radius of the tag polar chart at 73 Ω is much bigger than the one obtained with 290 Ω or 500 Ω. This clearly shows that a strict trade-off exists between the wireless power transmission and the backscattering communication.

6.7 Conclusion

A practical procedure was described to measure the modulation performance of a setup composed of a reader antenna and a tag antenna. This approach can be used in the design of UHF RFID systems when choosing the backscattering modulation impedances. Furthermore, it brings insight into the impact of the tag modulator characteristics on the interrogator architecture design as well as on the communication quality itself.

It should be mentioned that the material presented in this chapter is the result of research that was conducted after the design of the chip. Chapter 7 as well as chapter 8 do not take the presented results into account although the choices that were made are in good agreement with these.

7

RFID Tag design

This chapter takes advantage of the previous one to define the specifications at the system level of an RFID tag. The operational principle as well as the communication protocol chosen in the hereafter developed system are presented. The different building blocks and their design issues in light of low power consumption are described. Finally, the chapter concludes with the antenna choice and the experimental results [5].

7.1 UHF and μwave RFID circuit state-of-the-art

THE vast majority of today's available RFID tag ICs operate in the UHF band, i.e. 900 MHz. Table 7.1 lists examples of RFID tags from different industrials. All these products share similar forward and backward link communication techniques. This is a consequence of today's standards (see section 4.5). In terms of reading range, the ST XRA00 product leads the race with 10 m or 27 μW of necessary available power from the antenna. Atmel ATA5590 is not far behind, which is not surprising since both input impedances are very similar and the two circuits operate at the same voltage. It has to be mentioned that the Zuma design from Impinj achieves 8 m of read *and write* distance. According to [39], these performance are made possible using the Self-Adaptive Silicon (SAS) approach.

In the 2.45 GHz band, three products are industrially available (see Table 7.2) and one research work from Atmel shows a practical realization [33]. Both the EM4222 from EM and Philips Ucode are dual frequency systems. As can be seen in the Hitachi μ chip, at microwave frequencies the operating range is dramatically reduced compared to the UHF band. This is the result of input parasitics mainly due to the technology. Using a thinner CMOS process or insulated wafers (SOI) would reduce parasitics and improve the performance.

Table 7.1. Industrial passive tag products operating at 900 MHz

Model	Process	Input impedance Ω	Read distance m 4 W EIRP	Forward link	Backward link	Power at antenna μW	V_{DC} V
Atmel ATA5590	0.5 μm CMOS Schottky	$6.7 - j \cdot 210$	9.5	PWM 5-80 kbits/s	ASK, PSK 5-80 kbits/s	30	1.5
EM Micro. EM4222	0.5 μm CMOS Schottky	n/a	n/a	PWM <256 kbits/s	ASK <256 kbits/s	n/a	1
Impinj Zuma	0.25 μm CMOS SAS	n/a	8 r/w	PWM 40/80 kbits/s	FSK	42	n/a
Philips Ucode	n/a	n/a	7	ASK 40 kbits/s	AM (ASK) 40 kbits/s	55	n/a
ST XRA00	CMOS	$6.7 - j \cdot 197$	10	PWM 15-70 kbits/s	FSK 30-140 kbits/s	27	1.5

Table 7.2. Industrial passive tag products operating at 2.45 GHz

Model	Process	Input impedance Ω	Read distance m 4 W EIRP	Forward link	Backward link	Power at antenna μW	V_{DC} V
EM Micro. EM4222	0.5 μm CMOS Schottky	n/a	1	PWM	ASK	380	1
Philips Ucode	n/a	n/a	1.8	(ASK)	(ASK)	117	n/a
Hitachi μ chip	0.18 μm CMOS	60	0.4	n/a (none)	ASK	2200	0.5
Atmel Research	0.5 μm CMOS Schottky	$4 - j \cdot 89$	2.6	PWM	PSK	56	1.5

7.2 Tag specifications

The distance is clearly an important issue for RFID, but more generally for remotely powered devices. This work aims at maximizing this parameter. There are several aspects that influence this. At first sight, the carrier frequency is to be mentioned. Radio wave propagation tends to preach for the use of a UHF frequency band, e.g. 900 MHz. At this frequency, the per meter attenuation is indeed acceptable as can be shown using the Friis relation (see section 4.9). Secondly, to enable reader to tag communication and to comply with an ultra-low power approach, both a simple modulation scheme and a simple detection block are necessary. The envelope detector for pulse width demodulation represents a good compromise. Such a modulation scheme (see Fig. 7.1) implies a certain bandwidth that depends on the pulse width and on the shape factor (raised-cosine, etc.).

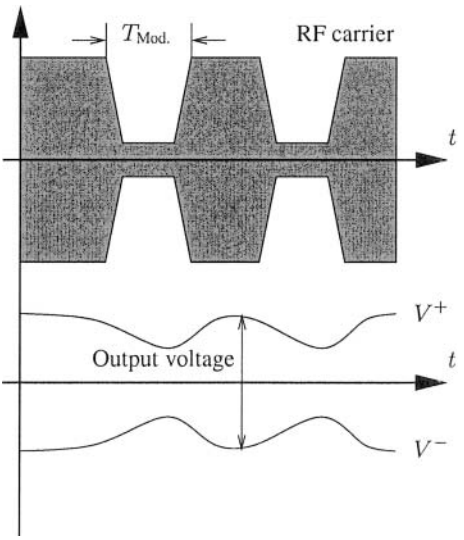

Fig. 7.1. Reader to tag waveforms and tag output voltage.

On one hand, if the modulation period $T_{\text{mod.}}$ is too large, no energizing signal is available on the tag side and the power supply could die. On the other hand, the period cannot be too small because of regulations and also because of the detectors receiving bandwidth. Therefore, a regulation/power consumption trade-off exists.

The Industrial Scientific and Medical (ISM) band at 2.45 GHz is interesting in this regard. The communication bandwidth there is rather large (about 80 MHz depending on the country) and it is widely available. Furthermore, the maximal Effective Isotropically Radiated Power (EIRP) is 4 W for indoor applications (see section 4.6).

The tag dimensions are also a central issue. It is well known that the antenna size scales with the carrier frequency. Again, microwave frequencies mean small

wavelengths and thus, a small antenna size. Different wavelengths for air propagation are shown in Table 7.3.

Table 7.3. Wavelengths for different frequencies (air propagation).

433 MHz	900 MHz	2450 MHz
70 cm	33 cm	12 cm

There are many antennas whose size depends on the half wavelength. Consequently, the 2.45 GHz band also inherently fulfills the small mechanical dimension constraints of the complete system (IC + Antenna + Packaging). The system specifications so far are summarized in Table 7.4. The operating range is difficult to specify

Table 7.4. Basic system specification.

Frequency	Available power	Size	Reader/Tag communication
2.45 GHz	4 W EIRP	5 cm × 1 cm Half wavelength antenna style	AM (short interrupts) with envelope detector at the tag side

without knowing the tag IC power consumption. We already know that there is a need for an envelope detector. The other blocks that are necessary to bring the tag to life are a rectifier to supply energy, a decoder to shape the received information from the reader, an oscillator, a modulator to enable backscattering communication, a power-on-reset and some control logic.

Part of our strategy to limit the power consumption of the tag is to avoid the use of an internal oscillator to clock the logic. As will be described in section 7.4.1, the clock signal is embedded in the emitted signal of the reader. This cuts significantly the power needed to charge all the logic gate capacitances at a constant rate. In other words, the tag developed in this work is a kind of state machine that operates *synchronously* with the reader. The biggest power consumption of this circuit will thus come from the oscillator when modulating the input impedance.

The power distribution pie chart of Fig. 7.2 where P_{NO} is the power consumption of the tag building blocks (without rectifier) during normal operation summarizes the situation.

The rectifier conversion efficiency η_c (see chapter 3) corresponds to the internal losses that occur during AC to DC conversion. It is given by

$$\eta_c = \frac{P_{NO}}{P_{in}}. \tag{7.1}$$

where P_{in} is the power that effectively enters the rectifier.

To introduce the power available from the antenna P_{AV}, it is mandatory to consider the power matching losses at the antenna/tag interface. One could use the overall

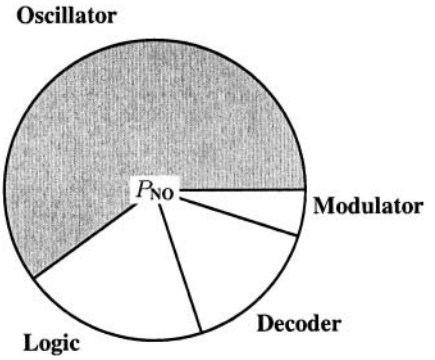

Fig. 7.2. Power distribution pie chart.

efficiency factor η_o but the reflection coefficient is preferred here. As a result, the following relation holds

$$\begin{aligned} P_{in} &= P_{AV}\left(1-|\Gamma|^2\right) \\ \Rightarrow P_{AV} &= \frac{P_{NO}}{\eta_c\left(1-|\Gamma|^2\right)} \end{aligned} \tag{7.2}$$

Using Eq. (7.2), we can compute the maximal operating range. For the distance d, the Friis relation holds and its value is given by

$$d = \frac{\lambda}{4\pi}\sqrt{G_t\frac{P_{EIRP}}{P_{AV}}} \tag{7.3}$$

where G_t is the tag antenna gain and λ the RF carrier wavelength. Eq. (7.3) represents the maximal *operating* distance which is not always equal to the communicating distance. The latter also depends on the reader receiving sensitivity. It is possible that even if the tag is working, the communication cannot take place because the return signal lays below the receiver sensitivity.

Eq. (7.3) is plotted in Fig. 7.3 using the specifications of Table 7.4, a 0 dB tag antenna gain, perfect matching between the antenna and the tag IC and 100% conversion efficiency. The curve represents the theoretically achievable ranges whereas Eq. (7.2) constitutes the design constraints for the tag IC in order to maximize the operating range.

As seen in chapter 3, a three stage modified Greinacher rectifier typically achieves 50% of conversion efficiency at an output power of about 20 μW. Using the developed model of the same chapter, such an output power corresponds to an input resistance on the order of 1 kΩ and an input capacitance of about 500 fF. The value of Γ for a 300 Ω folded dipole antenna can be computed at 2.45 GHz and is equal to

$$\Gamma \approx -0.63 - j0.65 \tag{7.4}$$

and the mismatch loss factor η_L is thus

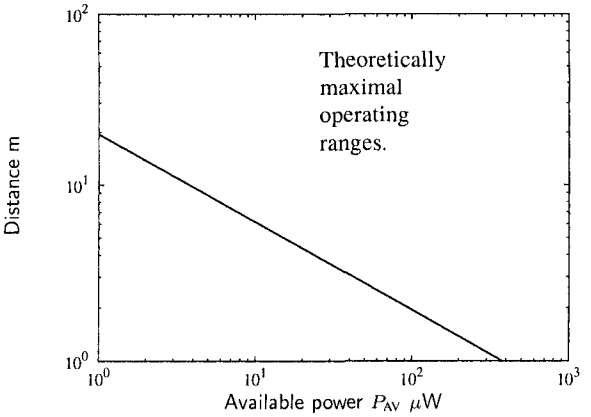

Fig. 7.3. Maximal achievable operating range.

$$\eta_L = 1 - |\Gamma|^2 \approx 17\%. \tag{7.5}$$

When the input capacitance of 500 fF is inductively matched, the loss factor rises to 29%.

There are, therefore, many losses due to impedance mismatch. By taking these into account, Eq. (7.3) becomes

$$d = \frac{\lambda}{4\pi}\sqrt{G_t \cdot \eta_c\,(1 - |\Gamma|^2) \cdot \frac{P_{EIRP}}{P_{NO}}} \tag{7.6}$$

which is plotted in Fig. 7.4 with and without inductive matching.

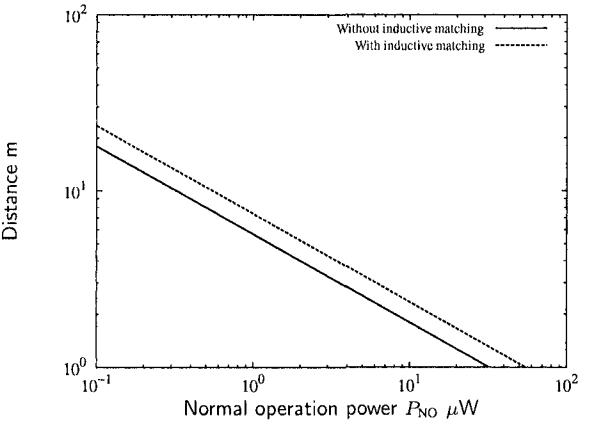

Fig. 7.4. Operating range taking typical losses into account.

Fig. 7.4 indicates that for a normal operation power consumption of 20 μW, the operating range reaches about 1.25 m, and raises to about 8 m for an operating power of 1 μW. These values are about one decade below the theoretical maximum. It is partly due to the rectifier conversion efficiency which cannot be easily increased since it mainly depends on the technology and the input power level. But the losses due to mismatch can be compensated to a certain extent. For example, the input capacitance can be reactively compensated either by proper PCB design or antenna design. This issue is discussed in section 7.7.

Concerning the tag-to-reader communication, the backscattering technique introduced in chapter 4 is used. In chapter 5, the pseudo-PSK modulation scheme was introduced as a good trade-off in terms of Bit Error Rate (BER) and power management. Moreover, this backscattering modulation technique is particularly suited to the input impedance nature of the rectifier. The only condition is to compensate for the reactive part of the input due to the capacitance.

Using what has been said, the system specifications can be established and their corresponding values are presented in Table 7.5.

Table 7.5. System specification.

Parameter	Value	Comment
Frequency range	2.4-2.4835 GHz	
Available power	4 W	4 W EIRP indoor in EU & US 0.5 W EIRP indoor & outdoor in EU.
Tag power consumption	<20 μW	
Size	5 cm×1 cm	Half wavelength antenna style
Read distance	1.25 m	That's arbitrary. It makes more sense to maximize this parameter.
Reader-to-tag communication	AM	
Tag-to-reader communication	pseudo-PSK	see chapter 5.

7.3 Technological issues

The goal of this work is to maximize the read range of a tag or more generally, a WPT system. The block that mainly limits the operating range is the rectifier. Without a power supply, even a sub-μW circuit is of no help! The sensitivity of the rectifier is defined as the minimal input voltage that allows an output voltage build-up. As seen in chapter 3, this event occurs when the current $i_D(t)$ flowing in one rectifying device integrated over one signal period T is equal to zero. Mathematically it is given by

$$\int_0^T i_D(v_D(t))\,\mathrm{d}t = 0, \tag{7.7}$$

where $v_D(t)$ corresponds to the voltage at the rectifying device.

From Eq. (7.7), it is clear that the $i_D(v_D)$ characteristics and as a consequence the technology should propose a low off-current I_{off}, a low threshold voltage V_t and a small sub-threshold slope S in order to improve the rectifier performance. Both a low I_{off} and a low V_t affect the sensitivity. A small V_t also makes low-power operations possible which is, of course, of importance to the present application. A small sub-threshold slope S increases the conversion efficiency since a small voltage amplitude variation on the device implies a bigger current drive (see Fig. 7.5).

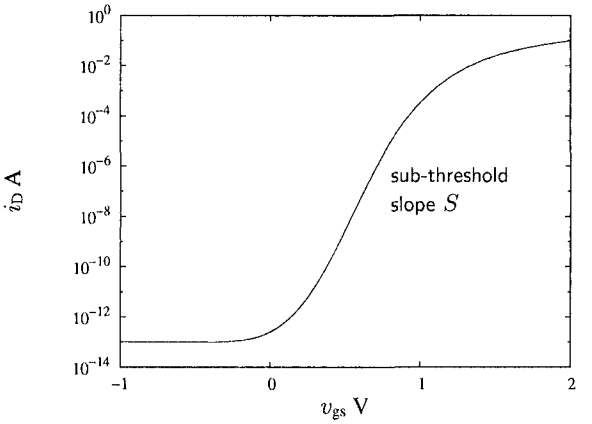

Fig. 7.5. Typical drain current i_D versus gate-source voltage v_{gs}.

Finally, microwave frequencies place high demands on the IC/antenna interface. A technology with low parasitics is thus desirable. The circuit realized in this work has been fabricated in a Silicon-On-Sapphire (SOS) technology [40]. This process offers a sub-threshold slope $S = 70$ mV/dec that is close to the theoretical limit value of 63 mV/dec for CMOS [41]. It also allies low V_t devices and excellent high frequency performance. Table 7.6 compares various device characteristics in the light of wireless power transmission.

Table 7.6. Comparison of various device characteristics for WPT applications

	SOS	Bulk Si	SOI	Bi-CMOS
High frequency performance	++	-	+	+
Low-power	++	-	++	–
Sub-threshold slope	++	+/-	+	+

The cost of sapphire wafers is greater than standard bulk Si but according to [42], their Ultra-Thin Silicon (UTSi) process uses fewer masks than performance equivalent bulk CMOS processes, ensuring competitiveness is maintained.

7.4 Operational principle

In the present work, a polling procedure is chosen to reduce complexity during implementation and testing. It is described in section 4.11.

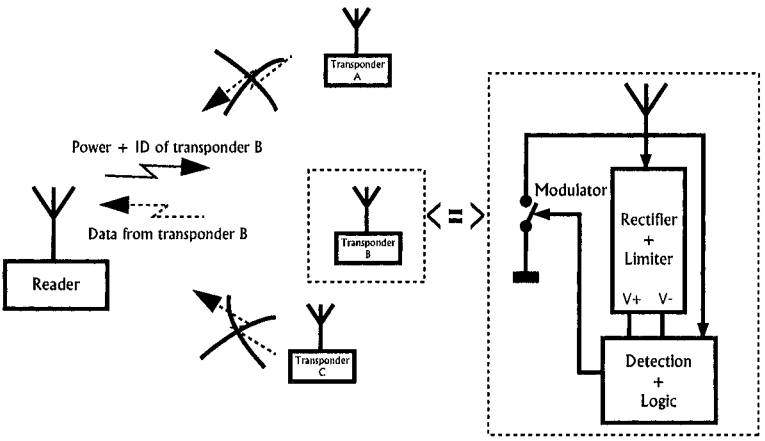

Fig. 7.6. Operational principle.

The general application framework is shown in Fig. 7.6. The concept is to address a group of hard-coded passive transponders in order to wake up only one of them. The reader sends an N-bit serial number and only the transponder that contains this serial number wakes up. All others switch to quiet mode. If a transponder with the emitted serial number is found, it starts modulating its input impedance to enable backscattering communication with the reader. The latter can then establish a communication with the tag and verify, for example, its serial number to check if it matches the one sent. As will be shown, every step in a communication session is reader controlled. Transponders that retrieve their operating power from the reader's transmitted energy thus operate in a master-slave configuration.

7.4.1 Communication protocol

Before describing the building blocks of the transponder, it is necessary to explain the protocol developed for this application. The present application was not intended to implement today's available standard [43, 24] although it could easily be modified to be compliant. The very low power available at the transponder side limits the

embedded intelligence. As a result, every step in a regular session is completely controlled by the reader. A successful session is split into three parts: the power-up mode, the addressing mode and the reading mode.

Power-up mode

A reader radiates high frequency power in the direction of one (or many) transponder(s). The power captured by the transponders' antennas is rectified and energizes the circuits. It is during the power-up mode that a Power-On-Reset (POR, see Fig. 7.7) occurs, turning the transponders to the *addressing mode*.

Addressing mode

In this mode, all the transponders that are within the interrogating zone wait for the reader information. The reader polls a serial number that is saved by all transponders. If a transponder successfully detects its serial number, it switches to the *reading mode* and modulates its input impedance so that the reader can detect its presence. All other transponders go into *quiet mode* where they wait for a power-off and possibly, a new interrogating procedure. In this configuration, no collision occurs since only one transponder should wake up. In the unlikely case where two or more tags respond, the reader should be able to detect the collision and restart the procedure.

To send a particular address, the reader generates a series of short RF interrupts, typically 200 ns (see Fig. 7.7). This duration cannot be too long since an RF interruption means an immediate voltage supply drop that could trigger a POR or a power off. The Start Bit is always equal to a logical "1" and corresponds to only one RF interrupt. For the following bits, the reader sends two RF interrupts if the emitted bit has the same logical value as the preceding one and only one otherwise (see Fig. 7.8). Like the interrupt duration, the gap between two successive interrupts is about 200 ns. The time between two successive bits has to be greater than twice this duration, i.e. > 400 ns.

The interrupt durations have to be short enough to avoid a power off of the circuit; there is a trade-off between this value and the charging capacitors Cv (see Fig. 7.9). Such a modulation choice offers the advantage of a very simple implementation, i.e. very low power consumption at the transponder side, at the cost of bandwidth. This can be solved by using a modulation signal profile that offers the least amount of side band spectrum, e.g. a sinusoidal profile.

Reading mode

Only the individual transponder that receives its serial number jumps to this mode. At this time, the control logic locks the shift register and turns on the Intermediate Frequency (IF) oscillator (square form). The oscillating signal switches on and off the modulator and as a result, the front-end impedance seen by the antenna is modulated at an IF rate.

The reader detects the reflected signal and is aware of the presence of a tag in its interrogating zone. In other words, the tag has acknowledged its presence and its data

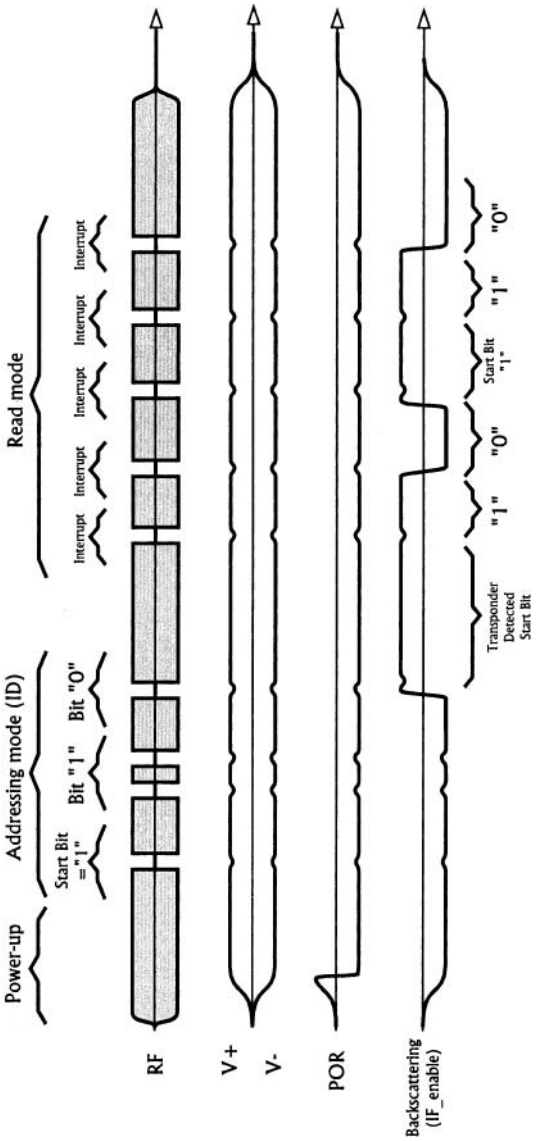

Fig. 7.7. Complete datagram of a communication session.

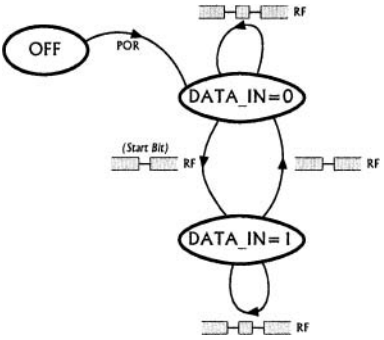

Fig. 7.8. State chart of the decoder.

can now be read bit by bit. The reader sends short RF interrupts similar to the Start Bit. The tag receives and decodes these interrupts that clock the shift register whose output is the next bit of information. If the next bit is a "1," the transponder keeps the IF oscillator on and the reader detects the backscattered signal. If the next bit is a "0," the oscillator is turned off and the reader detects the lack of backscattered signal. In that sense, no backscattering modulation occurs during "0" bits. The reason for this solution is because of the unstable IF oscillator frequency. No IF frequency tuning procedure was integrated in the IC or the protocol. The reader is thus responsible for locking on the IF frequency using a control loop. As one can imagined, this limits the achievable data-rate (see chapter 8). For each received interrupt, the transponder cycles its shift register and the reader can verify that the serial number sent matches the received one. For this particular work, the transponder sends its ID upon the reader's request but other data could be communicated depending on the application.

A comprehensive example session for a 3-bit transponder is drawn in Fig. 7.7. The code sent by the reader is $1 - 1 - 0$. After sending the code, the reader generates 3 interrupts to cycle the 3-bit transponder shift register.

7.5 Transponder architecture

Fig. 7.9 shows a block diagram of the transponder IC. A folded dipole antenna is the only external component of the system. It is connected to the circuit using 2 bond wires. Such an antenna has been chosen as will be described later for its naturally high radiation resistance (300 Ω). Passive transponders retrieve their energy by rectifying the incoming electromagnetic RF wave. This energy is then stored in storage capacitors to obtain a DC power supply. An RC detector allows data transmission from the reader to the transponder. When enough energy powers up the circuit, a power-on-reset is sent to the logic blocks. The transponder then "listens to" and decodes the incoming AM modulated signal as described previously.

The transponder architecture is rather simple compared to other communication systems. The only RF parts are the modulator, the envelope detector and the rectifier

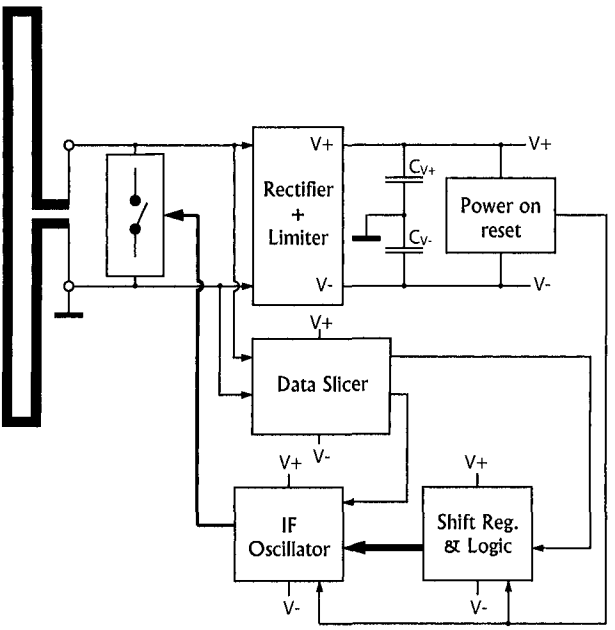

Fig. 7.9. Architecture of the system.

(and the antenna of course). As shown in chapter 5, the modulator design in terms of input impedance is a central issue to achieve acceptable communication quality.

7.6 Transponder building blocks

7.6.1 Rectifier and limiter

The rectifier and the voltage limiter are shown in Fig. 7.10. The rectifier consists of a three-stage full-wave voltage doubler cascade. The rectifying devices are diode-connected transistors with low threshold voltage, low reverse current and low parasitic capacitance. The negative wave rectification is made possible using a fully depleted silicon-on-insulator technology. This yields a higher rectifier efficiency at the cost of needing a differential structure for the other blocks.

In order to avoid a voltage over-drive, a limiter is added at the output of the rectifier (Fig. 7.10). An RC controlled loop (T3+T4) shorts the rectifier's output when the middle voltage exceeds two threshold voltages (T1+T2). Such a voltage regulation has the advantage of simplicity. The disadvantages are that for high received power, i.e. for low communication distances, the transistor pair will drive a quite high current that will dramatically reduce the input impedance seen by the antenna and thus, the modulation depth. Fortunately, in this case, backscattering communication is still possible since the range is rather small. The resistor Rl and the capacitor Cl are

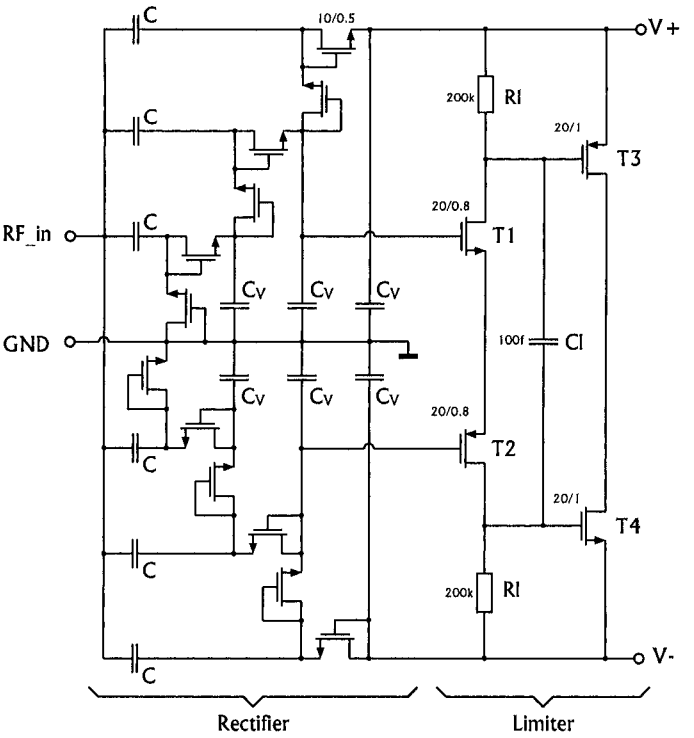

Fig. 7.10. Rectifier and limitation circuit schematic.

designed to match a reasonable damping ratio of the control loop to avoid oscillations of the power supply for the power dynamic range.

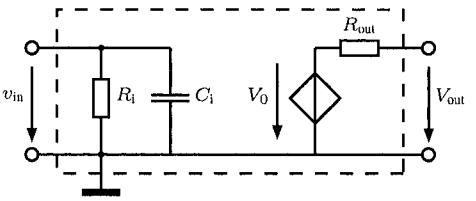

Fig. 7.11. Equivalent circuit for the rectifier.

The rectifier is a key block in every remotely powered system. A thorough study is available in chapter 3 and in [4] in which the circuit of Figure 7.11 models the rectifier fabricated in a given technology as an input and output impedance as well as a voltage controlled voltage source. The model allows the prediction of the power needed to supply a given DC output current at a constant output DC voltage. Furthermore, it provides the rectifier input and output impedance. If the input capacitance C_i is

inductively compensated, the input voltage amplitude $\widehat{v_{\text{in}}}$ is equal to

$$\widehat{v_{\text{in}}} = 2\sqrt{2P_{\text{AV}}R_{\text{s}}}\frac{R_{\text{i}}}{R_{\text{i}}+R_{\text{s}}} \tag{7.8}$$

where P_{AV} is the available power from the antenna and R_{s} is the real part of its impedance. From Eq. (7.8), it is clear that to increase $\widehat{v_{\text{in}}}$, one has to increase R_{s} while simultaneously keeping $R_{\text{i}} = R_{\text{s}}$, i.e. power matching. This is necessary in order to increase the performance of the rectifier.

The global rectifier efficiency defined as

$$\eta_{\text{o}} = \frac{\text{DC Output Power}}{\text{Incident RF Power}} \tag{7.9}$$

as well as the conversion efficiency

$$\eta_{\text{c}} = \frac{\text{DC Output Power}}{\text{Incident RF Power-Reflected RF Power}} \tag{7.10}$$

can also be calculated using the model. Based on [44], the minimal input power for a 3-stage rectifier with a 300 Ω radiation resistance antenna is equal to -16 dBm for an output current consumption of 1 μA. This power value could be reduced with better impedance matching (see section 7.7.1).

7.6.2 Power-on-reset

The power-on-reset circuit in Fig. 7.12 is composed of a cross-coupled pair of transistors and a NOR gate. It is a non-stable system and when the circuit powers up, one branch (T_1, T_3 or T_2, T_4) takes the advantage over the other. The NOR gate compares the two gate signals insuring a power-on-reset for the logic blocks. The capacitor C

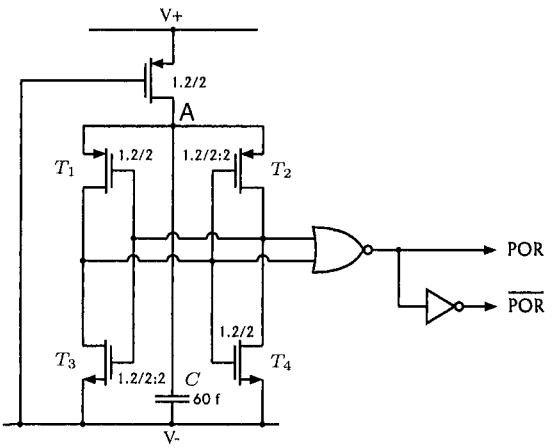

Fig. 7.12. Power-on-reset circuit schematic.

allows a slow charging of node A to force a delay between the rise of the voltage supply and the power-on-reset. In addition to this, it damps the circuit to avoid parasitic oscillations.

7.6.3 Detector, Data slicer and Decoder

The detector (Fig. 7.13) consists of an envelope detector and an averaging filter. The diodes in the detector are realized using low threshold voltage diode-connected transistors. In the fabrication process we used, the devices do not show significant temperature sensitivity.

Signals Venv and Vref correspond respectively to the envelope and the rectified average of the received RF signal. Signal Venv clocks the transponder and signal Vref allows voltage comparison in the decoding process.

When RF_in rises, the capacitor Ca charges to the RF envelope (see Fig. 7.13). When RF_in falls, Ca discharges through the resistor Ra due to the inverse current of the diode-connected transistor (or through the antenna if it is shorted at DC). The components' values are chosen to get a time constant within a few ns in order to follow the RF envelope Venv. The diode is designed so that its reverse current is high enough to discharge sufficiently rapidly the capacitor Ca.
Capacitor Cc and its touching diodes generate the signal Vref. Both diodes in series can be considered as a voltage divider. When RF_in rises, Cc charges down to the half amplitude voltage of the RF envelope signal. When RF_in falls, the retained voltage on Cc slowly reduces due to the inverse current of its parallel diode, which acts in this case as a parallel resistance.

The regeneration of signals Venv and Vref is realized by the data slicer in Fig. 7.13. The signal G_n (generated by the control logic, see Fig. 7.14) is tied to V- during addressing mode. When Venv is higher than Vref, CK1 rises to V+ and the D-flip-flop toggles since its logic has been designed to be sensitive to the rising edges.

The decoding process is ensured by the circuit of Fig. 7.13 following the state chart of Fig. 7.8. After the power-on-reset, the Data_in signal is 0. The start bit has to be a 1 (see Fig. 7.8) so that one RF interrupt is sent and the Data_in signal toggles to 1. This start bit is then registered and the rest of the ID is then sent as described in section 7.6.4.

In the reading mode, the input impedance is modulated in amplitude at an IF rate. As a consequence, the input RF amplitude varies and undesired bits could possibly be detected, decoded and registered. To prevent this, a transistor inhibits the data slicer when G_n goes high. The output signal of the decoder CK1 is thus always low.

System considerations

The radio system bandwidth B in this case is rather high since the envelope detector is not selective. An AM signal whose carrier is at 100 MHz or 5 GHz can be detected by the circuit. The upper limit is due to the fabrication process. The limiting bandwidth

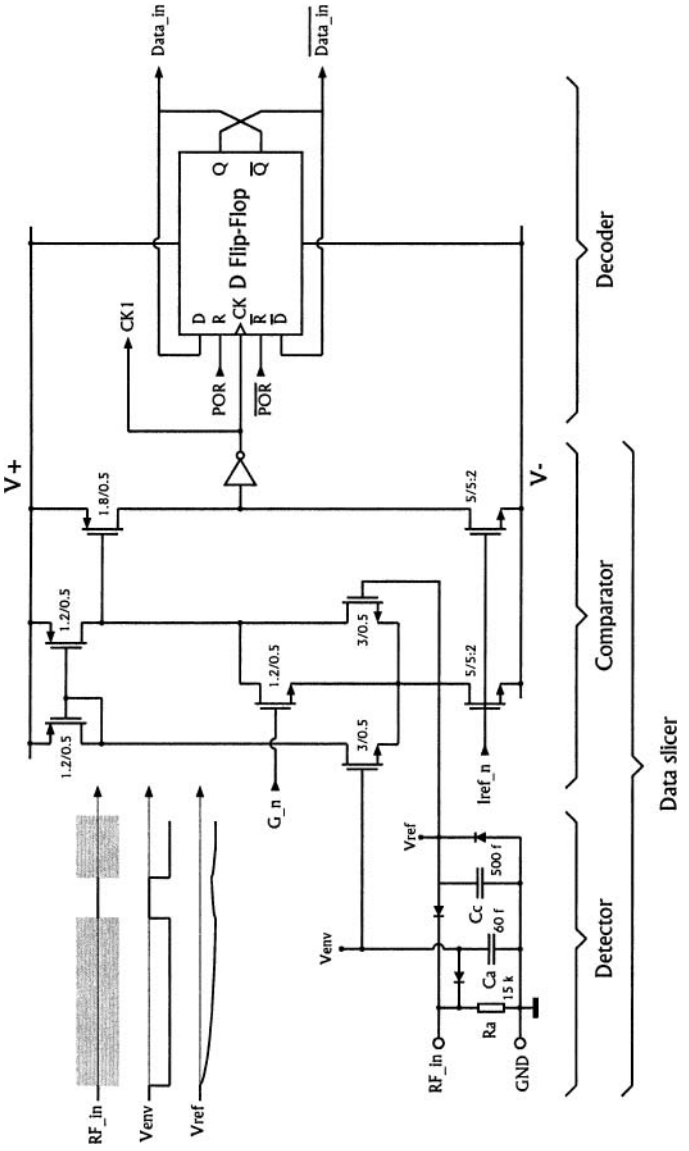

Fig. 7.13. Detector, data slicer and decoder schematic.

factor in this architecture is thus the antenna. According to [45], the Signal-to-Noise Ratio (SNR) at the input to the receiver is

$$SNR = \frac{G_t P_{EIRP} \lambda^2}{kT_A B(4\pi d)^2}, \tag{7.11}$$

where k is Boltzmann's constant, TA is the antenna temperature, G_t is the transponder antenna gain, P_{EIRP} is the emitted isotropically radiated power at the interrogator, λ is the carrier wavelength and d is the interrogator-to-tag distance. The SNR degradation due to envelope detection is

$$SNR_{out} = SNR_{in} \cdot \frac{2m^2}{2+m^2}, \tag{7.12}$$

where m is the modulation depth of the AM input signal.

Table 7.7. Receiver typical parameters.

Parameter	Value
λ	0.12 m
P_{EIRP}	4 W
G_t	1
T_A	300 K
B	100 MHz
k	1.38e-23 J/K
m	100%

Using the typical receiver parameters of Table 7.7, the SNR at the output of the envelope detector in dB is equal to

$$SNR_{out} = 89.4 - 20 \log d. \tag{7.13}$$

From Eq. (7.13), the SNR_{out} at 10 m is equal to 69.4 dB. Even with a 20 dB mismatch at the transponder input, the SNR at 10 m still achieves 29.4 dB. The forward link in passive RFID applications is thus not a problem. The voltage supply is really the limiting block in the system.

7.6.4 Shift register and logic

The shift register (SR) of Fig. 7.14 is responsible for loading the received bit of information from the decoder (Data_In). The POR signal sets the SR state to a logic "0." In this case we used a 3-bit SR but its depth can be increased to suit particular needs or an EEPROM can be used to avoid the programming pads. In addressing mode, Data_enable and Data_out are low. CK2 is thus equal to IF, i.e. the oscillator output

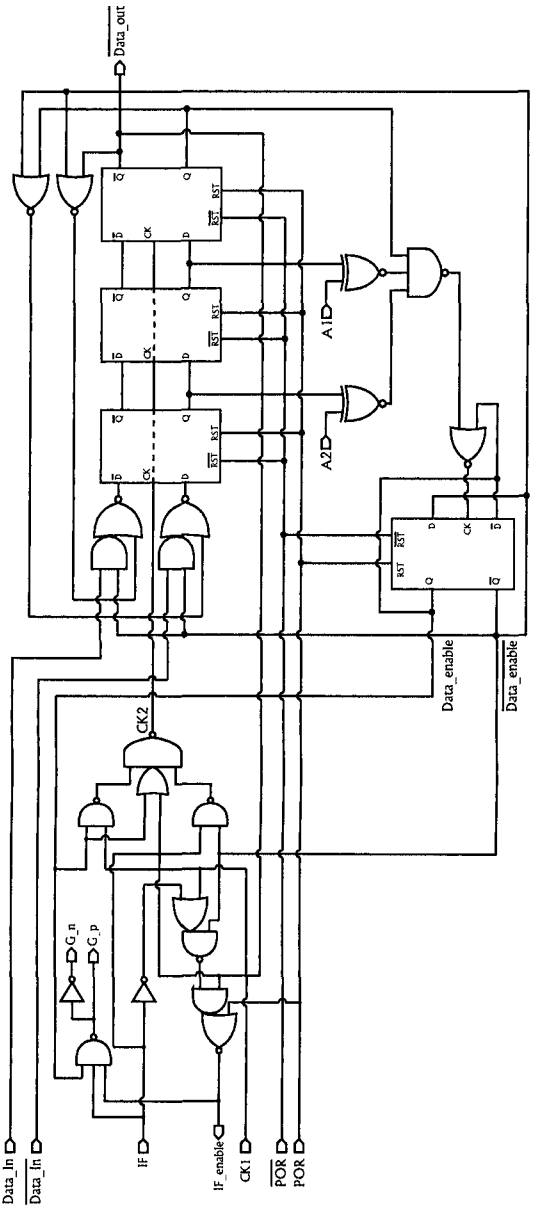

Fig. 7.14. Control logic and shift register schematic.

which operates as a mono-stable trigger in this mode (see section 7.6.5). The received bit Data_in is thus registered during each rising edge of the IF signal. The address of a transponder is programmed using the input A1 to A2. If the received address doesn't match the programmed one, Data_enable stays low, Data_out goes high (since the Start_Bit is always equal to "1") and CK2=1, i.e. no future bit is registered in the SR. In this case, the transponder enters the *quiet mode* until the RF signal vanishes.

If a matching code is received, the Data_enable flag turns on and the following control logic switches the IF oscillator on (IF_enable goes high) to establish the communication with the reader. Both signals G_n and G_p toggle the ASK modulator between its short and open configurations. The transponder is in the reading mode and CK2=$\overline{CK1}$. Furthermore, the SR operates in closed-loop, i.e. its output goes directly to its input. A communication session can start and at each rising edge of CK2 (or falling edge of CK1), the SR shifts its bits to the right. If Data_out is high (or low), IF_enable is high (or low), the IF oscillator is started (or stopped) and the communication session follows the protocol described in section 7.4.1.

7.6.5 IF Oscillator

The IF oscillator schematic is presented in Fig. 7.15. Depending on the logic state chosen, it can operate as an a-stable or mono-stable trigger circuit.

Mono-stable behavior (Addressing mode)

After power-on-reset, IF_enable is in the 0 logic state and the voltage V_C on the capacitor C is 0. When IF_enable rises up to V+ (or logic 1, see the datagram in

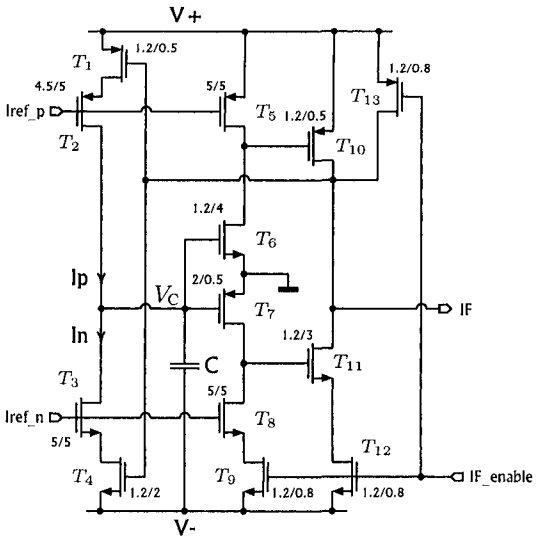

Fig. 7.15. IF oscillator schematic.

Fig. 7.16), T13 is switched off, T12 and T11 switch on and IF drops to V-. Due to the current Ip drawn from T2, V_C rises from V- up to the threshold voltage of T6 . At this point, T6 switches on, T10 starts to conduct and IF switches to V+. Simultaneously, T1 switches off, T4 switches on and In draws the charges from the capacitor C. As a result, V_C drops down to 0.

In this mode, the charging time of the capacitor C is slightly higher than the half oscillation period in a-stable mode since the capacitor charges from V- up to the threshold voltage of T1. This allows sufficient detection time before registering the received bit in the shift register at the rise of CK2 (equal to IF in this mode of operation).

A-Stable behavior (Reading mode)

In this mode, the starting phase is identical to the mono-stable behavior except that IF_enable is kept high. Hence, V_C doesn't drop to 0 but to the threshold voltage of T_2. At this point, T_1 and T_2 conduct and IF goes low. Simultaneously, T_1 switches on, V_C rises and the cycle continues until IF_enable drops to V-.

The IF oscillator is used to generate the modulation signals G_p and G_n. The oscillating signal delivered by this circuit presents two problems. Both *the central frequency* and *the duty cycle* of the output signal, which are controlled by the threshold voltages of transistors T_1 and T_2, the value of C, and the reference current Iref, strongly depend on the technology. The detection at the reader side is thus more challenging and is beyond the scope of this chapter (see section 8). Typically, the reader IF filter must have a wider bandwidth. Hence the noise power level at the demodulator input is higher and diminishes the reader sensitivity. One solution to this issue is to use a narrow-band IF filter that sweeps its central frequency through the receiving bandwidth.

7.6.6 Modulator

This is a key part of the backscattering communication principle used in this system. It enables the tag-to-reader communication by varying the impedance presented to the transponder's antenna in order to modulate the reflected power. Two modulation types are possible: phase and amplitude modulation. In PSK, the available power to the tag is kept constant during both modulation states. This could be an advantage over ASK. However, the process of absorbing power in PSK makes it impossible to achieve a 180° modulation angle (between the two modulation states). As a result, the communication in terms of Bit Error Rate (BER) is degraded. In fact, there exists a strict trade-off, which is detailed in chapter 5, between the power available to the tag and the power devoted to the communication.

To maximize the operating range, a low duty-cycle pseudo-PSK RF modulation has been chosen (see chapter 5). This means that the modulator can be realized using a simple switch if the reactive elements are compensated. Total power reflection occurs when the switch is closed. When open, the reflected power P_r is equal to the difference between the available power from the antenna P_{AV} and the absorbed

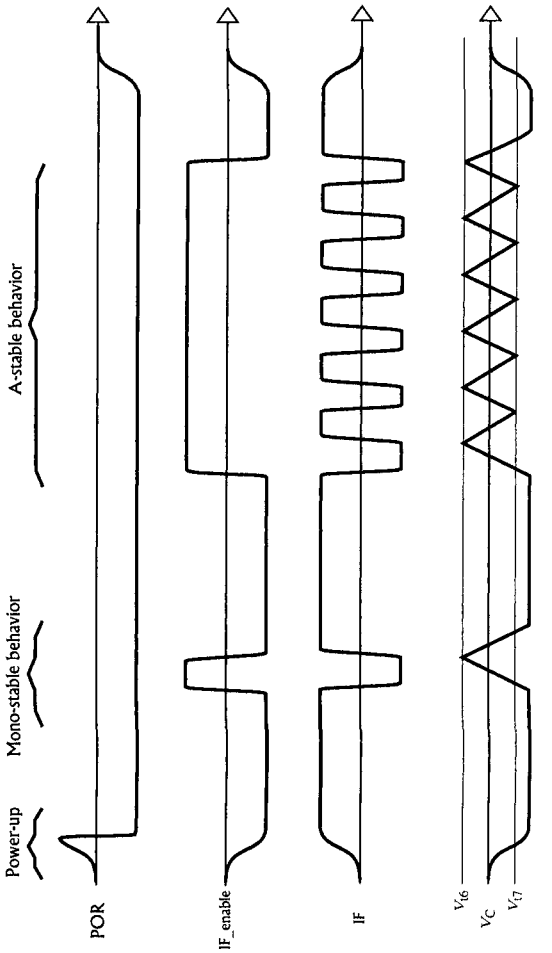

Fig. 7.16. Datagram for the IF oscillator.

power. It is thus dependant on the transponder power consumption P_{DC} divided by the rectifier's overall efficiency η_o, i.e.

$$P_r = P_{AV} - \frac{P_{DC}}{\eta_o}. \tag{7.14}$$

One can conclude from Eq. 7.14 that to maximize the distance d_M between the two modulation states, P_{DC} should tend to zero (see Fig. 7.17). This case is of course not realistic and as a result, the communication quality is slightly degraded (see chapter 5).

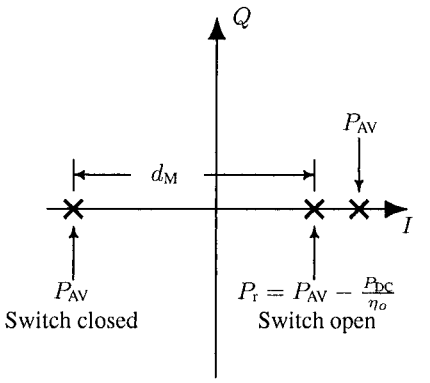

Fig. 7.17. Pseudo-PSK constellation diagram.

The parasitic capacitance can be taken into account when designing the matching network (or the reactive part of the antenna). Practically, the switch is realized using two minimal-length and simulation-optimized-width MOS transistors in parallel (see Fig. 7.18). Both transistors are controlled by the signals G_n and G_p.

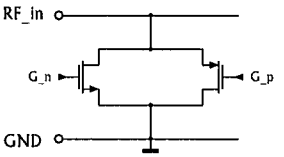

Fig. 7.18. Parallel modulator schematic.

7.6.7 Current reference

The current reference of Fig. 7.19 is used to bias the different blocks in the circuit. It consists of 2 PMOS transistors T_1 and T_3 forming a first current mirror of ratio 1:1. T_2 and T_4 NMOS transistors operate in weak inversion and have a $1{:}K$ current ratio. Neglecting transistor mismatch, the voltage V_R that appears on resistor R is equal to

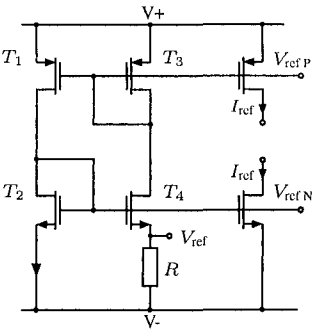

Fig. 7.19. Current reference block diagram.

$$V_R = U_T \ln K \tag{7.15}$$

and the current $I_{\text{ref.}}$ is thus given by

$$I_{\text{ref}} = \frac{U_T \ln K}{R}. \tag{7.16}$$

T_2 and T_4 have to operate in weak inversion. If operating in strong inversion, I_{ref} becomes much more sensitive to process and temperature variations [16]. This structure is especially suited for ultra-low power applications since very low current can be obtained by choosing a high value for R. Furthermore, by changing the resistor R to an active load, I_{ref} becomes much less sensitive to temperature variation. It is described in [16], [46].

7.7 Antenna

7.7.1 Transponder input impedance

The transponder input impedance is mainly influenced by the rectifier. Its impedance is composed of an imaginary part due to the parasitic capacitances and a real part that depends on the output current consumption. The other blocks of the RF front-end (the detector and the modulator) bring a small contribution.

As shown in [4] and section 7.6.1, to optimize the power transfer from the reader to the transponder it is necessary to have a high antenna radiation resistance as well as power matching. This scales the antenna voltage level for a constant received power and allows us to reach the rectifier sensitivity with less power. However, an upper limit exists due to parasitics that appear in parallel at the input of the rectifier. They limit very rapidly the real impedance level at the input and thus the global power efficiency at high frequencies. For that reason, SOI technology offers a clear advantage over standard bulk processes thanks to the high resistivity substrate.

At low received power, inductive matching can be added to resonate with capacitance C (see Fig. 7.20). In this case, optimum power transfer between the antenna

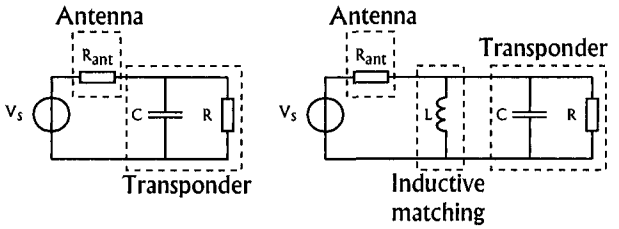

Fig. 7.20. Impedance matching for the transponder.

radiation resistance R_{ant} and the input resistance R is achieved if they two are equal. As a result, the global efficiency of the RF front-end increases. The inductance can be realized in conjunction with the antenna design with no added cost in terms of fabrication.

In section 7.8, the operating ranges for a transponder with and without inductive matching (see Table 7.9) for different antenna types are compared.

7.7.2 Choice of antenna

There are several types of antennas that can be used with a high frequency transponder. The choice is closely related to the target application [27]. Patch antennas are well suited for metallic objects since it is possible to make use of their bodies as a ground plane. Inverted-F antennas are also mountable on such objects [47]. Other types of materials, e.g. wood, cardboard, etc. also allow differential antennas. These antennas offer the advantages of higher radiation resistance compared to single-ended versions, and of less capacitive losses. As shown in [4], [44] and section 7.6.6, higher radiation resistance is desirable.

The folded dipole presents a radiation resistance of about 300 Ω, representing a significant improvement compared to a simple $\lambda/2$ dipole. The 3-wire folded dipole [48] can be used to raise this value. In that case, the radiation resistance takes on values of $540 - 2000\ \Omega$ according to [48]. Unfortunately, input parasitics do not allow such values due to finite quality factors of the matching elements. Moreover, the global communication bandwidth diminishes when the impedance level increases so that a compromise has to be found. For the circuit of this particular work, an impedance level of 300 Ω resulted in the best performance in terms of operating range.

7.8 Experimental results

A version of the circuit has been realized in a fully depleted silicon-on-sapphire technology [14]. This competitive process offers low threshold voltage CMOS transistors, a clear advantage for remotely powered devices[42]. The isolated devices present a low parasitic capacitance compared to a standard bulk process.

The chip micro-photograph is shown in Fig. 7.21. As can be seen in this figure, there is no ElectroStatic Discharge (ESD) protection on the pads. ESD protection

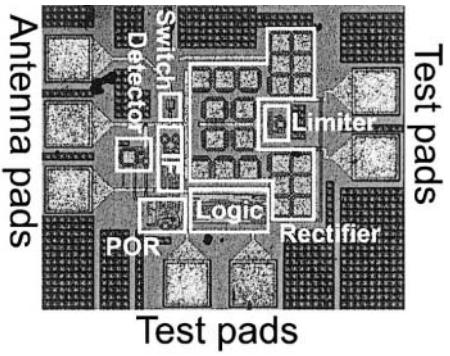

Fig. 7.21. Die micro-photograph (size: 400 μm×550 μm without the test pads).

brings too many parasitics at the antenna and results in power losses. The die area without test pads and only two antenna connection pads is about $400\mu\text{m} \times 500\mu\text{m}$, but can be reduced. The layout of the RF front-end has to be done with particular care, i.e. parasitic capacitances should be minimized. Extracted layout simulation is essential in order to estimate and reduce parasitics that are directly connected to the antenna.

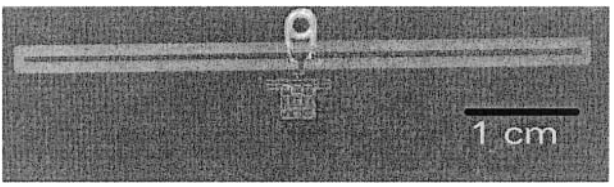

Fig. 7.22. Picture of the complete 2.45 GHz transponder.

A complete transponder is shown in Fig. 7.22. The antenna is optimized for 2.45 GHz. Its radiation resistance is approximately 300 Ω with a 2 dB gain.

An estimate of the maximal operating range can be calculated as follows. Simulations have shown that the minimal operating conditions for the tag circuits are: 600 mV & 200 nA in non-transmitting mode. In these conditions, the values of the power supply parameters are given in Table 7.8. For a 300 Ω antenna, this voltage

Table 7.8. Tag minimal operating conditions.

$\overline{V_D}$ mV	$\widehat{v_{in}}$ mV	R_i kΩ
50	120	>5

Table 7.9. Operating range for different antenna types

Frequency MHz	Antenna	Range m
2450	$\lambda/2$-dipole	6
2450	$\lambda/2$-dipole with inductive matching	9
2450	folded dipole	7
2450	folded dipole with inductive matching	12

$\widehat{v_{in}}$ corresponds to an available power P_{AV} of 6.74 μW. Based on Friis formula, with 2 dB gain antenna, this power is available at a distance of 9.52 m.

The measured operating ranges at 2.45 GHz are summarized in Table 7.9. It appears that the tag was still responding at 12 m with an acknowledgement bit. This result confirms that the model of chapter 3 is slightly pessimistic.

The distance could be increased by using a smaller operating frequency, e.g. 900 MHz. In this case, the achievable distance can be more than doubled.

7.9 Conclusion

This chapter presents the design of a remotely powered addressable UHF RFID transponder. Using state-of-the-art analysis and design techniques, a SOS 0.5-μm CMOS technology and inductive matching between the antenna and the transponder, an operating range of at most 12 m with 4 W EIRP transmitted power was achieved.

The system complexity is principally on the reader side (master-slave architecture). The available functions on the tag side are kept to a minimum with the goal of ultra-low power consumption. However, if a higher amount of power is necessary for a given application, this circuit is still usable at the cost of a smaller operating range.

Table 7.10. Operating range for 4 W EIRP 2.45 GHz RFID systems.

Range	Modulation type	Reference
1.8 m	n/a	[25]
2.6 m (Calculated value)	PSK	[33]
12 m	pseudo-PSK	This work

State-of-the-art RF design allowed us to reach an operating range of 12 m. This is an important improvement compared with the available technologies today at 2.45 GHz [33], [25] (see Table 7.10).

8

High frequency interrogator architecture and analysis

This chapter presents the UHF reader architecture that was used for the RFID system development. The distortion due to the direct coupling between transmitting and receiving antennas (or port-to-port isolation in a circulator-based architecture) is analyzed in detail. The phase noise impact is studied. The noise figure as well as the gain distribution is presented. Finally we conclude with the obtained results and possible improvements.

8.1 Introduction

THE interrogator or reader is a key part of a passive RFID system. It is responsible for many tasks such as powering the transponders in its interrogating zone and orchestrating the communication. As seen in section 4.11, the communication is either transponder-driven or interrogator-driven. In this work, we consider an interrogator-driven approach; more precisely, we're dealing with a polling architecture.

8.2 Communication protocol

The interrogating procedure is based on the operational principle described in section 7.4. From the interrogator point of view, it can be broken down into five steps:

i. Switch on the powering signal (RF carrier) and wait for the rectifier output voltage rise time.
ii. Poll the tag with a given code.
iii. Sweep the RF frequency until the down-conversion of the returning signal is coherent (or coherent enough to demodulate the data). Lock on the frequency

that output the maximal data power (RSSI)[1]. If no data power is available, it means that no transponder is in the interrogating zone or that an error occurred. In this case, go to step v.

iv. Transmit the pulses to cycle the transponder shift-register and simultaneously demodulate the received signal using the pulses as a reference sampling time.

v. Switch the RF off when all the data are received.

As explained in the previous chapter, an intermediate frequency (IF) is used. The data signal modulates this IF signal using OOK.

The IF signal is, unfortunately, unstable because of process variation. To solve this issue, an RSSI-based control loop is introduced at baseband before demodulating the OOK data (see section 8.9). The architecture thus belongs to the low-IF family.

8.3 Interrogator architecture description

The RF components necessary to satisfy the communication protocol are shown in the architecture of Fig. 8.1. The Voltage-Controlled Oscillator (VCO) generates the RF signal. It is on one hand amplified and radiated through the antenna. To enable interrogator-to-tag communication, the switch is used as a pulse modulator. On the other hand, the same RF signal (or carrier) is used to down-convert the returning signal backscattered by an individual transponder.

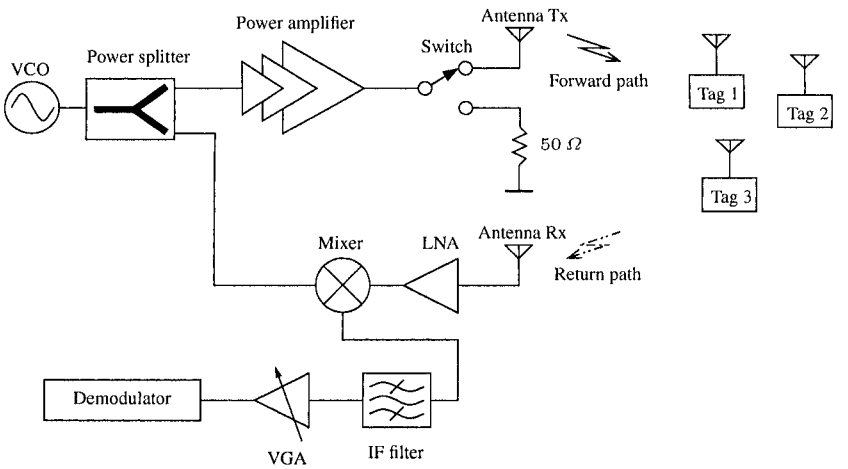

Fig. 8.1. Interrogator system architecture.

The architecture of Fig. 8.1 makes use of two antennas; i.e. one for the forward link and one for the return link. It is well known that the antenna is a reciprocal device,

[1]This occurs when a tag is present in the interrogating zone.

and with the help of a circulator, the architecture can be simplified (see Fig. 8.2). However, circulators are quite bulky devices, they cannot be integrated and their port-to-port isolation is typically 20 dB at 2.4 GHz [49]. The port isolation is central in this architecture as will be shown in section 8.4. At microwave frequencies, two parallel antennas typically present 30-40 dB of isolation. The circulator-based architecture is thus interesting at lower frequencies, e.g. at 900 MHz (UHF band) where high antenna gains are more costly in term of dimensions. For this reason, the antenna-based architecture was chosen for this work.

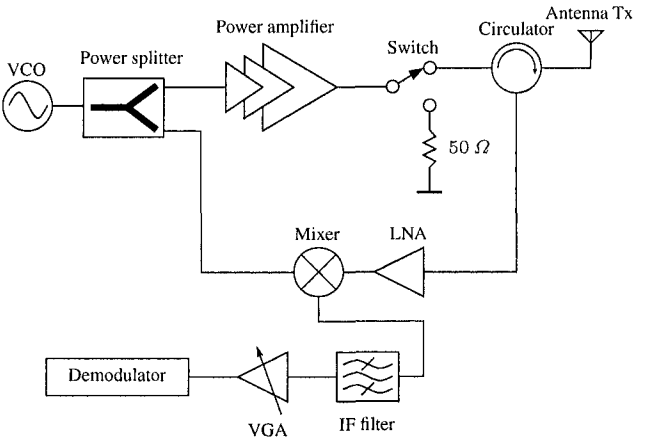

Fig. 8.2. One-antenna interrogator system architecture.

Interestingly, this architecture uses the same carrier for both transmission and reception. It is at first sight an advantage because the system could work with a free running oscillator. But upon closer inspection, this introduces a large interferer due to the antennas coupling (or circulator port-to-port isolation). The interferer level is rather high; about 0 dBm at 36 dBm EIRP. As a result, the receiver could be desensitized if not linear enough. This issue is studied in the next section.

8.4 Direct coupling

As described in [50], [51], a large interferer that lies within the receive band (see Fig. 8.2) can cause receiver desensitization resulting in a data signal loss. In the present case, this means a heavy distance reduction since the returning signal power decreases with the fourth power of the distance. This aspect is specified in terms of the third order interception point and is analyzed in the next subsection.

8.4.1 System input IP3

Signal distortion is a result of non-linearity in a system. The latter can be described by a time function

$$y(t) = \alpha_1 x(t) + \alpha_2 x(t)^2 + \alpha_3 x(t)^3. \tag{8.1}$$

Considering a large interferer $i(t) = A_I \cos(\omega t)$ and the returning signal in the form[2]

$$r(t) = A_R \left(\cos\left((\omega - \omega_d)t\right) + \cos\left((\omega + \omega_d)t\right)\right), \tag{8.2}$$

the inter-modulation terms at baseband for the system described by $y(t)$ are

$$IM = \alpha_1 A_R + \frac{9}{4}\alpha_3 A_I^2 A_R + \frac{9}{4}\alpha_3 A_R^3. \tag{8.3}$$

The term A_R^3 is negligeable and for this analysis we consider the worst case where α_3 is negative, i.e.

$$IM = \alpha_1 A_R - \frac{9}{4}\alpha_3 A_I^2 A_R. \tag{8.4}$$

When Eq. (8.4) is canceled, the system is desensitized and no data is transmitted. It occurs when the interferer amplitude reaches

$$A_I = \frac{2}{3}\sqrt{\frac{\alpha_1}{\alpha_3}}. \tag{8.5}$$

It is interesting to express the relationship between the interferer amplitude A_I and the system input IP3 $AIIP3$. From [51], we have

$$AIIP3 = \sqrt{\frac{4}{3}\left|\frac{\alpha_1}{\alpha_3}\right|}. \tag{8.6}$$

Substituting for α_3 we get

$$A_I = \frac{AIIP3}{\sqrt{3}}. \tag{8.7}$$

This occurs when the desensitization is theoretically complete. In reality, the system doesn't follow the function described by Eq. (8.1) but saturates at a certain input amplitude (this is what causes distortion). Because of this, Eq. (8.1) leads to a pessimistic estimation of $AIIP3$ and a certain amount of data power is still available.

Eq. (8.7) can be expressed in terms of power:

$$IIP3 \geq P_I + 4.8 \quad [\text{dBm}], \tag{8.8}$$

[2]For both BASK and BPSK modulation, the returning signal is either a Double-SideBand (DSB) signal or a DSB with carrier suppressed (DSB-CS) signal respectively.

where $IIP3$ is the system input IP3 and P_I is the power of the interferer. In this system, the typical antenna coupling at 2.45 GHz is 35 dB. Considering 36 dBm EIRP and an antenna gain of 15 dBi, the power at its input is 21 dBm. As a result, the coupled power at the receiver input is equal to

$$P_I = 36\,\text{dBm} - 15\,\text{dB} - 35\,\text{dB} = -14\,\text{dBm}. \tag{8.9}$$

Consequently, the system overall IIP3 has to be bigger than -9.2 dBm.

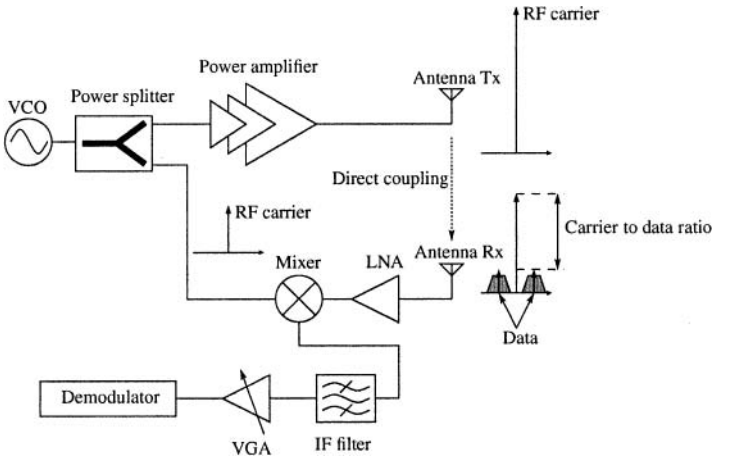

Fig. 8.3. Direct coupling phenomenon in the two antenna architecture.

Using the detailed architecture of Fig. 8.3, the received data power without baseband amplification is simulated for different antenna coupling as a function of the system IIP3 (represented by the amplifier in the schematic of Fig. 8.3).

The results in Fig. 8.4 show that the receiver linearity is a central issue. It also shows that a circulator-based architecture with 20 dB of port-to-port isolation (or direct coupling) is completely desensitized unless a highly linear system is realized. This can be a tough trade-off with the gain distribution.

8.4.2 Direct coupling compensation

Fig. 8.5 shows a simplified circulator-based architecture using a direct coupling compensation block. The idea is to cancel the direct coupled signal by generating its inverse before summing them up. As a result, only the signal returning from the tag is at the adder output. This block acts like a notch filter. Unfortunately, such a system is very sensitive to an attenuation mismatch between the two paths and even more to a phase difference. This sensitivity is illustrated in Fig. 8.6 where it can be seen that only a small error in phase or in amplitude quickly desensitizes the receiver part of the interrogator. Moreover, in practice, such a system is very tedious to implement at microwave frequencies.

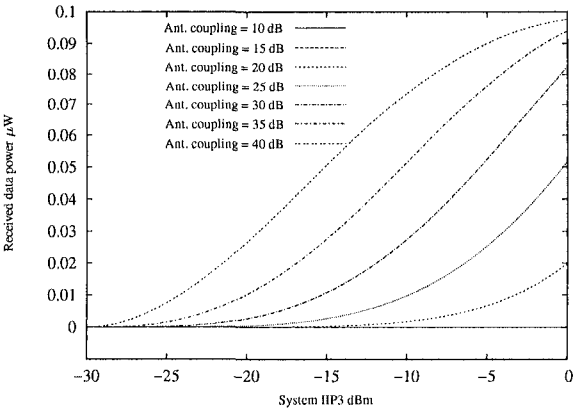

Fig. 8.4. Received data power versus the receiver IIP3 for different antenna coupling.

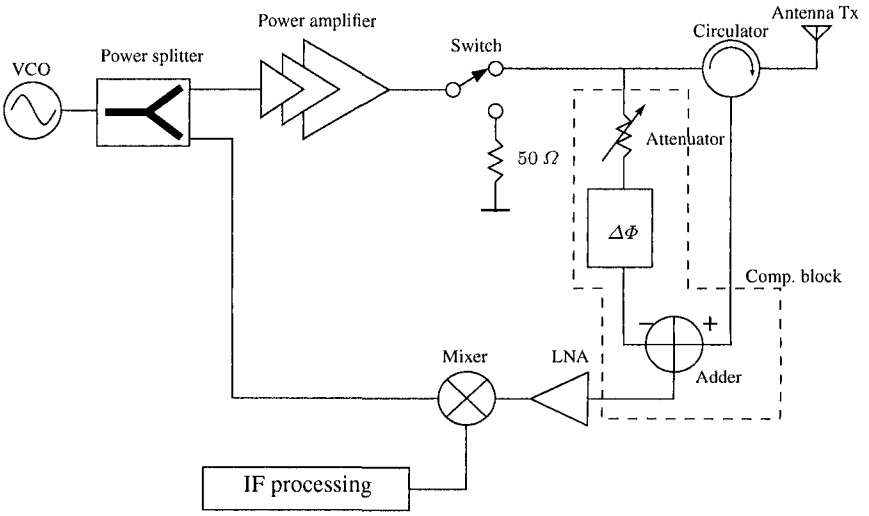

Fig. 8.5. Direct coupling compensation.

8.4.3 DC component suppression

Direct coupling implies the existence of a DC component at the output of the mixer. Its amplitude depends on the phase shift between the coupled and the LO signals. To suppress this unwanted signal, a second-order bandpass filter is introduced after the mixer. Its -3 dB bandwidth corresponds to the IF frequency spread due to the process, and to interrogator to tag distance variations. In the case of this work, the IF bandpass filter specifications are summarized in Table 8.1.

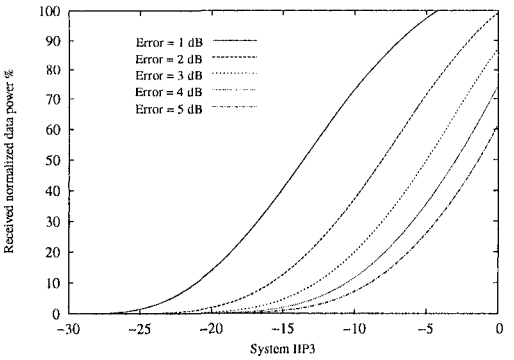

(a) Attenuation error

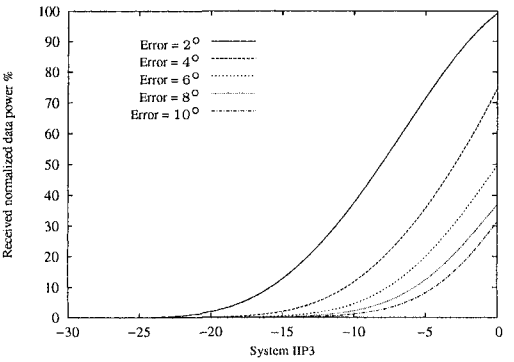

(b) Phase error

Fig. 8.6. The effects of attenuation and phase error on direct coupling compensation block.

Table 8.1. IF bandpass filter specifications

Parameter	Value
Type	Butterworth
Order	2
Center frequency	0.9 MHz
-3 dB bandwidth	0.6 MHz

8.5 Phase noise

8.5.1 Effect on down-conversion

In this section, we compute the noise introduced by the transmitter phase noise at the down-converted output (just after the mixer). As a basis, the following expression is used for the tone emitted at the antenna:

$$v(t) = A_v \cos\left[2\pi f t + \phi(t)\right] \tag{8.10}$$

where $\phi(t)$ corresponds to the VCO or frequency synthesizer phase noise. The signal at the receiving antenna is

$$r(t) = A_r \cos\left[2\pi f(t - 2\tau) + \phi(t - 2\tau) + \pi m(t - \tau)\right] \tag{8.11}$$

where $m(t)$ is the modulating signal (whose possible values are 0 and 1) and τ is the time delay due to the distance between the tag and the interrogator. At down-conversion, the signal of Eq. (8.10) and Eq. (8.11) are multiplied. The result is given by

$$\begin{aligned} s(t) &= A_r \cos\left[2\pi f(t - 2\tau) + \phi(t - 2\tau) + \pi m(t - \tau)\right] A_v \cos\left[2\pi f t + \phi(t)\right] \\ &= \frac{A_r A_v}{2} \cos\left[4\pi f \tau + \phi(t) - \phi(t - 2\tau) - \pi m(t - \tau)\right] \\ &+ \frac{A_r A_v}{2} \cos\left[4\pi f(t - \tau) + \phi(t) + \phi(t - 2\tau) + \pi m(t - \tau)\right] \end{aligned} \tag{8.12}$$

The effect of phase noise has to be analyzed in the signal bandwidth. Thus, the DC noise component due to phase error and the component at the double frequency are not taken into account. Using $S_\phi(f)$ as the Power Spectral Density (PSD) of $\phi(t)$, we can calculate the PSD of $\phi' = \phi(t) - \phi(t - 2\tau)$ using the usual linear system approach:

$$S_{\phi'}(f) = 2\left[1 - \cos(4\pi f \tau)\right] S_\phi(f) \tag{8.13}$$

At this point we can consider our signal to be

$$s(t) = \frac{A_r A_v}{2} \cos\left[\pi m(t - \tau) + \phi'(t)\right] \tag{8.14}$$

The constellation diagram of the signal without phase noise is composed of two points at $\pm\sqrt{E_b}$, where E_b is the symbol energy, as shown in Fig. 8.7. The noise adds a random phase component which rotates the data points on the circle with radius $\sqrt{E_b}$. This noise can be taken into account by finding the in-phase projection $\phi'(t)_I$ of the constellation point. This way, we get an additive noise component $n(t)$ equal to

$$n(t) = \phi'(t)_I = s(t) - \frac{A_r A_v}{2} \cos\left[\pi m(t - \tau)\right] = \pm(1 - \cos\phi') \tag{8.15}$$

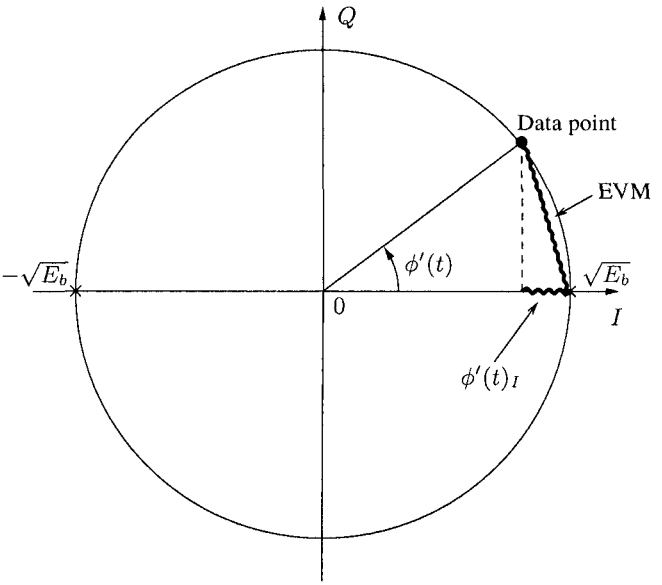

Fig. 8.7. Constellation diagram with phase noise and its in-phase projection for $m(t) = 1$.

It is difficult to find the SNR analytically because the phase noise ($\phi'(t)$) contributes to the output noise with the argument of a non-linear function. In order to get an underestimation of the SNR we use the Error Vector Magnitude (EVM) as an overestimation of the noise which is given by (8.15). The error vector is also shown in fig.8.7. It is clear that $|n(t)|$ is always lower than the EVM.

Considering the EVM, it is possible to write:

$$\langle n^2(t)\rangle \leq \sqrt{E_b}\left\langle \left[2\sin\frac{\phi'(t)}{2}\right]^2\right\rangle \approx \sqrt{E_b}\langle \phi'^2(t)\rangle \tag{8.16}$$

where the approximation holds for small angles[3].

If we use the known relation between phase noise and PSD of the phase ($L(\Delta f) = \frac{S_\phi(\Delta f)}{2}$) [52] and the following approximation for the phase noise

$$L(\Delta f) = \frac{k}{\Delta f^2} \tag{8.17}$$

the SNR can be calculated integrating the noise in the data bandwidth[4]:

[3]The small angle approximation could not be good enough for free running oscillators, but it is a reasonable hypothesis for PLLs.

[4]The factor E_b is present both in the signal component and in the noise and so it has no effect on SNR.

$$
\begin{aligned}
SNR = \frac{1}{\langle \phi'^2(t) \rangle} &= \left[2 \int_0^{\frac{B}{2}} S_{\phi'}(f) \mathrm{d}f \right]^{-1} \\
&= \left[8k \int_0^{\frac{B}{2}} \frac{1 - \cos(4\pi f \tau)}{f^2} \mathrm{d}f \right]^{-1} \\
&= \left[8k \cdot 4\pi\tau \int_0^{2\pi B\tau} \frac{1 - \cos(x)}{x^2} \mathrm{d}x \right]^{-1} \\
&\approx \frac{1}{32k\pi^2 B\tau^2}
\end{aligned}
\tag{8.18}
$$

The last approximation is possible by taking into account the magnitude of the upper limit of the integration interval; in the worst case (tag at a distance of 12 m) we have $2\pi B\tau \approx 0.05$ for a data bandwidth of 200 kHz and we can approximate the integrand function as constant and equal to 1/2 in this interval. In this worst case the SNR is

$$SNR \approx 70 \text{ dB} - k|_{\text{dB}} \tag{8.19}$$

With this equation it is possible to find the specification for the phase noise of the frequency synthesizer letting the SNR given by Eq.8.19 be much higher than the SNR due to other noise sources. The k parameter can be extracted from the phase noise spectrum in the following manner: one has to overestimate the phase noise in the bandwidth $\frac{B}{2}$ with (8.17). In this way system designers have a certain margin to consider the effect of phase noise negligible.

It should be mentioned that at longer distances, e.g. more than 20 m, the signal traveling time τ becomes important and the added noise due to the frequency synthesizer should be taken into account. However, power regulations usually limit the maximal operating range of a passive transponder. The phase noise issue thus shouldn't affect the performance.

8.5.2 Reciprocal mixing

Phase noise degrades receiver selectivity by causing down-conversion of signals located near to the desired frequency [45]. In Fig. 8.8, a Local Oscillator (LO) is used to down-convert the double-sideband signal to an IF frequency. Because of the presence of an unwanted signal, the LO phase noise located at an offset equal to the IF frequency is down-converted in the receive band (see the dark gray elements in Fig. 8.8). This process is called *reciprocal mixing*. In the case of the present work, the unwanted signal could come from a Bluetooth or WLAN transceiver. As a result, the maximum phase noise required to achieve a selectivity of S dB is given by

$$\mathcal{L}(f_m) = C[\text{dBm}] - S[\text{dB}] - I[\text{dBm}] - 10 \log B, \quad [\text{dBc/Hz}] \tag{8.20}$$

where C is the desired signal level, I is the unwanted signal level, and B is the bandwidth of the IF filter. Using Eq. (8.20), we can specify the phase noise of the LO. In our application, we consider only one interrogator, and as a result, the interferer or

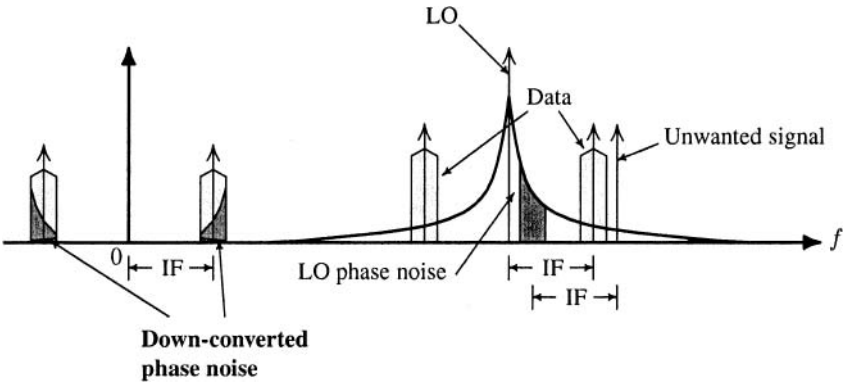

Fig. 8.8. Reciprocal mixing.

unwanted signal cannot come from another interrogator. If a multi-channel system is to be developed, the selectivity becomes critical and the carrier phase noise has to be specified.

8.6 Antenna noise temperature

Before analyzing the receiver, we consider here the noise received by the antenna. Antenna noise may be received from the external environment, or generated internally as thermal noise due to losses in the antenna itself [45].

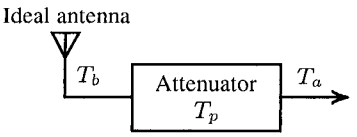

Fig. 8.9. Antenna representation using an ideal antenna followed by an attenuator.

An antenna can be represented by the equivalent system shown in Fig. 8.9. It is formed by an ideal lossless antenna with a brightness temperature T_b plus an attenuator with losses L. The overall noise temperature T_A appearing at the output terminals can be found by adding T_b and the equivalent noise temperature of the attenuator, both reduced by the attenuator loss

$$T_A = \frac{T_b}{L} + \frac{L-1}{L} T_p, \tag{8.21}$$

where T_p is the physical attenuator temperature. The brightness temperature T_b depends on the antenna direction. If looking toward zenith, T_b is rather small, e.g. 3-5 K. Toward ground, which is our case, the ambient noise sources are much larger and T_b

is close to 300 K. Considering a low loss antenna, the overall noise temperature is thus about 300 K.

8.7 Receiver design

A good starting point to derive the specifications of the receiving part of the interrogator (hereafter named the receiver) is to satisfy the linearity issue or the third order intercept point at the input $IIP3$. Then, the Minimum Detectable Signal (MDS) is calculated based on the chosen values. The $IIP3$ compliance guarantees that a nearby (less than a meter) tag is addressable and the MDS determines the maximal reading range of the system. As we will see, it is not the MDS that limits the operating range, but the tag rectifier.

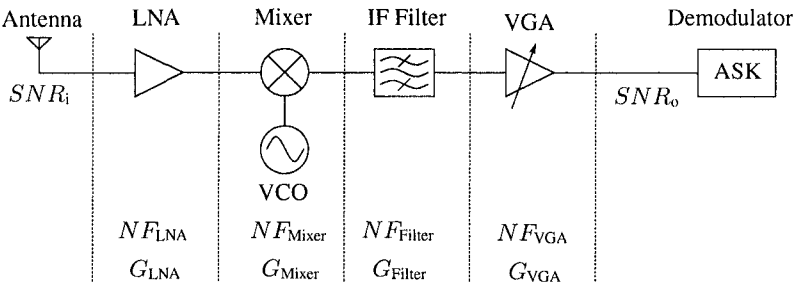

Fig. 8.10. Block diagram of the receiving part of the interrogator.

The specifications of the receiver blocks shown in Fig. 8.10 are shown in Table 8.2. G is the gain and NF corresponds to the Noise Figure.

From these values, we compute the cumulative output gain, noise figure and input $IP3$ using [50], [51]. The results are shown in Table 8.3. Finally, for a 200 kHz receiver bandwidth, a Bit Error Rate of 10^{-5}, and an OOK modulation scheme, i.e. a necessary output Signal-to-Noise Ratio of $SNR_o = 13$ dB, the MDS is equal to

Table 8.2. Receiver specifications.

Block	G dB	$IIP3$ dBm	NF dB	Product
Mixer	−5.8	17	5.8	Minicircuits MBA-18LH
Low Noise Amplifier (LNA)	19	−7	1.7	Hittite HMC286
IF Filter	−0.75	∞	0.75	Custom made
Variable Gain Amplifier (VGA)	Low:7.5 High:50	38	Low G:44 High G:4	Analog Device AD8331

Table 8.3. Receiver cumulative specifications.

Configuration	G dB	NF dB
VGA gain = 7.5 dB	20	31
VGA gain = 50 dB	62	2.1

−104 dBm. In terms of operating range, this corresponds to 24 m at 2.45 GHz. As said earlier, the tag's rectifier or wireless power transmission is the limiting factor. The noise figure in the case of a nearby tag reaches 31 dB. This is due to the VGA in which the gain is controlled by an attenuator. As a result, the noise figure is hugely degraded but with no consequence on communication since in this case, the SNR at the demodulator input is more than sufficient.

8.8 IF modulation frequency

In order to have an interrogator-driven communication and to avoid a data encoder at the tag side, an Intermediate Frequency (IF) is introduced. Upon request of the reader (a short interrupt is emitted during the read mode), the tag switches the IF carrier on or off depending on the data bit value. This is equivalent to an IF On-Off-Keying (OOK) modulation. The RF carrier is in turn modulated using the pseudo Phase-Shift-Keying (pPSK) scheme described in chapter 5. Such an approach has the advantage of an almost constant backscattered power as well as constant 180° of phase modulation depth. The difference of amplitude is due to the power absorbed by the application. The signal at different levels (from data to RF signal) is shown in Fig. 8.11.

The IF sub-carrier frequency has to be well chosen. When the modulator is closed, the voltage applied at the input of the rectifier falls, thus leading to an efficiency drop and more importantly, to an output DC voltage drop. The period must thus be short enough not to power off the circuit and long enough to lay within the interrogator's receiver bandwidth. In terms of power consumption, the frequency cannot be too high. A good trade-off in this case is 1 MHz which ensures a sufficient data-rate.

8.9 IF processing

As described earlier, the IF frequency value may vary from die to die. In the fabricated tags, its value varies from 600 kHz up to 1.2 MHz. Ideally, the data bandwidth we aimed at for the system is equal to 200 kHz to allow a sufficient data-rate (about 100 kbits/s). The modulated data are thus spread from 450 kHz to 1.35 MHz depending on the IF value. Integrating the signal over this bandwidth leads to a poor SNR compared to a 200 kHz bandwidth.

One could solve this issue by using a calibration technique at the cost of a larger protocol preamble and a higher circuit complexity. Our approach is based on the architecture shown in Fig. 8.12. The data bandwidth of the loop is kept to a minimum

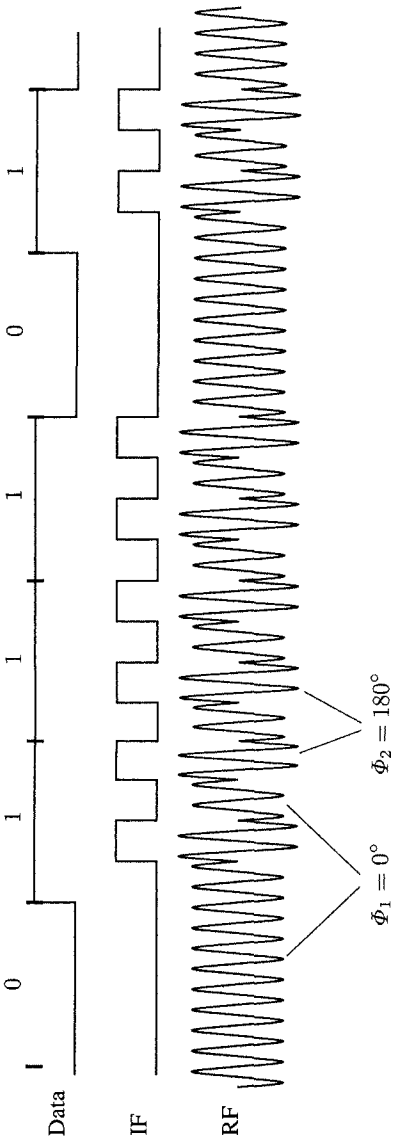

Fig. 8.11. Shape of the data, OOK modulated and RF signals.

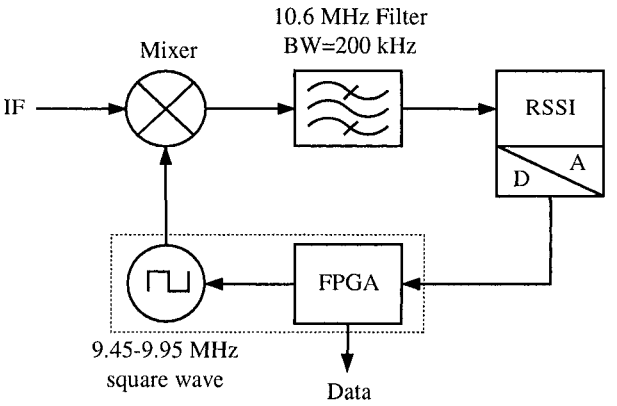

Fig. 8.12. Baseband processing architecture. The oscillator is realized with the FPGA in this work.

of 200 kHz, ensuring the desired data-rate, i.e. 100 kbits/s. The micro-controller or FPGA sweeps the voltage-controlled oscillator frequency over the IF spread until the Received Signal Strength Indicator (RSSI) circuit detects some signal power located at the tag's IF frequency. At this point, the loop is locked and the data communication session can start at the desired data-rate. The advantage of such an approach is that it is completely controlled by the reader thus reducing the tag complexity. In terms of time consumption, it is probably comparable to the calibration technique approach.

8.10 Conclusion

Possible architectures to detect backscattered signals have been presented. As seen in section 8.3, the emitted power is very high compared to the backscattered signal. Because of the direct coupling effect described in section 8.4, there exists a stringent constraint on the RF front-end design in term of linearity. Desensitization can occur and particular attention has been paid to this issue.

The impact of phase noise on the receiver performance has been studied. It has been shown that the effect on down-conversion is rather small. If a multi-channel system is to be designed, reciprocal mixing would place tougher specifications on phase noise. The antenna temperature and the receiver system design have also been described.

An Intermediate Frequency (IF) processing block that solves the tag IF signal tracking has been presented. The developed system achieves a theoretical Minimum Detectable Signal (MDS) value of -105 dBm.

The results of chapter 6 have important quantitative consequences on the interrogator design. The modulation impedance plane at the tag side is considerably transformed along the communication path depending on the particular antennas chosen. In this work, a variable carrier frequency approach at the interrogator side was used

to solve this issue. For a multi-reader, multi-channel system, such a solution is not viable. An I/Q down-conversion stage followed by an amplitude and phase demodulator should be independent on both the operating range and the carrier frequency value. The "dead-zone" problem nevertheless remains in such an architecture but could be solved using a frequency hopping technique.

9

Conclusion

MANY aspects of RFID systems have been discussed in this work. The order of the chapters is chronologically structured with the development of the presented system except for chapter 6. The latter is the result of research carried out after the fabrication of the transponder integrated circuit.

Three key issues concerning RFID systems were brought to light. Since passive tags have no embedded electrical energy, they have to be remotely powered. Wireless power transmission, RF to DC power conversion and the influence of some fundamental antenna parameters have been studied. A full-wave rectifier optimized using the model presented in chapter 3 showed performance (suited to passive devices) in agreement with predicted values.

The second important issue is the design of the tag modulator. Prior to this, an original study concerning the backscattering modulation was discussed in chapter 5. This study takes into account the three fundamental parameters for wireless power transmission devices, i.e. the available power to the application, the available voltage amplitude at the tag input when modulating and the communication link quality measured in term of Bit Error Rate. This development led to the proposal of the "pseudo-PSK" (see section 5.10) modulation scheme as an optimal trade-off for backscattering communication.

In the third place (although it could be in the *first* place!), the antenna plays a crucial role in this game. Its impact on the wireless power transmission and backscattering modulation can't be neglected. On one hand, its available voltage amplitude increases with its radiation resistance. But on the other hand, the same parameter should be kept as close to the reader antenna radiation resistance as possible to achieve a reasonnable communication quality (see chapter 6). A strict trade-off between the reader and the tag(s) thus rules.

The design of the tag itself (chapter 7) takes advantage of the previously presented results. The measured data in term of reading range at 2.45 GHz outperforms what is available elsewhere at the time of writing. Finally, the important points that prevail on the reader design are described in chapter 8. Above all, the system parameters, e.g. phase noise, linearity, gain and noise figure distribution have been presented.

At the end of this work, our personal points of view for future extension is the wide horizon opened by chapter 6. A "segmented" understanding of the analysis and optimization of UHF RFID systems is the result of chapters 2, 3, 4, 5, 7 and 8. In our opinion, chapter 6 links or "glues" these closely related topics and paves the way to a continuation of this work. The goal of such a continuation could be summarized in one sentence:
Optimize the UHF RFID system by synchronously designing the tag antenna, modulator and rectifier as well as the reader antenna, RF and IF blocks based on the results of chapter 6.

A

Appendix

A.1 Probability functions

The cumulative distribution function for the Gaussian distribution is

$$F(a) = Q\left(\frac{m-a}{\sigma}\right) = \frac{1}{2}\text{erfc}\left(\frac{m-a}{\sqrt{2}\sigma}\right) \tag{A.1}$$

where the Q function is defined by

$$Q(z) \triangleq \frac{1}{\sqrt{2\pi}} \int_z^\infty e^{-\lambda^2/2} \mathrm{d}\lambda, \tag{A.2}$$

the complementary error function (erfc) is defined as

$$\text{erfc}(z) \triangleq \frac{2}{\sqrt{\pi}} \int_z^\infty e^{-\lambda^2} \mathrm{d}\lambda, \tag{A.3}$$

m is the mean of the random variable and σ corresponds to the standard deviation.

The equivalence between the two functions is

$$Q(z) = \frac{1}{2}\,\text{erfc}\left(\frac{z}{\sqrt{2}}\right). \tag{A.4}$$

References

1. N. C. Bui and T. Roz, *Identification sans contact et applications low-cost*, 1st ed.Cours FSRM, 2004.
2. K. Finkenzeller, *RFID handbook, Radio-Frequency Identifications Fundamentals and Applications*, 2nd ed. John Wiley & Sons, Inc., 2003.
3. D. Parret, *Identification radiofréquence et cartes à puce sans contact*, 2nd ed.Dunod Electronique, 2001.
4. J.-P. Curty, N. Joehl, F. Krummenacher, C. Dehollain, and M. Declercq, "A model for μ-powered rectifier analysis and design," *IEEE Trans. Circuits Syst. I*, vol. 52, no. 12, pp. 2771 – 2779, Dec 2005.
5. J.-P. Curty, N. Joehl, C. Dehollain, and M. Declercq, "Remotely powered addressable UHF RFID integrated system," *IEEE J. Solid-State Circuits*, vol. 40, no. 11, pp. 2193 – 2202, Nov 2005.
6. W. Brown, "The history of power transmission by radio waves," *IEEE Transactions on Microwave Theory and Techniques*, vol. 32, no. 9, pp. 1230–42, Sep 1984.
7. H. Boot and J. Randall, "Historical notes on the cavity magnetron," *IEEE Transactions on Electron Devices*, vol. 23, no. 7, pp. 724–9, Jul 1976.
8. M. Ollivier, "Rfid-a practical solution for problems you didn't even know you had!" in *IEE Colloquium on Wireless Technology (Digest No.1996/199)*, London, UK, 1996, pp. 1–6.
9. Leonardi M. and Leuenberger P. and Bertrand D. and Bertsch A. and Renaud P., "A soft contact lens with a mems strain gage embedded for intraocular pressure monitoring," in *IEEE International Solid-State Sensors and Actuators Conference*, Boston, MA, USA, 2003, pp. 1043–6.
10. Hagerty J.A. and Helmbrecht F.B. and McCalpin W.H. and Zane R. and Popovic Z.B., "Recycling ambient microwave energy with broad-band rectenna arrays," *IEEE Transactions on Microwave Theory and Techniques*, vol. 52, no. 3, pp. 1014–24, Mar 2004.
11. M. E. Europe. (2004) Rfid comes up to a standard.
12. "Michelin embeds rfid tags in tires," 2003. [Online]. Available: http://www.rfidjournal.com/article/articleprint/269/-1/1/
13. I. T. U. (ITU). (1998) Question itu-r 210/1, wireless power transmission. [Online]. Available: http://www.itu.int/itudoc/itu-r/publica/que/rsg1/que210_ww9.doc
14. J. C. S. Woo. (1998) High performance silicon on sapphire technology. [Online]. Available: http://www.ucop.edu/research/micro/97_98/97_208.pdf

15. J. B. Kuo and S.-C. Lin, *Low-Voltage SOI CMOS VLSI Devices and Circuits*, 1st ed.Wiley, 2001.
16. E. Vittoz, "Conception de circuits intégrés analogiques," 2001.
17. W. C. Brown, "An experimental low power density rectenna," in *IEEE MTT-S International Microwave Symposium Digest*, vol. 1, Boston, MA, USA, Jun 1991, pp. 197–200.
18. J. McSpadden, L. Fan, and K. Chang, "Design and experiments of a high-conversion-efficiency 5.8-ghz rectenna," *IEEE Transactions on Microwave Theory and Techniques*, vol. 46, no. 12, pp. 2053–60, Dec 1998.
19. J. D. Chatelain and R. Dessoulavy, *Electronique*, 2nd ed., P. polytechniques et universitaires romandes, Ed. Presses polytechniques et universitaires romandes, 1995.
20. "A vintage rfid application," 2004. [Online]. Available: http://www.rfidjournal.com/article/articleprint/908/-1/99/
21. IDC, "U.S. RFID for the Retail Supply Chain Spending Forecast and Analysis," 2004.
22. J. Collins, "Rfid labels for less," 2004. [Online]. Available: http://www.rfidjournal.com/article/articleprint/770/-1/1/
23. (2004) Electronic Product Code. [Online]. Available: http://www.epcglobalinc.org
24. *ISO Standard 18000-4*, Std., 2004. [Online]. Available: http://www.iso.ch
25. Philips. (2004) UCODE HSL Product family. [Online]. Available: http://www.semiconductors.philips.com/
26. E. F. Knott, J. F. Shaeffer, and M. T. Tuley, *Radar cross section*, 2nd ed.Artech House, 1993.
27. F. P.R. and B. R.A., "Antenna problems in rfid systems," in *IEE Colloquium. RFID Technology*, London, UK, 1999, pp. 1–5.
28. Tagmaster. (2005) Product datasheet. [Online]. Available: http://www.tagmaster.se
29. R. Hansen, "Relationship between antennas as scatterers and as radiators," *Proc. IEEE*, vol. 77, no. 5, pp. 659 – 662, May 1989.
30. C. A. Balanis, *Antenna Theory*, 2nd ed. John Wiley & Sons, Inc., 1997.
31. L. W. C. II, *Digital and Analog Communication Systems*, 6th ed. Prentice Hall, 2001.
32. R. Collin, "Limitation of the Thévenin and Norton equivalent circuits for a receiving antenna," *IEEE Antennas Propagat. Mag.*, vol. 45, no. 2, pp. 119 – 124, Apr 2003.
33. U. Karthaus and M. Fischer, "Fully Integrated Passive UHF RFID Transponder IC with 16.7 μW Minimum RF Input Power," *IEEE Journal of Solid-State Circuits*, vol. 38, no. 10, pp. 1602–1608, Oct 2003.
34. G. D. Vita and G. Iannaccone, "Design criteria for the RF section of UHF and microwave passive RFID transponders," *IEEE Trans. Microwave Theory Tech.*, vol. 33, no. 9, pp. 2979 – 2990, Sep 2005.
35. J.-C. Bolomey and F. E. Gardiol, *Engineering Application of the Modulated Scatterer Technique*, A. House, Ed. Artech House, 2001.
36. J. Thaysen, K. B. Jakobsen, and J. Appel-Hansen, "A wideband balun - how does it work?" *Applied Microwave & Wireless*, vol. 12, pp. 40–50, Oct 2000. [Online]. Available: http://server.oersted.dtu.dk/publications/p.php?889
37. G. F. Engen and C. A. Hoer, "Thru-Reflect-Line": an improved technique for calibrating the dual six-port automatic network analyzer," *IEEE Trans. Microwave Theory Tech.*, vol. MTT-27, no. 12, pp. 987 – 993, Dec 1979.
38. G. Gonzalez, *Microwave transistor amplifiers: analysis and design*, 2nd ed.Prentice Hall, 1996.
39. Impinj. (2004) Impinj RFID Product. [Online]. Available: http://www.impinj.com
40. T. N. et Al, "Silicon on sapphire (sos) device technology," Oki, Tech. Rep., Oct 2004.
41. T. Skotnicki, "Cmos technologies for end of roadmap, lecture notes," 2004.

42. (2004) Utsi process advantages. [Online]. Available: http://www.peregrine-semi.com.au/Process/UTSIProcess2.html
43. "EPC Tag Data Standards Version 1.1 Rev. 1.24," Tech. Rep., 2004. [Online]. Available: http://www.epcglobalinc.org
44. J. P. Curty. (2004) A web interface for diode rectification ability evaluation. [Online]. Available: http://legwww.epfl.ch/direct
45. D. M. Pozar, *Microwave and RF Design of Wireless Systems*, 1st ed. Wiley, 2001.
46. E. Vittoz and J. Fellrath, "Cmos analog integrated circuits based on weak inversion operations," *IEEE Journal of Solid-State Circuits*, vol. 12, no. 3, pp. 224–31, Jun 1977.
47. L. Ukkonen, D. Engels, L. Sydanheimo, and M. Kivikoski, "Planar wire-type inverted-f rfid tag antenna mountable on metallic objects," in *IEEE Antennas and Propagation Society Symposium*, Monterey, CA, USA, 2004, pp. 101–4.
48. K. Rothammel, *Antennenbuch*, 7th ed. Franckh'sche Verlagsbuchhandlung.
49. (2005) Alcatel ferrocom. [Online]. Available: http://www.ferrocom.com/
50. T. Lee, *The Design of CMOS Radio-Frequency Integrated Circuits*, 1st ed.Cambridge University Press, 2001.
51. B. Razavi, *RF Microelectronics*, 1st ed. Prentice Hall, 1997.
52. U. Rohde, *Microwave and Wireless Synthesizers : Theory and Design*, 1st ed.Wiley, 1997.

List of Figures

List of Tables

Index